TU Clausthal

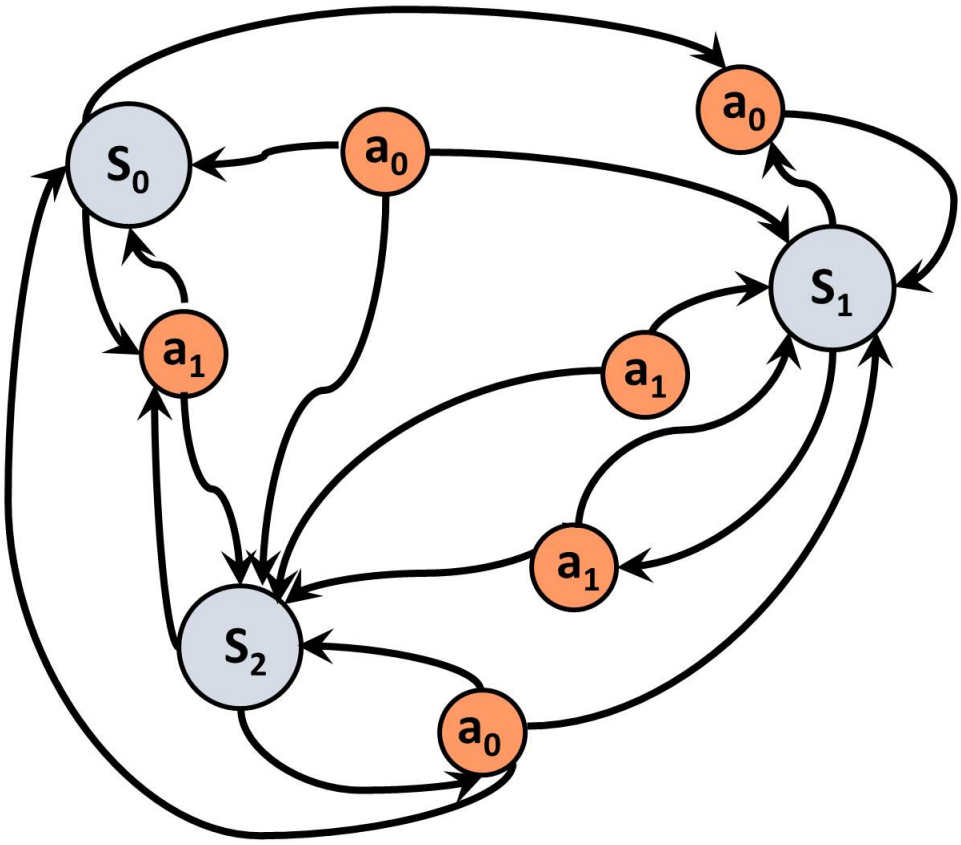

Stamatia Dimopoulou

Energy Management of a Hybrid Energy Storage System in a single-family House including E-Car Mobility

SSE-Dissertation 17

Software Systems Engineering

Department of Informatics
Chair of Prof. Dr. Andreas Rausch

Energy Management of a Hybrid Energy Storage System in a single-family House including E-Car Mobility

Doctoral Thesis
(Dissertation)

to be awarded the degree of
Doctor of Engineering
(Dr.Ing.)

submitted by
Stamatia Dimopoulou
from Athens, Greece

approved by the Department of Informatics,
Clausthal University of Technology

2018

Dissertation Clausthal, SSE-Dissertation 17, 2018

Chairperson of the Board of Examiners
Prof. Dr. Sven Hartmann

Chief Reviewer
Prof. Dr. Andreas Rausch

2. Reviewer
Prof. Dr. rer. nat. habil. Ekkehard Boggasch

3. Reviewer
Prof. Dr.-Ing. Joachim Landrath

Date of oral examination: November 19, 2018

To my parents

Abstract

The transition into the new era in transport sector after the invasive introduction of electromobility and the already established tactic of the installation of small-scale renewable energy units in the domestic sector force to the exploration of an undiscovered aspect of energy allocation if the individual components are synthesized into an ensemble which is supported from storage devices. The existence of a unique battery system is already a widespread policy in the new renewable installations. It is though common knowledge that none of the existing storage systems is from physical aspect steadily efficient under each operational condition, whereas it still remains partly explored the coupling of two storage systems, which from structural point of view are complementary.

Stimulated from the abovementioned concept in the frame of this research it is attempted to delimitate the capability of a hybrid energy storage system (HESS) so as to support the domestic load demand of a single family house in a central north area in Germany which is accumulated from the load demand of a E-vehicle which is used for commute reasons of the family and always charges at home. The designed HESS is composed of PV installation, two storage devices, namely a lead acid battery system (LAB) and a vanadium redox flow battery (VRB), as well as the respective load demand of the previously referred dwelling. The application ought to consume as much as possible of the on-site renewable generation and to minimize the interaction between the grid and the system.

So as to succeed an optimized utilization of the dual storage system a novel algorithm is developed based on the Markov Decision Process, according to which the priority for charging and discharging process is assigned to the storage facility which depicts a favorable performance under the given conditions. This is accomplished through a reward/ penalty policy which is by default integrated into the Markov Decision Process and is respectively adapted while it depends on the efficiency curves of the storage devices and the amount of the demanded or surplus of power. The main target is to reduce the great fluctuations between the building and the grid and succeed a higher rate of self-energy consumption.

The designed method tackles the problem of controlling a dual storage installation in the domestic sector, when considering the electric vehicle charging requirements and contributes to the management of the energy flow into a novel system topology with the introduction of reinforcement learning tools.

The results are evaluated after the comparison of the designed technique with a benchmark method which stems from the physical attributes of the battery systems and the evaluation metrics are two index factors which are respectively computed with real registered input data stemming from annual simulations as well as from an indicatively chosen sunny period, which is particularly selected in order to study the behavior of the complete system under high production PV rates. It is thereby proved that a control algorithm is essential in order to fully leverage the key resources.

Acknowledgement

This thesis was conducted in the frame of the Cooperative Promotion Program Electromobility (Kooperatives Promotionsprogramm Elektromobilität) which in terms of a schloraship aided financially for 3 years the current research, in cooperation and collaboration of the Institute for Applied Software Systems Engineering, TU Clausthal, Clausthal-Zellerfeld, Germany and the Laboratory of Electrical Engineering and Renewable Energy Systems, Faculty of Supply Engineering, Ostfalia University of Applied Sciences, Wolfenbüttel, Germany. Moreover, I would like to express my gratitude to the Rud. Otto Meyer-Umwelt-Stiftung which financially supported further my PhD study during the last months.

For the fulfillment of this thesis several people have contributed with their generous providing of input, comments and remarks. First of all I would like to thank my supervisors, Prof. Dr. Andreas Rausch and Prof. Ekkehard Boggasch for their continuous support during the individual steps of the research, their dedicate reading of the study as well as for their constructive comments after numerous brainstorming meetings and discussions.

In addition special thanks are due to the entire research team of the Laboratory of Electrical Engineering and Renewable Energy Systems of the Ostfalia University who steadily supported me and in particular to Dr. Lars Baumann and Patrick Kügler whom models of their studies and work were integrated in the current study, and Alice Oppermann whose daily and constant technical know-how but also psychological encouragement helped me go through this journey.

Last but not least, I would like to thank my family. My brother Dimitri, for his continuous support in every occasion that has arisen, my beloved husband George, since without his support, patience and inspiration in all terms I would not have completed this thesis, as well as my two adorable children, Anastasia and Alexandro, for their understanding for all the moments which I could dedicate playing with them but instead I had to sacrifice in order to keep writing and finalizing my PhD study.

Table of Contents

List of Figures

List of Tables

Abbreviations

AGM	Absorbed Glass Mat
BOP	Balance-Of-Plant
CHP	Combined Heat and Power
CO_2	Carbon Dioxide
DWD	Deutscher Wetterdienst (German Meteorological Service)
EER	Energy Efficiency Ratio
HESS	Hybrid Energy Storage System
LAB	Solar Lead Acid Battery System
LON	Local Operating Network
MBE	Mean Bias Error
MDP	Markov Decision Process
MPP	Maximum Power Point
OPC	Open Platform Communications
PDF	Probability Density Function
PLC	Programmable Logic Controller
PV	Photovoltaic
RES	Renewable Energy Source
RTU	Remote Terminal Unit
UPS	Uninterruptible Power Supply
VDEW	Verband der Elektrizitätswirtschaft
VRB	Vanadium Redox Flow Battery
VRLA	Valve Regulated Lead Acid Battery

1 Introduction

The increase of greenhouse gas emissions during the last decades, the challenge of global warming which threatens the orderly life on Earth and the Fukushima nuclear disaster have set the adoption of radical measures in the primary energy production as pivotal. The First and Second European Climate Change Programme, launched in 2000 and 2005 respectively and referring to all the EU Members [1], the Chinese Renewable Energy Law passed in 2005 and amended in 2009 [2], the Energy Transition (Energiewende) policy which was introduced in 2010 [3] in Germany are only some paradigms of the extended effort of the governmental and legislative organs to promote globally renewable energy sources and energy efficiency in order to substitute fossil fuels and nuclear energy in the overall energy mix.

The building sector has globally the highest ratio in energy-consumption, since the respective share is over one-third of the final energy consumption globally and is responsible for an equal proportion of carbon dioxide (CO_2) emissions [4-5]. Therefore an extensive effort to change the energy mix in this field would bring overall remarkable results. The integration of decentralized power systems in the energy portfolio of new buildings would help towards this direction and would substantially contribute in reduction of fossil fuels and nuclear share in the total energy mix.

The installation of small-scale renewable energy facilities in private houses is a common tactic in Germany nowadays. Due to the fact though that more than 98 percent of the installed power plants are connected to the low voltage grid [6], a high amount of energy exported to the grid leads to an extensive straining of its bounds during high energy availability and low demand timeframes, in particular in regions with high density of installed power plants. In this respect, the feed-in tariff policy adopted in Germany has been repeatedly reexamined during the last seven years, mainly due to the enormous spread of photovoltaic (PV) installations, resulting to a steady review of the Renewable Energy Sources Act (German: Erneuerbare-Energien-Gesetz or EEG) and the formed feed-in tariffs [7], so as to control and set boundaries to the growing tendency of installing renewable energy sources.

1.1 Motivation

From financial scope of view (although this aspect is not taken into account in the current study) it is identified that it has become more lucrative to consume the onsite produced energy from renewable sources than sell it to the grid. In particular, the present feed-in tariffs for small PV rooftop installations (till 10 kWp) do not exceed an amount of 12,3 Cent/kWh [8]. In addition, the primary cost for producing your own energy from small PV installations is currently between 7 and 13 Cent/kWh, according to a Fraunhofer Study [9]. From the occurring difference it is thus obvious that feeding the energy to grid is not considered a profitable approach, while the idea of the self-consumption of the on-site produced renewable energy becomes more attractive.

However it is common knowledge that the highest electricity demand and peak power periods in the residential sector occur when the PV panels are not producing energy. If no

storage facility is available, the self-consumption amounts to 20-40% of the onsite-generation [10]. However, when load and generation profiles do not coincide, battery components are favored in order to store the excess of on-site renewable produced energy and reallocate it to loads later when required. The unpredictable and intermittent character of renewable energy is thus overcome. According to Wirth [11] only if considerable storage capacities are connected to the grid it is possible that PV plants may substitute for fossil fuel and nuclear power plants. The German KfW, a German government-owned development bank, is encouraging such an attempt by supporting the integration of storage systems in dwellings through co-financing the investment [12] up to 660€ per kWp for PV installation with storage coupling.

Nevertheless, it's not only the production of energy which has changed the portrait of the energy market nowadays due to the penetration of renewable energy sources, but also the load demand profiles have been altering after the introduction of electromobility in the transport sector. Germany's vision to reach one million E-cars on German streets till 2020 and six million till 2030 [13] is going to change radically the standard load profiles from temporal and spatial aspect. It would be thus profitable for the household consumers to use the on-site produced energy to cover the E-car load demand. Consequently, they can save money from charging their private E-car at public charge points when they are out and about, simply by clever allocating the self-produced energy. This concept would be easier accomplished if the respective PV installation was also coupled from a stationary storage system.

It is concluded from the above mentioned that the integration of a stationary storage system in a household with a PV installation is lucrative in all circumstances. It is not only for the owner of the installation, who has profit from the self-energy consumption but also for the grid, which is no longer strained from the excess of the decentralized energy production.

The last three years more than 34,000 decentralized solar energy storage systems were installed in Germany, proving that these applications are considered already a routine by installation of new photovoltaic plants in the domestic field [14]. Although a wide range of those systems is marketable and commercially viable during the last years, it is also common knowledge that none of the existing storage systems regardless of their type (batteries, chemical-hydrogen storage, supercapacitors, etc.) is attributed with the ensemble of assets that such devices are featured. According to Daniel et al. since no system is able to meet all the needs of the customer or of the respective application, the final decision for the appropriate system choice is often a compromise [15]. In particular, there are residential storage systems that are characterized from high energy density and other which belong to high power systems. It would be thus of great interest to combine two or more of those systems in order to aggregate the complementary attributes and benefit from their coupling. In such a case consequently is more substantial to design a management system that would apply the devices at an overall higher efficiency. The optimal allocation of the self-produced energy is the crucial element, since an inappropriate energy management would eventually end up to a misuse of the available facilities and energy. The potential of such a coupling of storage systems in the building sector is actually the motivation of this thesis and the optimal operational mode of these facilities is regarded the core part of the study.

1.2 Aim & Objectives

The pairing of two storage devices is regarded as a Hybrid Energy Storage System (HESS) and their employment in swap mode stands as previously mentioned in the focus of this thesis. In particular, the present work is actually addressing a HESS which is composed of a Solar Lead Acid Battery, a Vanadium Redox Flow Battery and the peripheral components which are a photovoltaic installation, domestic loads of a dwelling and the load demand of an E-Car. A combination of a market-mature technology as the Solar Lead Acid Battery with a relatively new system as the Vanadium Redox Flow Battery and their integration in a residence which produces its own decentralized energy via a PV installation and whose load demand is also aggregated from the power needed to charge an E-Vehicle every day at the house premises is going to be explored. The upper target is to operate the two storage systems at a rational sequence which succeeds a higher rate of self-energy consumption and a lower grid interaction, which is interpreted as lower fluctuations.

This thesis is actually handling the energy management thematic of a HESS in order to deploy the available resources at a more efficient way. In this respect, a suitable technique which will predefine the respective operation sequence should be chosen and designed based on the features of the storage systems. It is thus examined and identified which is the optimal management technique that can be applied so as to take advantage of the physical and constructional attributes of the two selected storage systems that are applied in the respective residence.

The boundary conditions are playing a substantial role in the overall context, thus the planning of the environment is considered also fundamental. The choice and parametrization of the respective models for each device and the interactions among them were important sub steps in the design process while the plausibility of the modelling part and the validation of the designed models were considered vital parts of the developed method.

The previously mentioned indexes, i.e. the self-energy consumption and the grid interaction are the two evaluation criteria which actually assess the success and efficiency of the applied approach. Moreover, the technical feasibility of such an endeavor is discussed whereas financial and economic aspects are not considered under the spectrum of this thesis.

An evaluation of the developed controlled strategy is also conducted in the frame of this study and a comparison with a greedy approach to control the storage systems is performed. The objective is to prove whether the applied method is well and efficiently designed and if the given solution is the most optimal.

Summing up, the main research question addressed from the current thesis is enclosed in the following sentence:

- *"How can the energy flow in a single-family house be managed efficiently, so as to maximize the self-consumption of the produced renewable energy and minimize the grid interaction by controlling two different stationary storage systems?"*

Moreover, several sub-questions arise also from the studied case and there are in detail explained in Section 3.4.

It should be noted that such a system coupling is not yet fully reported in the literature while the energy management thematic of an analogous HESS is not extensively explored and examined. Subcases or sub-problems of this philosophy have been addressed [16-20] but an extensive study of such a concept has not been documented.

1.3 Methodology

Due to the complexity of the examined scenario and the specificity of the under consideration concept a preparation stage preceded the energy management system development. In particular, in the beginning the respective hybrid system had to be designed and modelled. The facilities should be accordingly selected so that their capacity scale is analogous to the energy needs of a one family house. Then since not only the input and output parameters were significant for the design part but also the interconnections among the different models as well as the specific attributes of each component, it was wiser not to create a black box with inputs and output signals but to precisely represent each one of the integrated facilities.

In this regard for each facility a suitable model should be selected and parametrized and subsequently all these formed the overall hybrid system. The parametrization was conducted in the frame of an iterative process of validation and verification and although the selected models were representing real facilities, great importance was also given on their design so as to take into account the physical principles that define their function and to develop models that are easily reapplicable.

In addition, after studying the individual attributes of the incorporated battery systems, an appropriate technique was chosen to control their charging and discharging process. This selection of the respective technique was based also on the given formed environment. An unstable and always changeable setting could affect drastically the outputs of the designed technique. It was decided after thorough examination of the available mathematical and statistical tools to design the control process based on the Markov Decision Process (MDP). MDP is considered as a discrete time stochastic process and is referred to problems where the output is partly random and partly dependent on the decision of the stakeholder [21]. This method, which belongs to reinforcement learning tasks, is ideal for problems in which after change of the system status new actions have to be taken, its target is to optimize the calculated return cumulative and not instantly, the decision maker needs to know only the current states and their respective rewards, and system may not be exclusively stationary [22]. Since all these conditions were in this case fulfilled, and till now such a technique in such a context has not been thoroughly documented in the literature, it was considered challenging its application and examination in the frame of this thesis.

Finally, given the overall hybrid system yearly simulations were conducted and the applied method was evaluated by comparing the extracted results with those stemming from a greedy method. This benchmark values for comparing the extracted results are occurring after applying a naive approach which hypothesizes that it is always optimal to operate by priority that storage system which has at examined point in time the higher efficiency.

In Figure 1-1 a graphical depiction of the applied methodology is given:

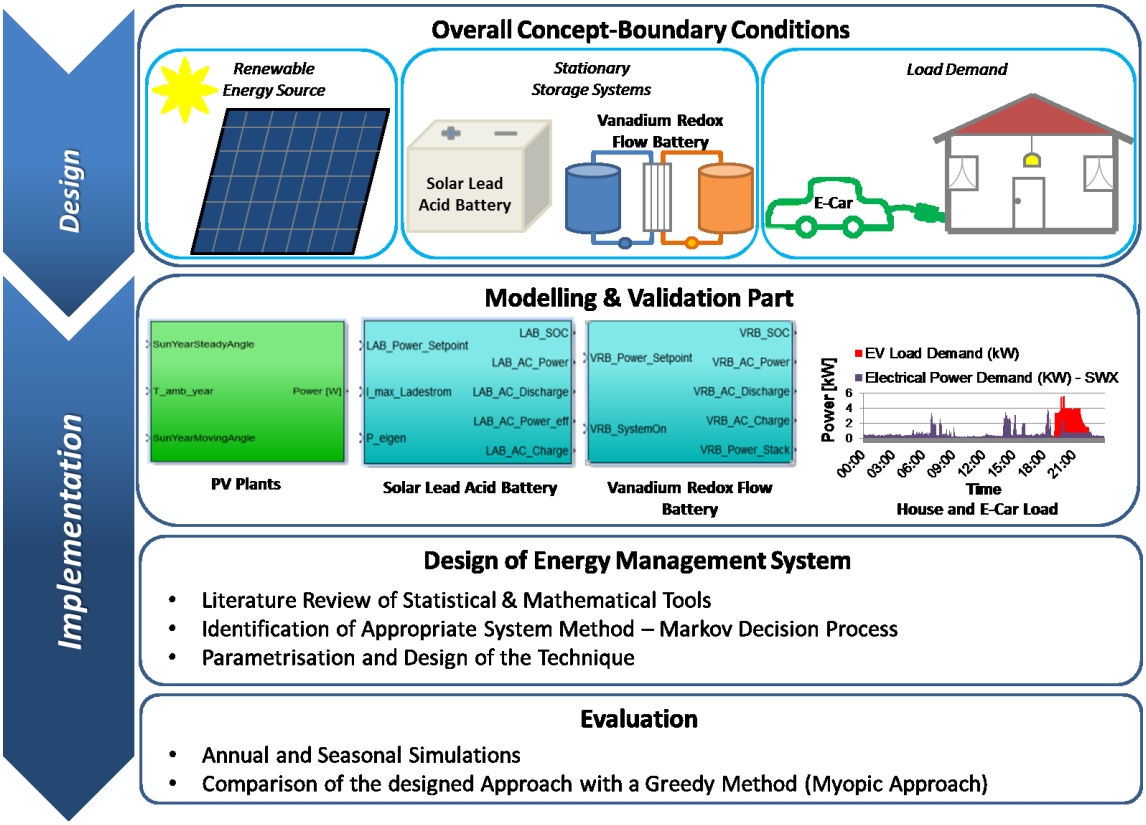

Figure 1-1: Followed Methodology

The entire process was designed and implemented in the MATLAB® / Simulink® environment while each of the selected facilities is a real part of the Energy Park in Faculty of Supply Engineering of the Ostfalia University in Wolfenbüttel. The required data for validation and testing purposes are also stemming from the database of the Faculty where weather parameters, such as global radiation and temperature, as well as values from the considered facilities, such as power, voltage and current, are registered, thanks to a Local Operating Network (LON) bus system, the Open Platform Communications (OPC) technology and the database system MySQL [23], which are enabling the transmission of measured values, the recording and provision, as well as the storage of them.

1.4 Thesis Layout

The rest of the thesis is structured as following:

In **Chapter 2** a detailed account of the state of the art in the field of photovoltaic plants and storage systems is given and the examined facilities from each category are thoroughly described. In this frame the Energy Park to which the referred systems are integrated is also depicted, setting thus the overall context of the current thesis.

In **Chapter 3** the state of the art round HESSs and the on-site HESS are presented, while focus was also given on the research questions accompanied from "Beyond the state of the Art". Methods applied to control similar HESSs are documented and advantages and disadvantages of them are justified. The logic to select the suitable in this case control

management method is then explained while limitations of scope and challenges during the design phase were addressed.

Chapter 4 includes the modelling part for each facility, namely the PV installation, the two selected storage systems, the domestic loads as well as the load demand of an E-Car. In particular, in MATLAB® / Simulink® environment all of the considered components of the examined HESS are designed and respectively parametrized so as to depict the real facilities. The validation was also included in the design phase by using data which are registered in the database of the Energy Park.

Consequently the methodology chosen to control the two storage systems is explained in detail and the applied technique is fully described in **Chapter 5**. The problematic which arose during the design phase relating to the efficiency grade of the storage systems is referred and the decided approach is justified. In addition the greedy method which will be used as benchmark to evaluate the extracted results is also analysed and the differences with the designed control technique are documented.

In **Chapter 6** the annual and seasonal simulation results are included while the evaluation is performed by comparing the outputs with the ones extracted for an analogous naive approach. Comparison is not only made between the selected evaluation criteria which are considered the metric for assessing the optimal method but also with graphical representation of the systems which operate with a stand-alone battery and hybrid ones and it is justified why the developed Markov method outperforms the others.

Finally in **Chapter 7** the examined concept and the contribution of the thesis are summarized while suggestions for future work are mentioned.

2 System Fundamentals & Experimental Setting

In the previous chapter an introduction to the thematic of the current thesis was presented through setting the boundary conditions and concretizing the topic. The motivation for handling such a domain and the specific objectives which are related to it are described while emphasis is also given on the followed methodology, which is explained. This Section is primarily devoted to describe the facilities which exist in the Energy Park of the Ostfalia University and are to be integrated in the designed HES. Beside that the state of the art around photovoltaics, storage technologies and load profiles applied, which are considered the fundamental components of this study is to be outlined.

2.1 Energy Park of the Ostfalia University

In order to create a research test bed of a hybrid energy system on which various measurements and different topologies can be examined so as to emulate a semi-autonomous residence, a modular energy park was designed and gradually developed at the premises of the Faculty of Supply Engineering at the Ostfalia University. It is composed of RESs, storage systems and loads that can imitate the power consumption and cover the electrical demand of a residence. The individual components are depicted in Figure 2-1, while the interconnection among the different systems is also represented with lines between them. It is to be noted that the selected units are appropriate for residential purposes and the applied topology is three-phase AC. Although the examined synthesis is used for experimental purposes, all constituent parts are commercially available.

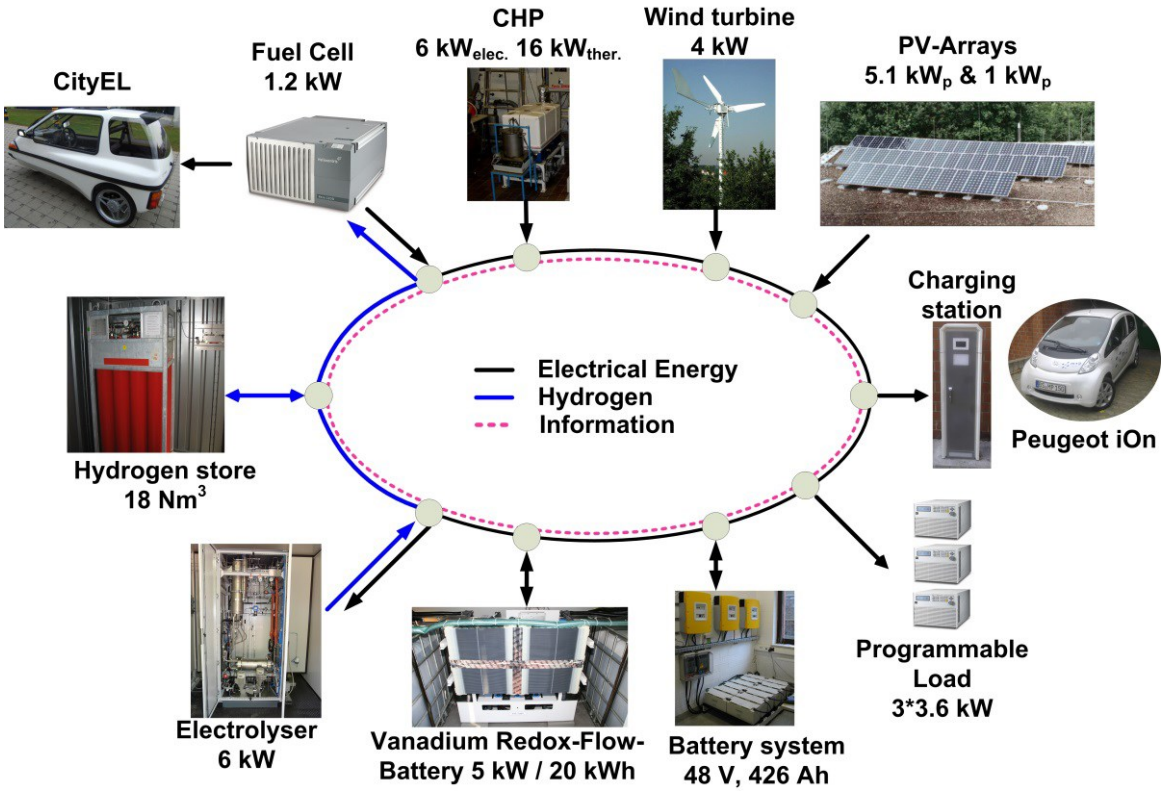

Figure 2-1: Graphical Representation of the Energy Park [18]

In particular, the available on-site devices are two PV plants of 5.1 kWp and 1.02 kWp peak power, a wind turbine of 4 kW, a combined heat and power system (CHP) of 6 kW_{el} and 16 kW_{ther}, a fuel cell of 1.2 kW, an electrolyser (6 kW) with a hydrogen store unit, a vanadium redox flow battery (VRB) of 5 kW, a solar lead acid battery system (LAB) of 6 kW, a charging station for E-Vehicles and programmable loads that can be respectively controlled to imitate house load profiles. However, from the installed facilities not all have been integrated to the examined study case. The photovoltaic plants, the vanadium redox flow battery, the solar lead acid battery and the E-Vehicle are those which were adapted in the examined concept in the framework of this thesis, with upper target to investigate under which circumstances it is optimal to operate two storage systems for covering local demands of a residence with an E-Vehicle, by exploiting maximally the locally produced renewable energy. It is to be noted that since the installed facilities are connected in such a way that may operate as part of the described system, as well as elements of a configuration with partial exploitation of the available facilities or as stand-alone systems, no disorders or malfunctions have arisen.

The described interconnected system is supported also from a LON (Local Operating Network) based data acquisition with a sampling rate of 1 sec and a weather station is also integrated so as to extract weather data, useful for validation and testing purposes.

2.2 Solar Photovoltaic Systems

PV Trend

As mentioned in previous Section, PV power generation is a widespread tactic nowadays. In Germany over 1.5 million of solar photovoltaic systems have already been installed which are equivalent to 39.8 GWp installed power and 38.7 TWh electricity production. In the South and West the majority of the systems are rooftop plants while in the East and North large photovoltaic parks have been built [24]. In Figure 2-2 the PV evolution of the installed facilities among the last fifteen years in Germany is depicted.

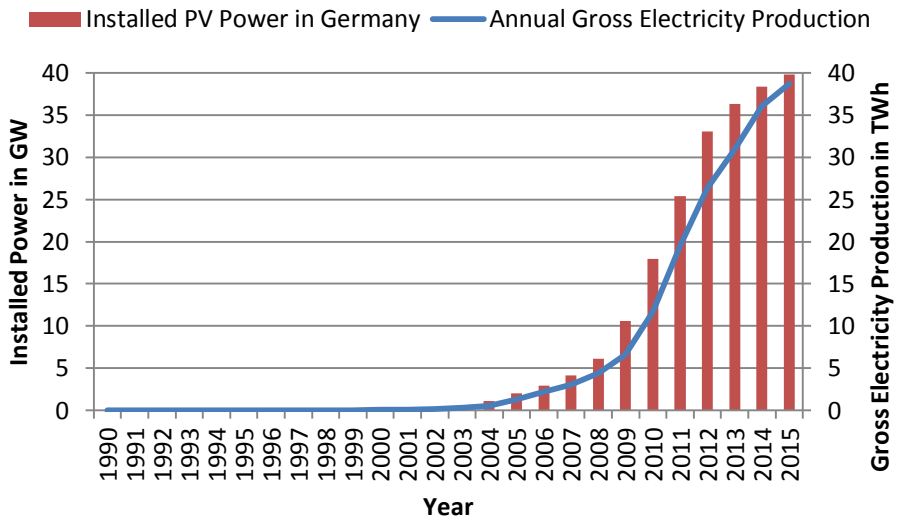

Figure 2-2: PV Data in Germany during the last 15 years [25]

It is obvious that the widespread installation of PV systems took place after the 1st Renewable Energy Sources Act (Erneuerbare-Energien-Gesetz) came into force in 2000. The introduced favorable feed-in-tariffs contributed to the exponential interest of the public and soon the installation of a PV system on the house rooftop turned out to be a profitable investment.

In the next sections the state of the art around the PV technology and the integrated to the examined HESS PV facility are explained in detail.

2.2.1 State of the Art of Photovoltaic

Solar energy is indefinite, renewable and sustainable, as well as one of the most abundant sources that can be used to produce heat or electricity. Photovoltaic systems can transform via solar panels solar energy into electricity by exploiting the photoelectric effect. According to this phenomenon, electrons are dislodged from a pn junction when light under specific circumstances hits the material. This movement of electrons is actually the physical representation of electricity.

The main components of the photovoltaic systems are the panels, which are connected in series to achieve the anticipated output voltage, or in parallel to reach the required current level. Panels are formed from one or more modules, and are preassembled, while modules

consist of the PV cells, which are the semiconductor units that convert the incident irradiance into electricity. Since the produced current is direct, an inverter is in most cases required to convert it in alternating current.

Different types of PV cells have reached commercial maturity to form the PV modules and panels consequently. These are described by the following clusters:

- *Monocrystalline PV Cells:* They are considered the most effective technology of all but also the most expensive, since cells must be sliced into wafers resulting to a high waste of material, if it is considered that during the process almost 50% of it is turned into dust [26]. Typically over 16% of the solar irradiance is converted into electricity [27].
- *Polycrystalline PV Cells:* These cells consist of multiple layers of crystal which are grown between the material. The deficit of such a technique is though that the area between the formed layers creates resistance thus its performance deteriorates (almost 15% efficiency) [27].
- *Thin Film PV Cells:* The thin film PV cells are made by depositing silicon on a thin surface which can be glass, or other material so as to form the solar module. They are characterized by a lower efficiency (6%-11%) [27], though their production is simpler and cheaper [28].
- *Organic PV Cells:* They take advantage of organic electronics to produce electricity from the photovoltaic effect and their low cost manufacturing increases their potential application in the future. However the low efficiency (~10%) and the duration still inhibit a broader employment [29].
- *Hybrid PV Cells:* This type of solar cells combines organic and inorganic components. In particular, the parts that absorb light are made from polymers while the surface which receives the excited electrons is made from inorganic materials. It is a promising technique that has already high efficiency grades achieved at experimental stage (~40%) [29].

For household installations, since the space capacity is usually limited it is thoughtful to install panels with a higher efficiency grade so as to achieve a higher gain and consequently lower installation costs. On the other hand, when solar parks are planned on land areas the efficiency grade is not that important.

The rooftop installations use building mounted solar arrays. The tilt angle of the panels is calculated based on the specific constructional characteristics as well as on the site of the building. When referring to ground-mounted systems, different installation structures can be applied, in order to increase the incident angle of the sun on the panels:

- *Fixed arrays:* With a fixed angle towards the south and a tilt angle usually smaller than the latitude of the installation area, so as to achieve the maximum annual power yield, this type of structure is widespread due to its low installation costs and simplicity in manufacturing. The tilt angle can also be monthly manually adjusted, benefiting from seasonal changes.
- *Single axis trackers:* This cluster of floating mount foundation includes the trackers with one degree of freedom, which is represented from one axis that can rotate. They favor the tracking of sun's movement during the day but they are unable to modify their angle

adjusting to seasonal changes. Their performance can be increased up to 30% over the static panels [30, 31].

- *Dual axis trackers:* Target of those systems is to follow sun's orbit during the day and yearly. With the primary and secondary axis they can angle themselves so as to have always the optimum orientation. Their added complexity in manufacturing is however not always worthwhile, since it is proved that only an added performance of 6% from the single axis trackers are noted [30, 31].

The best technique to be applied depends on various factors such as the installation site, the size of the planned solar park, the weather conditions of the area etc.. A higher investment cost for installing dual axis trackers may ultimately not yield the expected profit in the annual energy collection. So a systematic analysis is required and several aspects are to be taken into account before concluding to a specific mounting system.

Finally, another categorization of photovoltaic systems is between grid-connected or stand-alone systems which operate in island mode. Grid-connected systems are connected to the public power grid while those in island operation are feeding the produced energy only to on-site loads or to installed storage systems.

The characteristic I-V curve of the PV cells is an additional significant attribute of the respective facility. Given a steady solar irradiance and a steady temperature there is always a point on the curve which yields the highest output power. This point is called Maximum Power Point (MPP) and target is to operate always the system at this power point. This is succeeded via varying the resistance in the PV circuit which consequently influences the voltage and current level.

2.2.2 Description of the on-site Phovoltaic (PV) installation

The PV installation which is considered as the RES for the hybrid system is compiled from two smaller PV plants of 5.1kW and 1.02kW (Figure 2-3). These plants exist both in the facilities of the Laboratory for Electrical Engineering and Renewable Energy Systems and have been installed at the roof top of the Faculty of Supply Engineering at the Ostfalia University of Applied Sciences in Wolfenbüttel.

Figure 2-3: The installed PV Power plants of (a) 5.1kWp Plant with 30 modules; (b) 1.02kWp Plant with 12 modules

The 1st Plant with installed power of 5.1 kW is consisting of two strings of 30 modules each. Each string consists also of two times of 15 modules in series and then in parallel connected. The module is composed of 36 monocrystalline cells from the BP company and each cell has

a maximum power (P_{max}) of 85 W. In Table 2-1 manufacturer's specifications of the installed PV modules are given. The solar panels are south oriented with a fixed angle to the ground of 30° and the plant is connected to the grid via 2 string inverters Sunny Boy 2000 from the SMA company with a nominative AC power (P_{ACnom}) of 1.8 kW. The efficiency curve of the selected inverter is depicted in Figure 2-4.

Table 2-1: Manufacturer's Specifications of installed panels

Manufacturer's Specifications	BP 585
Maximum Power (P_{max})	85W
MPP-Votlage (U_{mpp})	18.0 V
MPP-Current (l_{mpp})	4.72 A
Guaranteed Minimum Power (P_{min})	80.8 W
Short Cut Current (I_{sc})	5.0 A
Open Circuit Voltage (U_{oc})	22.1 V
Temperature Coefficient (l_{sc})	(0.065±0.015) %/°C
Temperature Coefficient (U_{oc})	-(80±10) mV/°C
Temperature Coefficient P_{max}	-(0.5±0.05) %/°C
NOCT	47±2°C

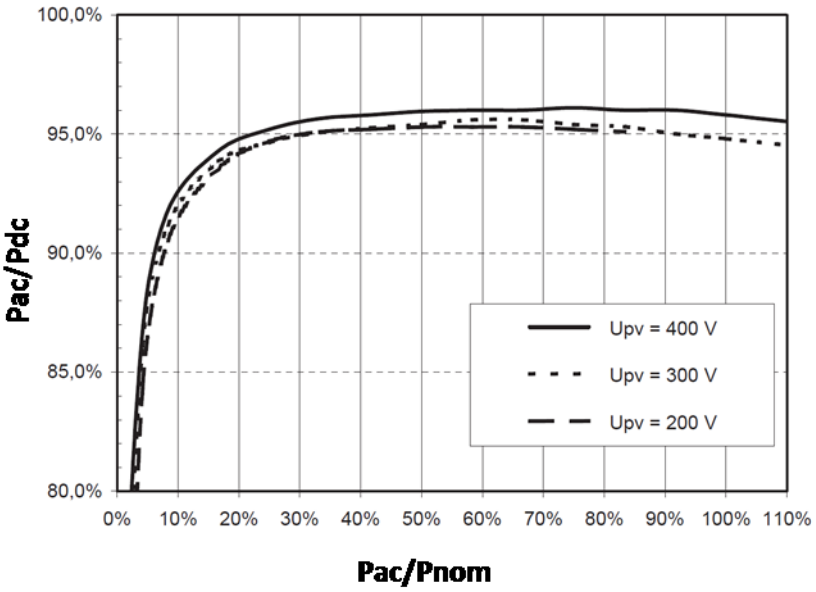

Figure 2-4: Efficiency Curve of the Sunny Boy 2000 [32]

The 2nd plant with installed power of 1.02 kW is composed of one string of 12 modules, it is also south oriented but its angle is adjustable and for every month in the year anew determined, so as during winter to benefit from the increase of the tilt angle (avoiding snow accumulation) and in summer coming to a more flat position. In Table 2-2 the respective tilt per month is illustrated. The module characteristics are the same as for the abovementioned facility and the installed cells are from the same manufacturer as these of the 1st plant and have the same attributes, presented in Table 2-1. In this case the on-site produced energy is fed into the public grid via the Inverter Sunny Boy 1200 from the SMA with a P_{ACnom} of 1.2 kW and an efficiency curve shown in Figure 2-5.

Table 2-2: Tilt Angle per Month of 1.02kWp PV Plant

Month	Tilt angle
January	70°
February	60°
March	50°
April	40°
May	30°
June	30°
July	30°
August	40°
September	50°
October	60°
November	70°
December	70°

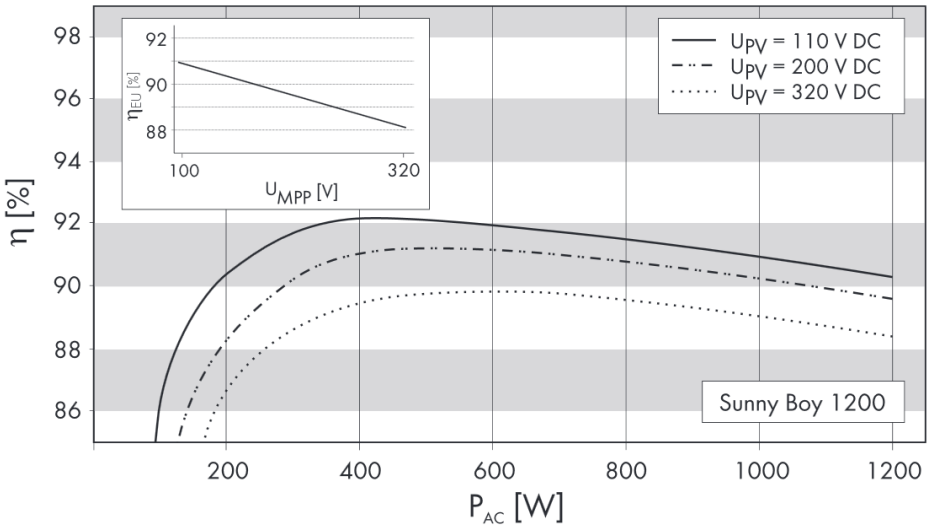

Figure 2-5: Efficiency Curve of the Sunny Boy 1200 [33]

2.2.3 Modeling of Photovoltaic Systems

There are two different approaches to model a PV cell and calculate its performance [34-36]. First as shown in Figure 2-6 a single diode model can be used to represent quite adequately the function of a PV cell with a sufficient accuracy. Other studies apply models with two or three diodes so as to take into account the effects which with the one-diode model are not considered [37-40]. This type of modeling is representing the equivalent electrical circuit of a PV cell and parameters such as series resistance R_s, shunt resistance R_{sh}, saturation current are needed in order to calculate the power output while the output power is also estimated based on the IV characteristic curves of the cell.

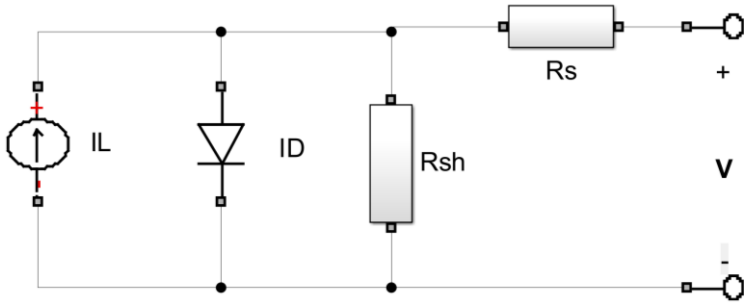

Figure 2-6: Model for PV cells with a single-diode

On the other hand, mathematical models which are mixture of empirical knowledge and physical laws can be applied to describe the cell's function [41-44]. Using manufacturer's characteristics and input data such the solar irradiance and the ambient temperature the power generation of a cell is calculated and respectively scaled for panels, arrays and plants.

The simplicity and the preciseness that characterize the mathematical model, given the available input data, make the choice of it as the most appropriate for the examined case. Subsequently, the respective PV installation was modelled and the extracted output power was estimated based on the mathematical power model from Perpiñan et al. [41] as it was considered adequately precise and easy in implementation. A detailed description of the applied model is given in Section 4.

2.3 Stationary Storage Systems

Storage systems can be divided into two extended categories based on their portability, those built for stationary applications and those intended to be used for mobile systems and/ or are portable. Although storage devices are more familiar to the public from mobile devices which are useful in their everyday life to keep them functioning, great progress has been made the last years in the development of storage systems for stationary applications in the residential, industrial or commercial sector. What differentiates the stationary storage systems from those for mobile applications is mainly their capacity, since those must cover a higher load demand.

As Luo et al. [45] report there are also various other methods to use in order to categorize the several storage techniques that exist. For example the response time, the application that are suitable for or their function, are only some of these criteria that a researcher may choose to apply to the respective clustering. Adopting the classification of Fraunhofer ISE [46] and classifying the available storage technologies according to their form of energy stored in them the following categories are identified: mechanical, electrochemical, electrical, chemical and thermal. A graphical illustration of this categorisation is in Figure 2-7 depicted. To each category various technologies are assigned.

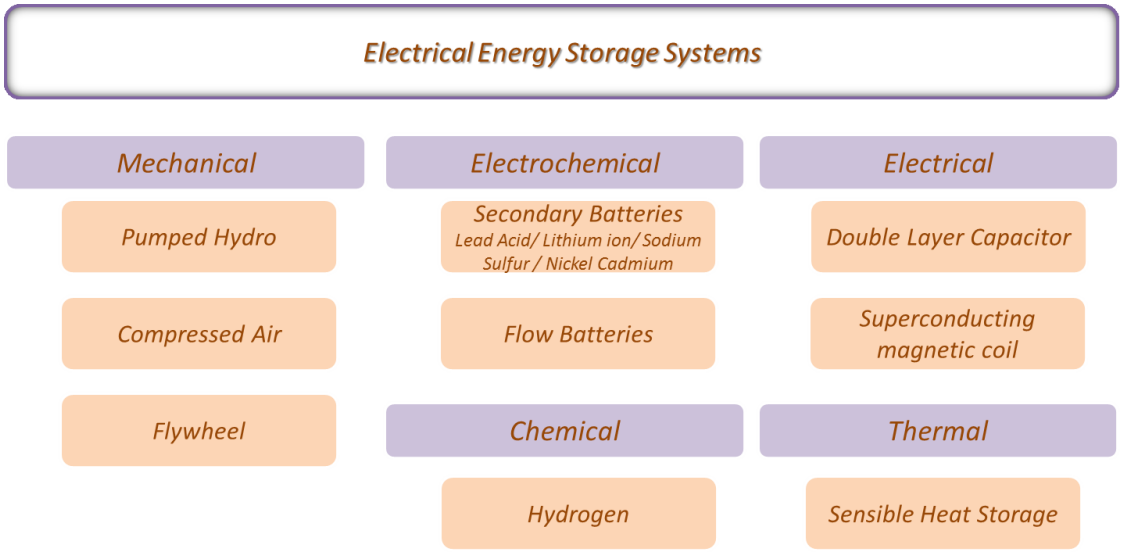

Figure 2-7: Storage Systems Classification according to type of stored energy [46]

2.3.1 State of the Art of Electrochemical Storage Systems

In case of electrochemical technologies (batteries) as the two integrated storage technologies in the examined HESS topology belong to this type of energy storage, a chemical reaction is responsible for creating a voltage difference between two electrodes and the chemical energy is thus converted to electrical. To this category as stated in the abovementioned diagram the following battery types are assigned:

- ***Lead Acid batteries*** is the most widely used rechargeable battery and is composed of two lead based plates and an electrolyte which is sulfuric acid. They are often used as back-up devices (UPS) and are characterized by low self-discharge rate, low capital cost, relatively high efficiency and fast response times. However the low energy density and low cycle life are prohibiting their expanded use. An extended description of their function and on the reactions that take place is presented in the next section.
- ***Lithium ion batteries*** have plates from lithium metal oxide and graphitic carbon, while the electrolyte usually consists of lithium salts in an organic solvent [45]. They are preferred in portable and mobile applications and they are the main component in an electric vehicle [47]. Their high gravimetric energy density [47], the high life span time and the relative high efficiency are considered the most significant advantages which advocate that they are predominant battery type the last years. Though, they still lack in capital investment as the cost is relatively higher in comparison to similar technologies. This is not only due to the fact that the technology is relative new in the market but also because they require a special control unit which protects them from deep discharging and overcharging.
- ***Sodium Sulfur (NaS) batteries*** with liquid sodium and sulphur composing the two electrodes and a solid beta alumina electrolyte, which separates the two active materials require internal high temperatures to ensure that the electrodes remain in liquid form. The high energy density and capacity and the high power rate which they can provide make them particularly attractive for high power application from

utilities or large consumers [47]. One special characteristic of this type of storage system is that the utilized materials are fully recyclable, setting their disposal as environmental friendly. The high operational and capital cost as well as the need for a heat source which is needed for operating the system are on the other hand included in the drawbacks of such systems.

- ***Nickel Cadmium (NiCd) batteries*** are considered a mature technology and have been commercially available already from the beginning of the last century. Electrodes' materials are nickel hydroxide and metallic cadmium while the electrolyte is an aqueous solution [45]. Their capability to operate efficiently under low temperatures makes them competitive in the storage market and their low maintenance cost is contributing to their employment in storage applications. However, the high toxicity of the used materials as well as the memory effect which characterizes the battery are the most important disadvantages of those systems.

Although ***flow batteries*** are characterized by similar chemical reactions as in the conventional battery systems, the storing technique of the electrolyte is the attribute that differentiates them [48]. The electrolyte is stored in external tanks and through pipes is driven to the cell stack and circulated where the voltage difference is created. Their main asset is that the power and capacity are independently scalable, thus providing a flexible dimensioning of the facility according to the needs of the respective customer. On the contrary they have a high constructional complexity and the capital cost to obtain them remains relatively high. Different configurations of flow batteries are reported with main difference in the species in the anolyte and catholyte. Main types are the vanadium redox flow (which have the same species but different oxidation states) and the hybrid ones [49].

In Table 2-3 the main features of the abovementioned technologies are summarized and an overview of their technical and economic features is concise presented:

Table 2-3: Characteristics of Battery Systems

	Energy density (Wh/L)	Efficiency	Cycles	Cost per kW	Cost per kWh
Lead Acid	50–80 [50], 50–90 [51]	75 %-90 % [52]	500-2,000 [53]	950-5,800 $ [52]	350-3,800 $ [52]
Lithium ion	200–500 [50], 200–400 [46], 150 [51]	70 %-95 % [54]	Ca. 3,000 [54]	200-4,140 € [54]	200–1,000 € [54]
Sodium Sulfur	150–250 [50], 150–300 [46]	70 %–90 % [54]	Ca. 3,300 [54]	1000–3,000 € [54]	210-500 € [54]
Nickel Cadmium	60–150 [50], 15–80 [46], 80 [51]	72–78% [45]	1500-3,000 [55] 2000-2,500 [50]	400-2,400 $ [55] 500-1,500 $ [50]	800-1,500 $ [50]
Flow	16–33 [50], 25–35 [49]	65%-75% [52]	>10,000 [52]	3,000-3,700 $ [52]	620-830 $ [52]

2.3.2 Lead Acid Battery

Lead acid batteries are perhaps the most common rechargeable battery technology nowadays and they are considered a benchmark in the storage market. There are characterized from low capital costs, easy maintenance and a sufficiently good efficiency.

However their short life cycle due to accumulative deposition of lead sulphate on the electrodes and their limited energy density has forced the market in research and development of other storage technologies which could replace it [56]. Nevertheless, it remains dominant in the storage market although various other types have been commercial and technological mature.

The electrical energy for such a battery type is stored chemically and is converted into electrical energy in a chemical reaction. The transition from electrical to chemical energy and vice versa occurs after a reversible redox reaction. The reaction equations which occur during discharge, are shown below [57].

When the battery is fully charged, the positive plate is composed from lead dioxide, the negative plate from lead and the electrolyte is sulfuric acid. When it is fully discharged both plates are composed of lead sulfate ($PbSO_4$), while the electrolyte has been primarily converted into water.

Oxidation (Anode/Negative Pole):

$$Pb(s) + HSO_4^{2-}(aq) \xrightarrow[discharge]{} PbSO_4(s) + H^+(aq) + 2\,e^- \quad | -0.36\,V \tag{2-1}$$

Reduction (Cathode/Positive Pole):

$$PbO_2(s) + HSO_4^{2-}(aq) + 3\,H^+(aq) + 2\,e^- \xrightarrow[discharge]{} PbSO_4(s) + 2\,H_2O(l) \quad | +1.68\,V \tag{2-2}$$

Total Reaction

$$Pb(s) + PbO_2(s) + 2\,H^+(aq) + 2HSO_4(aq) \xrightarrow[discharge]{} 2\,PbSO_4(s) + 2\,H_2O(l) \quad | +2.04\,V \tag{2-3}$$

From the electrochemical series of voltages, the reduction and oxidation potentials and thus the potential difference (= electrical voltage) can be obtained from:

$$\Delta E^0_{Ges} = 1.68\,V - (-0.36\,V) = 2.04\,V \tag{2-4}$$

This voltage is applied to the electrodes of the battery during the chemical reaction, being influenced by the following circumstances [58]:

- Current charge level of the battery;
- Charge / discharge current related to capacity (current rate);
- Ambient temperature;
- Age of battery.

Lead acid batteries can be clustered in different categories according to chosen criterion. In the market exist flooded, and sealed or valve regulated lead acid batteries (SLA or VRLA). Their chemical synthesis remains in both cases the same, though their main differences are identified in their design. Specifically, SLA or VRLA batteries are so constructed that do not

need topping up of electrolyte, they do not require regular ventilation of produced hydrogen and they are in total low-maintenance systems, in contrast to flooded batteries which need all the above mentioned services to operate optimally [59-60].

Moreover SLA or VRLA batteries are classified in wet, gel and absorbed glass mat (AGM) type. Wet type batteries are normally characterized from low cycle life but also low price. AGM and gel type differ from each other in the storage composition of the electrolyte. Usually AGM are less durable in deep discharge and have a shorter cycle life than gel type [60].

One last categorization is between deep cycle and shallow cycle lead acid batteries. As their name indicates the first may be deeply discharged without damaging the battery, though being able to provide lower rate but for longer time period. The second type is preferred in automotive field for starting engines and ignition purposes producing higher currents in shorter time.

2.3.2.1 Description of the on-site Lead Acid Battery

The battery system to be integrated in the HESS belongs to the renewable energy park of the Ostfalia University of Applied Sciences in Wolfenbüttel. Theoretically, it could serve as an electrical buffer storage system, which will shave load peaks and store excess energy. In practice, however, it is used only for experimental purposes and is charged from renewable energy generators (photovoltaic systems, wind turbine, combined heat and power plant) and from public grid [58].

This solar lead acid gel battery is composed of blocks from HOPPECKE, with a deeper discharging capability and technological maturity to charge with low current levels. The electrolyte between the plates is in gel form avoiding the gassing effect and leading to lower maintenance costs.

The system consists of 16 interconnected 6V lead-gel battery blocks with a single capacity of 229 Ah at a 10-hour discharge rate (C_{10}). In this case, always eight batteries are connected in series (two rows) so that the total battery voltage is U_N = 8 x 6 V = 48 V. The charge rate C (in Ah) is increased by the parallel circuit so that the two rows lead to a total nominal capacity of C_N = 2 x 229 Ah = 458 Ah. With the nominal voltage of U_{nom} = 48 V, the storable energy of the battery system is:

$$E_{el} = 458Ah \times 48V = 21.98\ kWh \qquad \textbf{(2-5)}$$

Since the energy park is constructed on a three-phase AC topology, the battery system is connected to the energy park via three bidirectional inverters SUNNY BACKUP 5000 with an Automatic Switchbox from SMA (Figure 2-8), so that the current is inverted in direct form when battery is being charged and back into three-phase alternating current which can be fed to cover the load demand when it is being discharged [58].

The charging process of the battery is controlled from the inverters starting with a constant current charge (Constant Current Mode) and going into a constant voltage charge (Constant

Voltage Mode) after the charging end voltage is reached. After a fixed time period, the charging voltage is abruptly reduced to a lower value (Float Phase). Finally, the charge state is set to 100% when the predefined time lapse is completed [58, 61] (Figure 2-9).

The discharging process is on the contrary not controlled; in each time step the required current is supplied as long as physical and constructional threshold limits of the system are not exceeded.

Figure 2-8: Lead Acid Battery with Sunny Backup System 5000

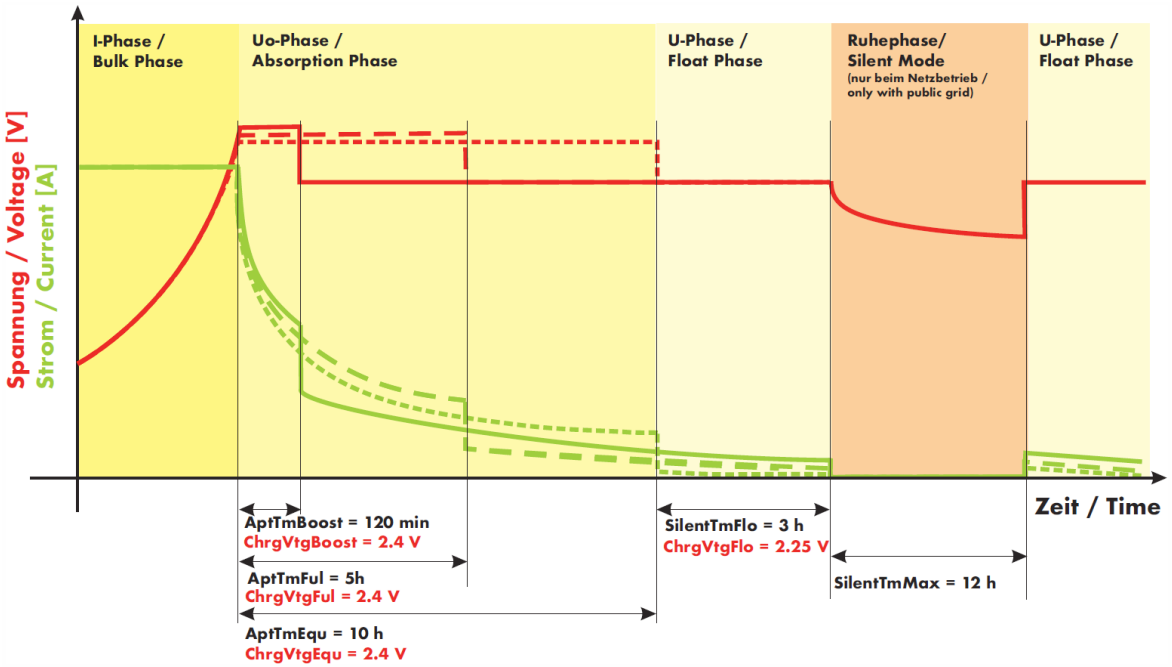

Figure 2-9: Charge Control of the Sunny Backup 5000 [61]

The presented battery type used here is offered by the manufacturer as an uninterruptible power supply (UPS) which is continuously connected to the power supply and is only rarely discharged. In the present arrangement, the batteries are not connected to any real loads and therefore serve as laboratory test facility without real utility as UPS [58].

2.3.2.2 Modeling of Lead Acid Battery System

Battery models fall into different categories which include mathematical, electrochemical, thermal and electrical models [62]. So as to describe the different processes inside a battery various models have been developed which can be represented with equivalent circuit diagrams. This type of models use simple components such as resistors, capacitances and voltage sources so as to build the respective electrical behavior that matches the respective battery. The more components (RC elements) the circuit diagram includes the more precise it is; though it lacks in computational speed, and vice versa [58]. When adding further parallel-connected components self-discharge effects or other capacitances are taken into account. In general, it is important to consider how important a high accuracy is, since each additional calculation requires further computation time [58]. In Figure 2-10 a generalized equivalent circuit diagram with n different RC parallel elements is depicted:

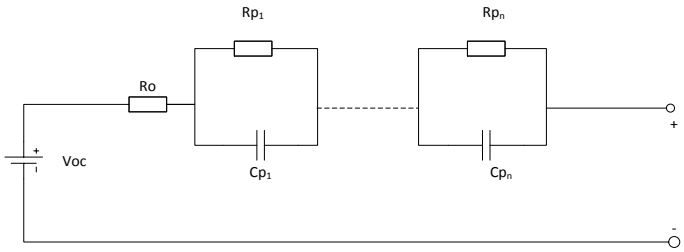

Figure 2-10: Equivalent Circuit Model for Battery

In the literature three of the most commonly applied battery models are the Resistive Thevenin model, the Thevenin and the Linear Model [63-64] and belong to the equivalent circuit-based models (Figure 2-11). The resistive Thevenin model [65-66] consists of an ideal voltage source and an internal resistance. The Thevenin model [67] has additionally an RC element, so as to take into account the delay effect caused by the capacitance of the parallel plates. Finally the Linear Model [68] has an additional parallel connected resistor which considers the self-discharge of the battery.

It is important in the frame of this thesis to develop/ integrate models that simulate the performance of the existing facilities as best as possible, without neglecting the generalization factor that has to be maintained. Trying to strike a balance between accuracy and computational speed, it was thus decided to apply the Linear model to simulate the performance of the existing lead acid battery, since it is considered the most complete (the self-discharge factor is taken into account) without demanding extremely high measuring effort to parametrize it. Its equivalent circuit model was interpreted into a mathematical model and the respective parameters were defined after a series of experiments. However, it is to be noted that although in the abovementioned models the resistances are assumed to be constant, in the designed model the battery conditions were affecting their value. In addition due to the fact that different phenomena take place during the charge and discharge process the equivalent circuit model was designed, so as to choose in each case the respective resistance. Finally temperature effects are not considered as the battery is kept in a room and great variations are not noticed. For this reason a non-linear model was excluded from this review.

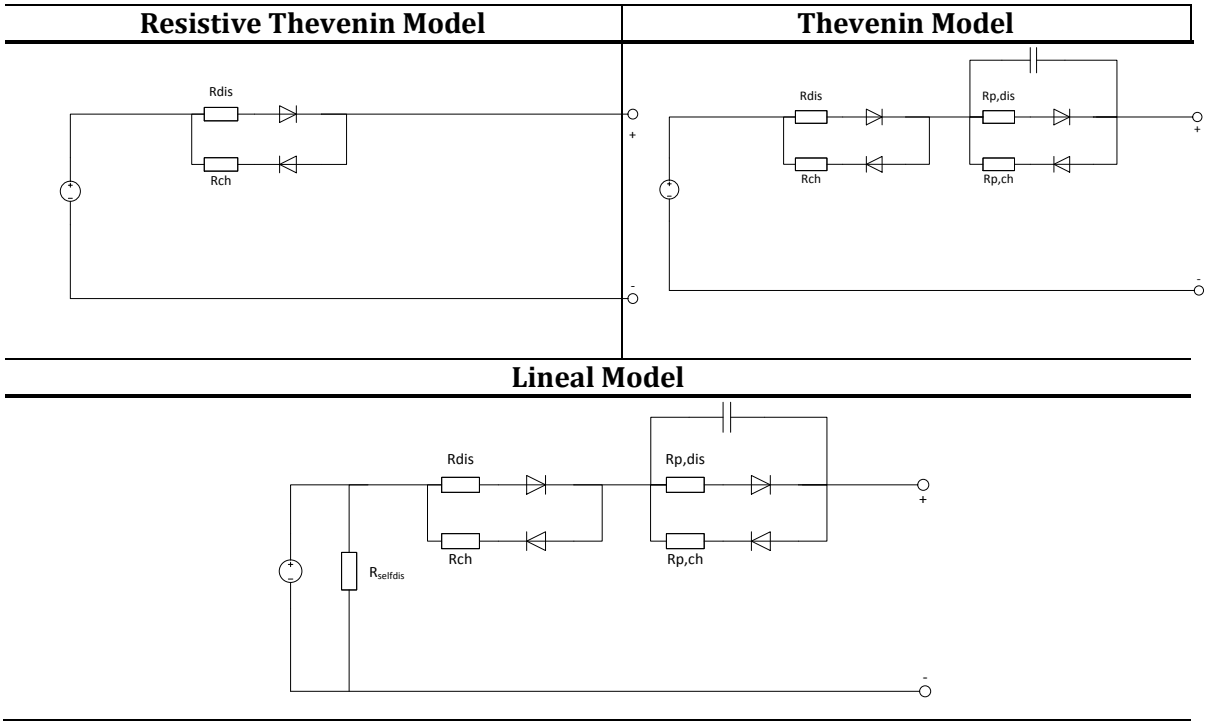

Figure 2-11: Graphical Representation of the Equivalent Circuit Models

The diodes in the above graphical representation serve for modeling purposes and have no physical meaning in the battery. They are in parallel connected, so that only one diode is forward biased during the charging or discharging process, and accordingly current flows only through one resistor. This increases the accuracy of the model compared to a simple internal resistance, since it becomes possible to consider different losses for charging and discharging [58].

2.3.3 Vanadium Redox Flow Battery

Flow batteries are considered as one of the electrochemical storage technologies with the highest capital costs. Though due to their extended life span end up to have a lower cost per kWh than the lead acid batteries [69]. Another advantage of these batteries is that the power and capacity can be independently scaled and so as to meet the required demand. In particular, the size of the tanks and therefore the quantity of the electrolyte is defining the amount of energy that can be drawn while the size of the cell stack is component which differentiates the power. It is more than clear nowadays that a storage technology which can be at will scaled up is required in the energy market for domestic or industrial use [70]. Among the advantages of the vanadium redox flow battery is also the fact that the two types of electrolyte are not incompatible and there is no concern for contamination of the two solutions [49].

This type of battery is composed of one cell stack where the chemical reaction takes place and two external tanks with two different electrolytes. The electrodes are contained in the cell stack and charging and discharging is accomplished after the oxidation/ reduction reaction of vanadium [60]. The circulation of the electrolyte through the cell stack happens by the electro-pumps which pass the electrolyte from the external tank into the cell stack in

order the two types of electrolyte to mix and react. In particular the chemical reactions that take place are described by the following equations [71]:

$$VO_2^+ + 2H^+ + e^- \rightleftarrows VO^{2+} + H_2O \quad \textbf{(2-6)}$$

$$V^{2+} \rightleftarrows V^{3+} + e^- \quad \textbf{(2-7)}$$

Total Reaction

$$V^{2+} + VO_2^+ + 2H^+ \rightleftarrows VO^{2+} + V^{3+} + H_2O \quad \textbf{(2-8)}$$

The change in oxidation state that takes place on both sides of the membrane is the incident that causes the charge or discharge of the battery [49]. It should also be stated out that electrodes do not corrode during charge/ discharge process if the battery is under ambient temperature [18].

2.3.3.1 Description of the on-site Vanadium Redox Flow Battery

In the beginning of 2012 a Vanadium Redox Flow battery of 5kW/20 kWh from Prudent Energy (Figure 2-12) was installed and integrated in the Renewable Energy Park of the Ostfalia University. It is composed of the cell stack and the two tanks which contain the electrolyte. The cell stack in this case is composed of 36 cells in series connected [18]. The same cells are however hydraulically connected in parallel [18]. The installed battery controller is actually monitoring the charge and discharge process. Depending on the applied DC power the electric pumps are speeding up or slowdown in pumping the electrolyte and the respective energy is stored or drawn from the battery. Although vanadium batteries are mainly preferred for large customers, decentralized systems or for supporting grid needs as back-up systems, in small unit sizes (kW range) they can also serve as stationary storage systems for residential purposes. Via two bidirectional Sunny Island inverters of 5kW from SMA the relevant power is converted in AC form during discharge and vice versa.

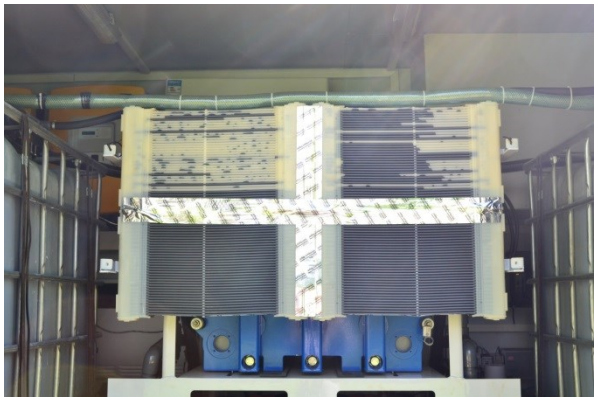

Figure 2-12: Vanadium Redox Flow Battery coupled at the Energy Park at the Ostfalia University

According to Baumann [18] it was found out after various experimental tests that this specific battery has an optimal SOC and therefore a useable SOC range between 33% and 74% which corresponds to an open circuit voltage of 1.362 V and 1.481 V respectively.

Instead of the overall documented opinion that these types of batteries are able to be fully discharged without damaging internal components, this does not represent the reality. By high SOC values a higher oxidation rate is accomplished in the internal components causing gradual performance deterioration [72]. Moreover in low SOC fields the peripheral losses are enormous, setting its further discharging unbeneficial. For these reasons the battery operates in this case study always between the abovementioned SOC scale.

As indicated from the schematic illustration in Figure 2-13 the battery system is divided into two areas, the main and the communication part. The first refers to the part where energy is converted from chemical to electrical form and vice versa and the second to the intermediate stage (MODBUS Remote Terminal Unit (RTU)) between the user or grid and the battery. The WAGO Programmable Logic Controller (PLC) undertakes the direct communication with the battery controller while the energy management block is actually the communication coupling of the system with the rest of the Park. The data acquisition for further processing is succeeded via an Ethernet connection and via the LabVIEW program. In Figure 2-13 a schematic approach of the installed system is illustrated, including also the peripheral elements, important for the coupling to the existing local grid. These include the inverters and the modules which constitute the energy management of the device and through which the communication with the external "world".

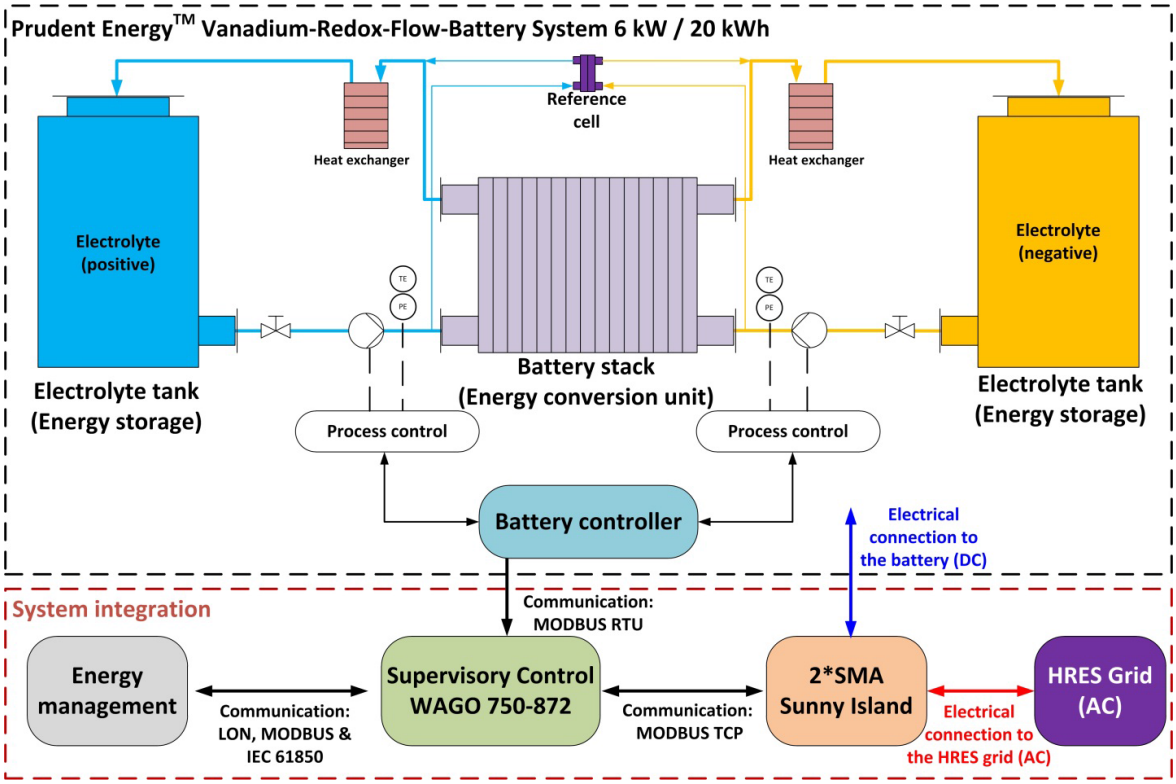

Figure 2-13: Schematic illustration of the installed Vanadium System with its auxiliary components [18]

2.3.3.2 Modeling of the Vanadium Redox Flow Battery System

Although vanadium battery systems are quite newly introduced in the market, in literature exist already various models which simulate the behavior of such systems. In particular, Clausen et al. [73] have developed a mathematical model to describe the electrochemical

reactions that take place in a vanadium battery. However, the developed model did not take into account physical phenomena that take place, similarly implemented from Shah et at. in [74]. Moreover, studies such as the one from Ma et al. [75] focus on modeling one cell behavior and not on an overall system. The proposed model from Li and Hikihara [76] is concentrating on the transient behavior of a vanadium redox flow battery, though arising time delays are not counted.

The model decided to be adopted and integrated in the overall system considers internal losses from the Balance-Of-Plant (BOP) and coulombic losses, and is developed and parametrized from Baumann [18]. Another attribute of the used electrical model is that incorporates the startup and standby behavior of the vanadium redox flow battery. The performance and efficiency, mainly due to internal losses vary from operating mode, thus it was considered significant to integrate these two states to the developed model. Finally the model was validated based on experimental data from the on-site vanadium system, verifying its appropriateness for such a system class.

In Figure 2-14 the equivalent electrical circuit model is depicted, including also the representation of all the important components and sizes. A detailed explanation of the referred sizes is given in Section 4.

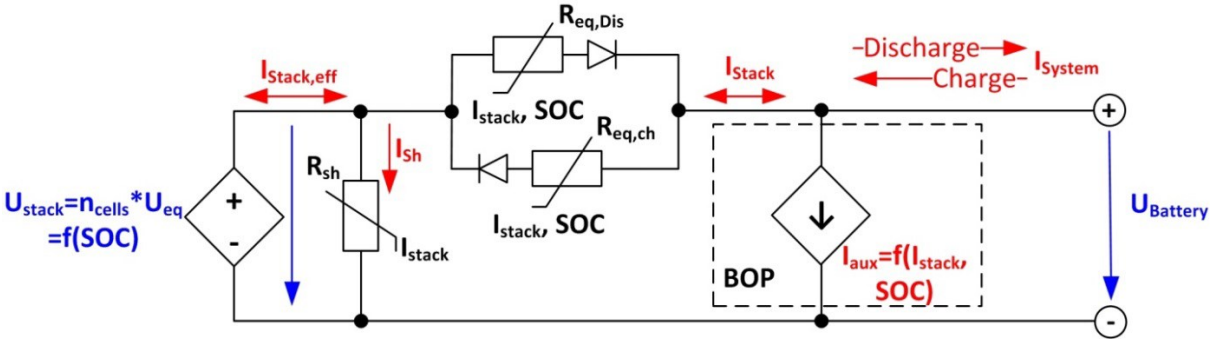

Figure 2-14: Equivalent Electrical Model of the Vanadium Redox Flow Battery [18]

2.4 Residential Load Demand including E-Vehicle Charging

So as to test the abovementioned facilities and investigate the optimal way to discharge the available battery systems, load profiles are needed to imitate the load demand of a residence with an E-Vehicle. In the next sections a literature review is conducted, including the state of the art of the existing load profiles for dwellings and E-Vehicles while the most appropriate modeling solution for the examined case study is advocated.

2.4.1 Residential Load Demand

House Load Demand Trend

According to a study from BDEW [77] the private households are considered the second greater electricity consumer after the industrial sector. Almost one-third of the overall

electricity consumption is allocated to residential sector and it is thus considered particularly crucial the energy management in this segment. However electricity consumption in Germany for residential sector shows since 2006 a slight downward tendency as it is depicted on Figure 2-15. The introduction of the renewable energy sources and the awareness around the climate change have obviously contributed towards this direction. On the other hand, the increase of the households with up to 2 residents is still keeping the consumption to these levels.

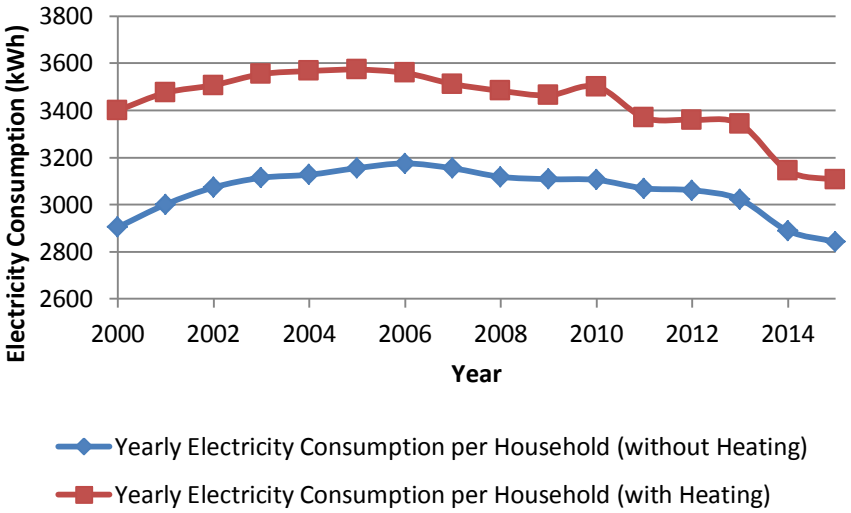

Figure 2-15: Yearly Electricity Consumption per Household with & without Heating [78]

Lifestyle aspects, socio-demographic factors, user practices and efficient appliances are some parameters which affect the house load demand and a better and deeper understanding and examination allows the more precise estimation of it. Moreover the inauguration of new technological trends, such as the integration of the E-Vehicle load demand is another issue which recalibrates the existing electricity consumption in households. In addition, modern techniques of demand side management and load shifting are also defining a new era in the configuration of the load profiles that refer to the residential sector.

2.4.1.1 Modeling of the Load Demand of a Residence

Since at the premises of the faculty a real test bed with home appliances does not exist, so as to register and utilize it for discharge purposes, house load profiles had to be created based on literature data and studies. Defining an ideal or optimal house load profile is from etymological terms wrong formulated and from practical point of view impossible. The forecasting of the exact consumption of a residence or the adoption of synthesized or even real house load profiles of a day does not guarantee that the power consumption will have the exact same fluctuations in the next days. However, several studies already exist and in their context load profile models were developed. In the following paragraphs a indicative review of three categories of the most applied load prediction techniques is conducted.

In particular, the German Association for Electricity Industry (Verband der Elektrizitätswirtschaft e. V. (VDEW)) had conducted a report in 1999 [79] on load profile

methods that can be applied for small customers in Germany, which have a yearly energy consumption till 30,000kWh. These load profiles are also adopted from grid operators for analyzing system requirements and studying grid expansion. With the H0 profile all load profiles for households are described and comprise the following sub-profiles: the load demand for winter, summer and transition days and for working days, Saturdays and Sundays. These are formed on quarter power values from the three daytime periods and the three time zones. They are regarded as standard load profiles and can be adopted in any case if the consideration of load peaks during the day is not important in the examined study case.

The study from Richardson et al. [80] is focusing on the development of a pattern of electricity use in one-family house, taking into account the individual activities and the physical presence of the dwellers. In its framework and via a software platform the user can choose which appliances are operating. Based on the selected house occupancy the appliances' operation is configured and then one-minute electricity load profiles are generated. Although this tool is offering great flexibility, it is difficult to extract a generalized profile. Moreover, the validation of the platform was based on data stemming from dwellings in UK, which by nature defer from respective ones registered in Germany.

In the frame of this thesis the adopted load profiles were eventually developed according to the VDI 4655 guideline [81]. This guideline is intended to be used in order to create reference load profiles for single-family and multi-family houses for the use of CHP systems, but it can be used in any other case where the electricity load demand is required. The load curve comprises electrical energy and energy for domestic-hot-water heating. The generated profiles are with one-minute resolution and refer to three different year periods, two types of day and two types of typical-day category. Moreover, the climate zone of the referenced building as well as the occupancy of the residence is also affecting the extracted load profiles. This systematic technique to create reference house load profiles is more appropriate for integration to the examined system, since it is focusing on the German electricity demand, it takes into account various parameters that may affect the extracted profiles and offers a sufficient time resolution.

2.4.2 E-Vehicle Load Demand

E-Vehicles are considered an environmental friendly solution to the conventional internal combustion engine vehicles if the electric energy used to charge the battery vehicles from renewable energy sources. Nowadays they are an emerging trend in Germany since the strategy to establish one million cars in the German streets till 2020 and 6 million till 2030 has been announced from the German government. In addition a law which came into force in 2015 is giving additional privileges to e-vehicle owners and further promoting electromobility in the country [82].

The capacity of storing devices in the E-vehicles has been improved drastically since a great importance is attached to research and development in the specific sector. During the last years battery capacities have reached levels of 90kWh and allowed travelling ranges till 500 km, making the electromobility friendlier to user and diminishing steadily the consumer 'range anxiety'.

The different options to charge an e-vehicle are:

- With a single-phase home outlet with 230 V und a max. current of 16 A (3.7 kW) [83];
- With a three-phase home outlet with 400 V und a max. current of 16 A (11 kW) [49];
- Fast charging (from 20% to 80% capacity in 20 - 30 min) reaching today power rates till 150 kW [84].

In addition techniques such as inductive charge or battery changing station also included in the charging alternatives for an electric vehicle but are not yet widely spread and applied, mainly due to immature technology.

Referring to the available charging techniques which exist in the literature, the following ones are those who dominate: the uncontrolled charging, the application of external charging techniques and the individualized charging strategies [85]. In particular, during the uncontrolled charging the electric vehicle may charge as long as it is connected to an outlet. The external charging techniques are usually applied by an aggregator who decides based on specific input parameters the optimal way to charge the vehicle. Finally, the user may also adjust the start and end time of charging prompted from personal incentives. This is the individualized charging strategy. It should be stressed out that the abovementioned charging patterns refer to unidirectional charging (Grid-to-Vehicle).

2.4.2.1 Description of the On-Site E-Vehicle & Charging Station

For the examined case a Peugeot iOn with its 14.4 kWh Lithium iOn Battery is the e-vehicle integrated to the overall hybrid system (Figure 2-16). Moreover via a charging point for electric vehicles, which is equipped with a WAGO charge controller, the EV battery can be charged either via a single-phase connection or via a Type 2 power plug with a step 3-phase current mode of 6/10/16 or 32 A. The charging station is integrated in the Energy Park and over a PLC program the charge process can be controlled given the availability of instant on-site produced renewable energy.

Figure 2-16: EV Peugeot iOn with Charging Station

2.4.2.2 Modeling of E-Vehicle Load Demand

Based on the three charging patterns previously described (Section 2.4.2), various charging modes have been designed and developed. Indicatively, Darabi et al. [86] used transportation data to produce charging load curves based on American driving profiles. Fernández et al. examine the penetration of EV in an urban area with regard to the expansion of the local distribution network while Lee et al. focus on creating probabilistic driving cycles for estimating the impact of the charging process on the grid [87-88]. Westermann et al. have developed an averaged model which stems from measured load profiles, based on fleet data from fifty electric vehicles [89]. Due to the fact though that the consumed energy could not be correlated and subsequently predicted, a generalized model which could be used for individual trips was not feasible. Moreover great emphasis is given on the impacts of the EV load profile on the distribution grid [90-92] but the effect after the integration of the charging process of an EV on the house load profile is not widely discussed or described in the literature.

As in the current study emphasis is given on a residence in Germany and a microscopic examination is entrenched in a hybrid house installation, an analogous driving cycle should also be considered. Reports based on charging profiles from other countries can unfortunately not be utilizable since there is a differentiation in driving behavior among countries. According to the VDE Studie Elektrofahrzeuge [93] the mean daily vehicle distance travelled in Germany for a passenger car is approximately 60km. Considering this parameter as a basic variable of defining a charging profile of an EV, a naturalistic driving combined cycle of 60km was decided to be performed given that the EV was fully charged at the beginning of the trip and the charging process was registered. Although such a charging profile is considered static it has the advantage that is customized to the German driving behavior and represents the mean passenger. Based on the hypothesis that the driver always charges at home and the trip end-time is at 19:00 daily, the specific charging method can be assigned to the uncontrolled charging strategies. Finally another fact which advocated the adoption of such a charging method is the lack of time-based utility pricing (or dynamic pricing) from the German grid operators, setting an uncontrolled charging technique as favorable.

3 Hybrid Energy Storage System

In the previous chapter a thorough literature review in batteries and PV installations used in the domestic field was conducted. It is scope of this chapter to present the thematic around the hybrid energy storage system (HESS), which is actually a combination of the two different types of facilities already described. The examined HESS with its individual components will be presented and the problematic which arises is going to be analyzed. In this context the scope of this work is concretized. After a presentation of the existing HESS control methods it is justified why the Markov Decision Process (MDP) was the selected applied technique to control the given system. Finally the research questions and the challenges which were faced during the design of the optimization strategy are addressed and the limitations of scope are clarified.

3.1 Introduction to Hybrid Energy Storage System (HESS)

The rapid penetration of decentralized energy systems in the energy market during the last decade and the encouragement to increase the share of self-energy consumption have set the adoption of storing ideas as substantial in the domestic field. The deployment of one storage device to gather the surplus of the renewable energy and redirect it to the loads when a deficit in power occurs is already a standard tactic nowadays. The operation simplicity of such a system makes it particularly attractive. However, it is common knowledge that none of the existing storage techniques or battery types for domestic purposes is optimal for use under any conditions. There are systems whose technology is already mature but they still lack in other characteristics such as the degradation, the energy density or the self-discharge. On the contrary, systems with better attributes in cycle life-time and energy density may underperform in reaction time or in system efficiency. HESSs are considered optimal to give a solution to such inadequacies since they combine two (or more) different storage types and consequently they combine also the advantages of them. They are designed to take advantage from the best of two or more worlds, so as to exploit and use the positive aspects of each one of the applied stationary storage systems. The adaptation of a storage system combination is a challenging and highly promising approach from which a stand-alone installation or a grid-connected system may profit if the different storage systems are managed to be controlled in an optimal way so as to benefit from the advantages of the heterogeneous technologies.

Already discussed HESS applications in the literature include among others [94]:

- HESSs for hybrid and plug-in vehicles;
- HESSs for large scale installations;
- HESSs for stand-alone installations in remoted areas;
- HESSs for grid connected systems targeting to lower interaction with the Electrical Power Distribution System.

3.2 Description of In-Situ HESS

In the framework of this thesis a HESS, which constitutes a partial configuration of the described Energy Park (Figure 2-1), is studied and different case studies are examined. Its individual parts and their attributes are analytically reported in Section 2 whereas a graphical illustration of the examined system (Figure 3-1) and a comprehensive overview are following below:

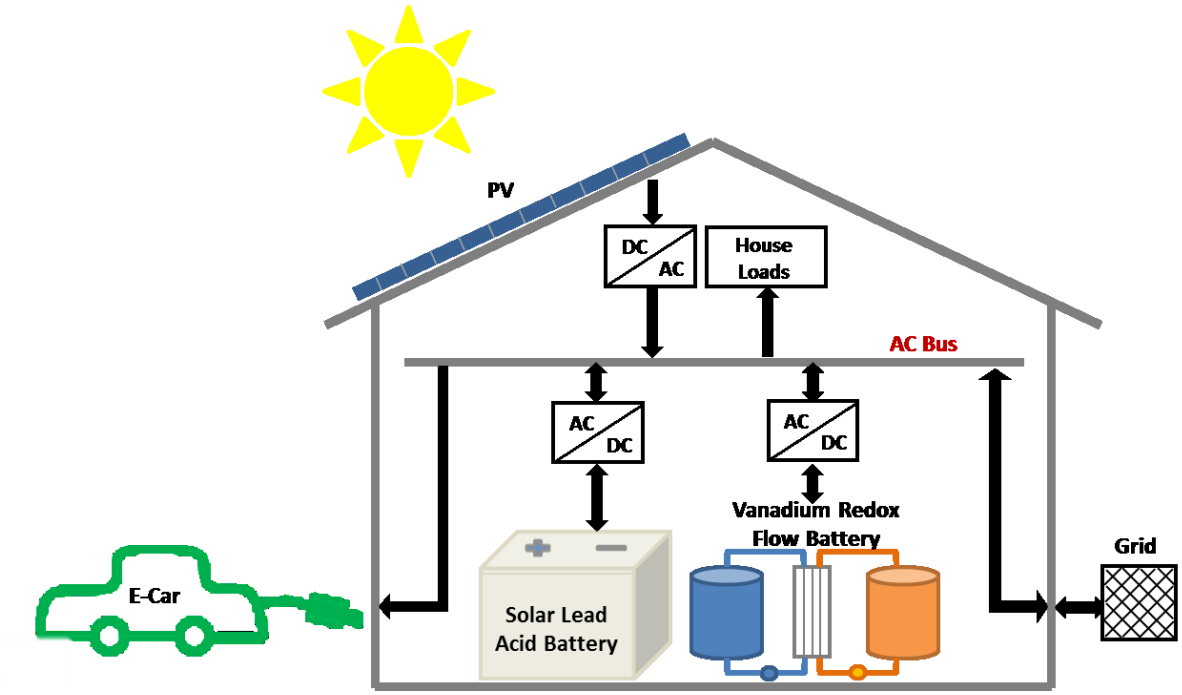

Figure 3-1: Hybrid System Synthesis

In particular, the under examination HESS consists of the following facilities/ components:

- **Two PV installations of 5.1 and 1.02 kWp power.** The two PV plants constitute the renewable energy source of the system. The 1st Plant with installed power of 5.1 kW consists of two strings of 30 modules each. Each string consists also of two times of 15 modules in series and then in parallel connected. The solar panels are south oriented with a fixed angle to the ground of 30°. The plant is connected to the grid via 2 string inverters Sunny Boy 2000 from the SMA company. The 2nd plant with installed power of 1.02 kW is composed of one string of 12 modules, it is also south oriented but its angle is adjustable and for every month in the year new determined, so as to benefit from the increase of the tilt angle during the winter avoiding the snow accumulation, and from the flat position in summer months. In this case the on-site produced energy is fed into the public grid via the Inverter Sunny Boy 1200 from the SMA [23].
- **A Solar Lead Acid Battery (SLAB) from HOPPECKE.** The SLAB has a total C_{10} capacity of 458 Ah. The system consists of two strings of 8 blocks each and each block is composed of 3 cells in series. With a nominal voltage of 48 V the storable energy amounts to roughly 22 kWh. The battery is connected to the energy park through three bidirectional inverters and in comparison to usual lead acid batteries this one is characterized from a particularly long life and shows a better behavior at lower discharge rates [58].

- **A vanadium redox-flow-battery (VRB) system from Prudent Energy™.** The VRB has a storable electric energy of approximately 20 kWh. The liquid electrolyte of sulphuric acid solution, which amounts to 1,800l, is stored in two tanks and contains vanadium at different oxidation states. During charging or discharging process the liquid is pumped to the cell stack, which is composed of 36 single cells, that are electrically connected in series with nominal voltage equal to 48 V and maximal current of 130 A and the cell stack is converting chemical energy to electrical and vice versa [18].
- **A yearly domestic electric load for a notional single-family house in region of** North-West Germany **with four occupants.** So as to create a yearly reference load profile for a single family house with four occupants in a region which belongs to the "North-West German Lowlands" climate zone the guideline VDI 4655 [81] was taken into account. Registered data from net meters could also be retrieved and utilised though it was assessed that the proximity to real data would be at the expense of the generalisation of the study and of the further exploitation of the results. So a common used procedure has been adopted in order to facilitate the redimensioning of the load demand in other cases. So as to determine these reference day load profiles the following parameters were taken into account:
  - Type of the Building;
  - Climate Zone of the Site of the Building;
  - Number of occupants.
- **The yearly load demand for charging the Lithium iOn battery of a Peugeot iOn pure electric vehicle.** The Lithium iOn battery has a capacity of 14.4kWh and can be charged with 10A, 13A or 16A current in flex charge mode and a voltage of 220/230V or 330V when charging in fast mode. To estimate this daily load it was claimed that the mean vehicle distance travelled each day for a passenger car in Germany is 60 km [93]. With a fully charged EV and after a real driving combined cycle of 60 km the charging process of a 14.4 kWh Lithium iOn Battery from the Peugeot iOn has been registered till its battery was again full and so the yearly load demand of the E-car was created and aggregated to the yearly domestic electric load, assuming that the E-vehicle charges always at home.

In the composed scenario the PV plants are considered the energy sources of the system supported whenever required also by the local grid supply. The vanadium redox flow battery and the lead acid battery will constitute the stationary storage systems and will be appropriately utilized to store renewable energy and feed it back to the household whenever it is required. Finally the electric vehicle and in particular the battery of it as well as domestic load profiles form the consumer's behaviour.

3.3 Problem Description & Scope of this Work

Given the abovementioned concept and under the generalized context of energy management of HESSs in the next sections the overall problem will be defined, the examined approach will be analyzed, while the boundary conditions and the argumentation round the selected technique to be applied will be addressed.

3.3.1 Overall Problem

All HESSs, no matter which topology is deployed, need an additional management system, which will undertake their control and apply them in a rational sequence with ultimate goal to increase the total efficiency of the system. Why at all is it such a system necessary? There are two cases of power allocation that can be applied: either the storage systems share the amount of power demanded or fed to them, or at each moment only one of them is prioritized against the other and they operate exclusively interchangeably. In both described cases it is though substantial to define the external actor which decides in the first case which proportion of power is ought to be allocated to each facility, and in the second case which storage system has at the current moment higher priority and should operate as stand-alone device at this time (i.e. without the support of the other storage facility).

As mentioned in Section 3.1, HESSs are optimally featured with complementary characteristics and the target of coupling them is to benefit from the strengths of each one. In a fictional application were two different storage systems are operating alternately the selection of the most appropriate technique to control the facilities is considered a crucial matter. Incongruous methods may lead to unadvantageous employment of the storage systems, resulting in an unprofitable usage of a HESS. Given the specific initial and boundary conditions and assumptions and the respective selected storage systems which form the HESS one method outperforms the other or one technique delivers better exploitation of their attributes. The dynamic energy storage control is responsible for the coordination of the HESS and the power distribution between the two facilities. Charge and discharge allocation is undertaken from the control system and the optimal operation solution is defined.

Referring to the architecture of the HESSs, different types of topologies can be applied to interlink the storage systems with the rest of the facilities. Direct coupling of the devices with a single DC converter is a favorable architecture from financial and implementation aspect; though the constraints in controlling the energy flow make it ineffective. A topology with a DC-DC converter for each battery and a grid-connected inverter is a better alternative, increasing the flexibility of the system. Another promising architecture is the connection of each facility with a DC-AC inverter which introduces higher degree of freedom in handling the individual components.

3.3.2 Examined Approach

Under the abovementioned context a robust energy management algorithm is to be developed in the framework of this thesis so as to operate the storage systems, already described in the Section 3.2, namely the solar lead acid battery and the vanadium redox flow battery, in the most efficient way in the overall setting consisting of the rest of the facilities.

The utilized storage systems are optimally featured with complementary characteristics and the target of coupling them is to benefit from the strengths of each one. Having a closer look to their characteristics, lead acid battery systems are characterized from intolerance at deep discharges, and short cycle life, especially when high currents occur. Though this is not the case for the VRB, since such types of batteries are attributed from cycle durability, being possible to deeply discharge it without damaging the system and they can be easily

dimensioned since the capacity and power are independent sizes. Simply, by enlarging the storage tanks the capacity may increase while if the stack of the battery is replaced with a more powerful one, the battery will be able to operate in higher power ranges. On the contrary lead acid battery systems are financially favorable, have a short reaction time, medium energy density and a sufficient efficiency rate, while VRBs are still considered an immature technology in comparison to the lead acid battery systems, their price remains high and their efficiency is proven to be lower than the theoretical values referred in the literature [18].

The designed hybrid system will avail itself of the combination of the two storage systems by operating them interchangeably so as to benefit in each case from the respective facility with the most efficient characteristics. It is to be noted that a power division between the two storage systems at each moment was considered insufficient for such a system scale. Moreover, in such a case the fictional agent will apply the designed controlling at AC connection level after the installed inverters and the already available management systems. A graphical depiction of this topology is depicted in Figure 3-2. Although such a technique increases the costs and losses of the entire system, it is considered optimal if a power management policy is to be applied and parameters such as voltage or frequency level don't belong to the sphere of examination.

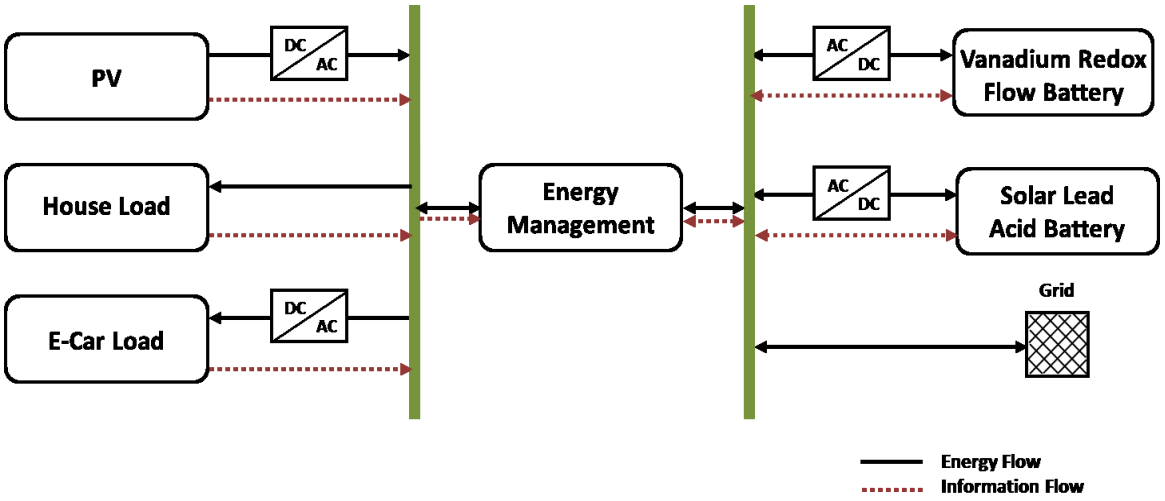

Figure 3-2: Block Diagram of the installed facilities depicting the energy & information flow

Such a topology is requiring input information from the PV installation as well as from the current loads in power level, and stand of the batteries' SOC. Subsequently, the energy management based on the given input decides which one from the storage systems should undertake the excess or demand of energy and gives the corresponding signal.

3.3.3 State of the Art of Control Management Concepts

As referred in Section 3.3.1 there is variety of techniques that can be applied to control a HESS. The criteria which are considered each time in order to design the optimal control method may vary among different applications. After a thorough and extensive literature review the most common cited techniques to control HESSs that are identified can be clustered in the following five identified categories [17, 95-102]:

- Low and High Pass Filters;
- Rule-based Algorithms;
- Linear Programming Methods;
- Reinforcement Learning Techniques;
- Hybrid Approaches.

The nature of the considered attributes of the storage systems as well as the type of evaluation criteria influence the selection of the suitable applied control method. If the reaction time is the critical decision characteristic then methods based on low- or high-pass filters are favored [98, 101]. When specific operation boundaries ought to be kept rule based algorithms are preferred [97, 101, 102] and when these boundaries and the expected requirements are represented by linear relationships linear programming methods are applied [96]. If the environment of the controller is deterministic, i.e. the employed models do not learn from the action evolution, and the degree of freedom during parametrization is also significant for the developed optimization technique, while a sequential decision-making problem is to be solved, a decision making algorithm which does not factor in the preceding states is ideal [17]. Finally hybrid methods are employed when a combination of characteristics should be taken into account [99-100].

Delving into the already reported control systems for HESSs, it is accrued that the different employed methods are not ideal for optimizing the current studied system. In particular, in Zhang et al. [97] rule-based algorithms are applied so as to manage the energy flow between a supercapacitor and a conventional battery. Parameters such as load demand and battery output current are compared with threshold values and the respective rule is applied. Takeda et al. in [101] compare the results extracted from applying two of the above-mentioned methods so as to control a HESS which is constituted from a LAB and a Lithium ion battery. The amplitude sharing algorithm, which is a rule-based approach, delivers better results in comparison to the first order filtering. Moreover, Ise et al. in [102] fuzzy control logic has been applied so as to manage the power allocation between two storage systems, namely a superconducting magnet and a secondary battery for an energy storage system with high energy and power density. This control technique, which belongs to the rule-based algorithms, has the benefit that it is based on a set of rules which are designed from experts and the most appropriate alternative is selected without requiring extreme complicated mathematical knowledge. However, the configuration is becoming extremely difficult if the system is quite complex [95]. Under the given conditions, the attribution and setting of a group of rules in advance during the design of the management method for the examined HESS is considered rather demanding and puzzling, so such a method is not preferred in the frame of this thesis.

In the literature, the most widely used technique to manage HESSs is the first-order filtering method. According to it, the high power fluctuations are allocated to one storage system, often a supercapacitor, and the rest is undertaken from a conventional battery system [98, 99]. This linear filtering is actually designed based on the response time of the two storage technologies; nonetheless various other parameters are not being considered. Filtering methods as the ones applied from Li et al. and Takeda et al. [98, 101] are regarded also unsuitable for system cases as the one described in the current study, since the response time of the storage systems is not the determinant factor for designing the present

management system. Such technique is preferable when for instance a supercapacitor is integrated in the HESS and in both previously referred cases such a device is part of the examined system.

Another HESS is also studied from Nikolai et al. [96], referring to the project on the island Pellworm of the North Sea. By exploiting all the renewable energy sources installed on it (a PV park of 700kWp and a wind farm of 300kWp) and with the support of several storage systems (mainly lithium-ion batteries and redox flow batteries) a stable and cost-effective energy supply is pursued. In this case a mixed integer linear programming method is applied for the optimization approach. While linear programming algorithms are easily comprehensive and simply applicable, though they lack in the generalization part, and therefore avoided if a global solution is claimed, as in the examined case.

Hybrid methods are recommended because they combine different techniques and they are often preferred in the literature. For instance, Abbey et al. in [100] apply a low-pass filter combined with two neural networks decide the percentage of the reference power which should be allocated to each facility. Such a technique is though unfavourable because the partitioning of the demanded energy or the surplus of the on-site generation between the existing two storage devices which constitute the examined HESS could worsen their efficiency behavior. Moreover, as already explained earlier, low pass filters do not apply in a case as the one designed here. For this reason, the combination of a rule based algorithm with a filtering technique, as the one conceptualized from Li et al. in [99], still cannot fulfill the needs addressed from this topic.

Conclusively, as it is argued in [100], it is concluded that an ideal energy management system which can be applied in any case cannot be nominated, since every application of hybrid energy storage systems is attributed from varying characteristics, which must be taken into account during the design of the control process and the optimization goal or parameter can be different in each case. However, advanced control algorithms which are optimized-based are considered as more efficient in acquiring better results. It is also to be noted, that the selection of the appropriate technique to manage the energy flow in the HESS is considered crucial when an optimized solution is sought and case specific solution is in most cases addressed.

3.3.4 Beyond the State of the Art

The designed platform under the examined concept is deterministic, because the respective models which represent the individual components of the system are validated and correspond to the real applied facilities which exist in the Hybrid Renewable Energy Park of the Ostfalia University in Wolfenbüttel. In addition, the adopted models do not include a learning process, i.e. for the same inputs values and under the same conditions the extracted output remains always the same. Finally, the ageing process of the stationary storage systems or other intermittent parameters do not intrude in the design process so as to modify the already formed environment and affect the output values. Based on these prerequisites it is decided that the optimal controlling of the existing HESSs can be accomplished using the Markov Decision Process.

MDP is considered a mathematical framework to support the decision making. The decision maker (agent) after taking into account the rewards (which are calculated each moment based on the efficiency grade and the state of charge of the two stationary storage systems) is favoring one action and subsequently one battery system against the other. The ultimate target from applying this process is to optimize the alternate modus of the storage systems by operating them under high-efficiency conditions in the long-term. Such a technique is appropriate in cases where the next time step action is exclusively dependent on the current states of the system (i.e. the SOC of the storage systems and the required/ abundant power) while the precise calculation of these variables is considered determinant for the correct design of the MDP. In this study, the use of validated and verified models guarantees the systematic approach that is chosen.

Such a method is applied to solve several energy allocation problems. Jimenez in [16] applies an MDP to succeed resource allocation and load shedding in a system consisting of a decentralized energy source, one storage system and loads. Zhou et al. in [103] conclude that an MDP applied in a system composed of a wind farm, a storage facility and a transmission line to the grid, delivers 15% better results in comparison to a Naive policy. A similar system with the one referred from Zhou et al. [103] has been studied from Murtaza and Tahir in [104], with an ultimate target to minimize the data transmission level and keep the battery energy between specified levels, though in this case renewable energy generation stems from not from wind but from PV facilities. Moreover, in the study of Xu et al. [105] the MDP is applied in a load-serving entity having as evaluation criterion the decrease of energy costs. Grillo et al. have applied a control policy, based again on the theory of MDP, though in this case the scheduling refers to a test network in medium voltage (MV) level. The authors tried not only to minimize the cost of energy but also to reduce the network losses [106].

Qiu in [17] studies a HESS in microgrid operation. It is composed of a LAB, a VRB and target of the study is to minimize the system losses, via controlling the storage devices with an MDP. Although the stationary storage systems are of the same type as the ones examined in the framework of this thesis and the applied control technique is the MDP, there are several design points and physical characteristics that differentiate substantially the abovementioned study with the current one. Specifically, for simplicity and dimensionality reasons much fewer states are selected during the design of the MDP as the ones predefined under the current study in Section 5.2. Another differentiation point is the level of accomplished generalization. In particular, although the applied method was developed for the already described HESS, scope of this work was also to design a technique that can be generalized for every other similar HESS simply by respectively parametrizing the analogous sections in the designed process, given equivalent boundary conditions. This part is however not succeeded from Qiu in [17] due to physical constraints of the storage systems. A more detailed description of this argumentation is provided in Section 5.2. Furthermore, in the discussed study a power distribution via a DC bus is the selected topology while in the examined case the components are connected over an AC bus. Last but not least, the overall target in each study is heterogeneous. In the abovementioned system losses should be ultimately minimized whereas scope of this work is to maximize the consumption of the on-site renewable energy by covering the local demand and to minimize

the power interaction between the fictional building and the grid, as described in Section 3.3.4.

Concluding from the abovementioned, the current study differentiates from other similar ones in the design and modelling of the individual devices as well as the interactions among them which depict precisely the reality. The systems are designed considering their functional specifications and no simplified version of models has been used. Moreover, all energy losses are taken into account when modelling each facility as well as when the interconnections among them were captured and represented at the design of the entire system. It is also to be noted that in many studies the coordination of the systems is undertaken from an external actor. In the framework of this thesis the management is implemented from the local controller of the decentralized platform showing that individual solutions contribute to relieve the strain of the grid from peak power and increase the self-energy consumption grade of the residence. Although as abovementioned, HESSs which are utilized to store abundant PV energy and reallocate it back to existing loads are already registered in the literature, the management of a hybrid system which consists of a VRB, which operates as a mid-term storage system and a LAB, which is considered a short-term equivalent, in combination with the fluctuating and occasionally acute load demand due to the charging process of a pure E-Vehicle has not yet been studied. In addition, VRB systems applications in the residential sector are barely mentioned in the literature [107]. In addition, in the described HESS each PV plant as well as storage device is equipped with a respective DC-AC inverter and the facilities maintain their own internal energy management system. It should be also noted that the HESS operates in grid-connected mode, so when a surplus or shortage of power occurs the grid accommodates each case.

3.3.5 Evaluation Criteria

So as to evaluate the applied technique a benchmark method was also implemented, according to which priority in charging and discharging was always given to the battery system with the higher efficiency grade on the examined time slot. This naive approach is considered a heuristic tactic and the evaluation criteria, according to which the two policies were assessed, are two energy indexes, i.e. supply cover factor and the grid interaction index which are described from the following equations [108]:

- **The Supply Cover Factor, F_{supply}:**

$$F_{supply} = \frac{\int_{\tau_1}^{\tau_2} min[P_{PV}(t) - P_{Storage}(t), P_{Load}(t)]dt}{\int_{\tau_1}^{\tau_2} P_{PV}(t) - P_{Storage}(t)dt} \quad \textbf{(3-1)}$$

- **The Grid Interaction Index, I_{grid}:**

$$I_{grid} = \sigma\left(\frac{E_{Grid\_Exchange}}{\max(|E_{Grid_{Exchange}}|)}\right) \quad \textbf{(3-2)}$$

Where: $P_{Storage}(t) = P_{Charge}(t) - P_{Discharge}(t)$, which is the storage power balance, $\tau_2 - \tau_1$: the examined time period, $E_{Grid\_Exchange} = E_{Feed} - E_{Draw}$, the Net exported energy, E_{Feed}: Energy Fed to the Grid, E_{Draw}: Energy Drawn from the Grid, $P_{PV}(t)$: PV On-Site Power Generation, $P_{Load}(t)$: Load Demand

The first index is actually the factor which describes the grade of the self-energy consumption and is given from the rate of PV energy allocated to cover local demand in an evaluation period which is defined from the time values τ_1 and τ_2. In the frame of this thesis and the storage optimization process this index is ought to be maximized. The on-site storage existence affects the result by reducing/ increasing the local power generation depending on the instant function of the batteries, i.e. if they operate as sink or source of energy in the examined time span [109]. Due to the fact that by designing the control algorithm it is assumed that the PV generation is used by priority to cover first the load demand and then the occurred difference is demanded or fed to the batteries and then the grid, it is always the load demand that has the minimum value when the production exceeds the loads. However, when the PV generation is lower than the needed amount of energy, then the power difference $P_{PV}(t) - P_{Storage}(t)$ is the term with the minimum value.

The Grid Interaction Index is depicting the fluctuation of the energy exchange between the building and the grid and the scope of this research is to minimize this factor so as also to minimize the grid stress, since great grid fluctuations lead to strain the grid tolerance. It is actually calculated as the standard deviation of the ratio of the energy exchange to the maximum value of it within an annual cycle [109].

3.4 Research Questions

In the previous sections the term of HESS has been introduced and the respective considered facility has been presented. Moreover, the problematic around the examined case was also described. From the abovementioned information the main research question of this thesis is formed as follows:

- *"How can the energy flow in a single-family house be managed efficiently, so as to maximize the self-consumption of the produced renewable energy and minimize the grid interaction by controlling two different stationary storage systems?"*

Solution Approach: After defining the overall concept and the boundary conditions of the studied case, each facility is modelled in MATLAB® / Simulink® environment and after precisely representing the interactions among the designed blocks, an energy management policy is applied, which will undertake the role of the "decision-maker" and will mandate the storage systems by triggering them when a surplus or a demand of power is occurring, according to their SOC as well as their efficiency grade and power level.

Several sub questions emanate from the main research problem, which is previously described. These are formulated as follows:

- *"Which are the appropriate models to represent the existing facilities?"*
- *"Which method is optimal to be applied in order to implement the selected energy management policy so as to control the charging and discharging process of two stationary storage systems?"*
- *"How can the chosen technique be evaluated?"*

Solution Approach: After specifying the examined environment by identifying and developing the most suitable models and after creating the charging scenario for the E-Vehicle based on literature and experimental data, a thorough literature review was conducted for evaluating the possible methods that can be applied to control the given HESS and the most appropriate was selected. Finally, a benchmark method for controlling the facilities was also provided and analyzed and the results from the two case studies were compared, based on the evaluation criteria presented in Section 3.3.4.

3.5 Limitations of Scope & Challenges

Due to the fact that the design of the control algorithm requires the exact knowledge of the remaining stored energy, it was quite challenging to model the existing facilities by applying common used techniques, which represent the physical fundamentals and principles of each facility, and simultaneously taking into account the explicit specifications of the respective module. The validation and verification of the designed models contributed towards the correct representation of them. For this reason the modelling part occupies a substantial part of the current thesis and the applied methods are discussed in detail in the following chapter (Section 4).

In addition, the randomness in the weather conditions in the central north region of Germany forms a highly fluctuating PV production profile. The intermittency of the power generation was another challenge to be faced when planning the management policy, because the great fluctuation in the current shortage or surplus of energy demanded a robust algorithm which could manage these situations. In finite state-action problems, as the one tackled in the frame of this thesis, if the system model would be running in minute-step intervals, the application of the Q-Learning algorithm to solve the MDP optimization problem would cause slow convergence to the optimal action-value function. It was thus decided to work in hour-step intervals, trying to reduce the complexity of the applied algorithm by making a compromise between accuracy and convergence. An alternative would be the application of the speedy Q-Learning algorithm as implemented from [110].

4 Hybrid Energy Storage System Modeling

So as to proceed to the development of the control algorithm for the designed HESS, as explained in the concept analysis in the previous chapter, the included facilities should be modelled in a simulation environment, which will be the test platform for testing and validating. Target of this Section is not to provide pioneer or novel methods for modeling systems such as storage facilities, photovoltaic modules or load demand for dwellings and E-Vehicles, rather than utilize existing physical models that are appropriate and suitable for application in this case study and adapt them as well as parametrize these in order to fit to the respective system. In particular, in the next sections a thorough description of the physical rules that are applied to the Simulink models is reported and whenever possible the validation results are also presented. The individual developed models are graphically reported in Annex 1 for reasons of clarity.

4.1 Photovoltaic Model

As it is concluded from Section 2 a mathematical model is adequately accurate and appropriate to be applied for the simulation of on-site PV application. So as to calculate the output DC power delivered from a solar module the study of Perpiñan, Lorenzo and Castro [41] was used and the designed model was based on the Carnot Toolbox Source ("CARNOT - Conventional And Reneawable eNergy systems Optimization Toolbox"), which is an open source toolbox developed by the Solar Institute in Jülich [111] and on the master thesis of Riccardo D'Agostino [112]. According to it the DC output power of one module is analogous to the radiation that hits the panels and the nominal power of the modules and is also related to the temperature which is developed on their surface. Mathematically it is described from the following equation:

$$P_{DC}=\eta_{ext\ losses}\cdot\left\{P_{peak}\cdot\left(\frac{G_{eff}}{G^{*}}\right)\cdot\left[1-\beta\left(T_{c}-T_{C}^{*}\right)\right]\right\} \quad \textbf{(4-1)}$$

where:

- $\eta_{ext\ losses}$ are losses for modules mismatching, diodes and dirt (9%);
- P_{peak} is the rated power of one module (W);
- G_{eff} is the effective global radiation (W/m²);
- G^{*} is the radiation in standard conditions (1,000W/m²);
- β is the temperature losses coefficient (0.005/°C);
- T_C is the operation cell temperature;
- T_C^{*} is the standard operation cell temperature (25°C).

The operation temperature T_c is calculated as follows:

$$T_c = T_{amb} + (NOCT - T_{NOCT,std}) \cdot \left(\frac{G_{eff}}{G_{NOCT}}\right) \quad \textbf{(4-2)}$$

where:

- T_{amb} is the ambient temperature (°C);
- $NOCT$ is the nominal operation cell temperature (47°C);
- $T_{NOCT,std}$ is the ambient temperature at $NOCT$ conditions (20°C);
- G_{NOCT} is the radiation at $NOCT$ conditions (800W/m²).

So as to calculate the AC output of the plants the inverters were also modeled as Lookup Tables in Matlab/ Simulink based on the characteristic curves of the manufacturer SMA.

According to the sun theory the global radiation is formed from three different components, namely the direct, the diffuse and the reflected part of radiation as shown in Figure 4-1. The registered radiation data are measured values of the global radiation on a horizontal surface. However, so as to calculate the output power of the PV installation according to [41] the radiation on the inclined surface is required for the correct computation. Therefore, the given numbers have to be decomposed in the diffuse and direct elements and subsequently the respective components have to be recalculated considering the tilt of the PV panels. In Section 4.1.1 an analytical comparison of three different decomposition models is performed and the direct and diffuse components of the radiation on the inclined surfaces of the PV installation are computed. The reflected fraction is negligible, so it was not taken into account during the computation phase.

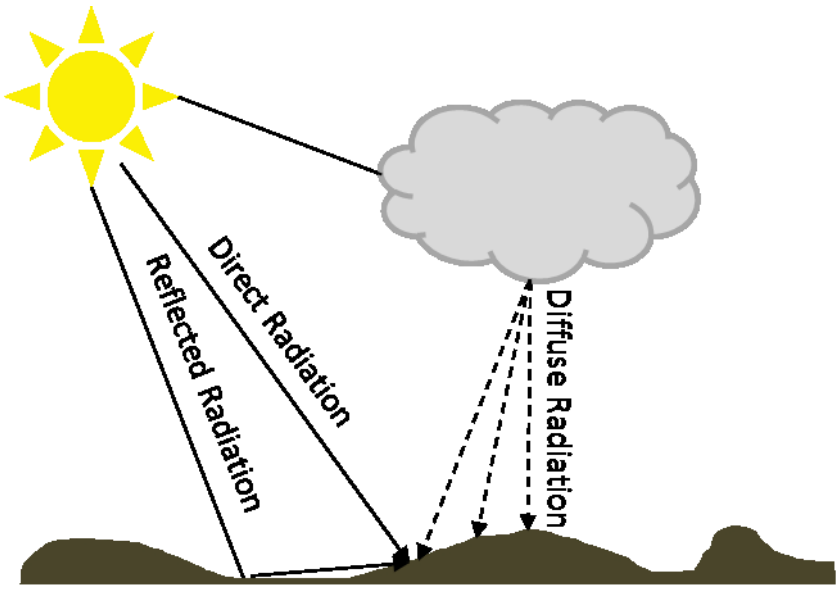

Figure 4-1: Global Radiation Components

For the calculation of the effective global radiation G_{eff}, i.e. the global radiation on the inclined surface of the solar panels, the sun azimuth and altitude had to be specified. In Figure 4-2 the various angles that appear in the following calculations are graphically explained. The adopted method for computing these values was based on the DIN 5034 Norm [113]. According to it the parameter $J^{'}$ as well as the solar declination $\delta(J^{'})$, which represents the angle that is formed if a direct line is drawn from the center of the sun to center of the earth and the equatorial plane, and the time equation T_{eq} are calculated as follows:

$$\mathrm{J}^{'}=360^{\mathrm{o}}\cdot\frac{\text{Day of the Year}}{\text{Total Number of Days in a Year}} \tag{4-3}$$

$$\begin{aligned}\delta(\mathrm{J}^{'})=\{&0.3948-23.2559\cdot\cos\left(\mathrm{J}^{'}+9.1^{\mathrm{o}}\right)-\\&0.3915^{*}\cos\left(2\cdot\mathrm{J}^{'}+5.4^{\mathrm{o}}\right)-0.1764\cdot\cos\left(3\cdot\mathrm{J}^{'}+26^{\mathrm{o}}\right)\}^{\mathrm{o}}\end{aligned} \tag{4-4}$$

$$\begin{aligned}T_{eq}(\mathrm{J}^{'})=\{&0.0066+7.3525\cdot\cos\left(\mathrm{J}^{'}+85.9^{\mathrm{o}}\right)+\\&9.9359\cdot\cos\left(2\cdot\mathrm{J}^{'}+108.9^{\mathrm{o}}\right)+0.3387\cdot\cos\left(3\cdot\mathrm{J}^{'}+105.2^{\mathrm{o}}\right)\}\mathrm{min}\end{aligned} \tag{4-5}$$

From the Local Time *LT*, the time zone and the longitude of the region the Local Mean Time *LMT* is extracted as given below:

$$\mathrm{LMT}=\mathrm{LT}-\mathrm{Time\_Zone}+4\cdot\mathrm{Longitude}\cdot\mathrm{min}/^{\circ} \tag{4-6}$$

Then the Local Apparent Time *LAT* and the time angle ω, which is the true solar time and represents the difference between noon and the local apparent time, are calculated before completing with the calculation of the sun altitude γ_s and the azimuth a_s [114].

$$\mathrm{LAT}=\mathrm{LMT}+T_{eq}(\mathrm{J}^{'}) \tag{4-7}$$

$$\omega=\left(12.00\mathrm{h}-\mathrm{LAT}\right)\cdot15^{\mathrm{o}}/\mathrm{h} \tag{4-8}$$

Finally the Sun Altitude γ_s and the azimuth a_s are extracted from the calculated time angle ω, the solar declination δ and the local Latitude φ:

$$\gamma_s = \arcsin(\cos\omega \cdot \cos\varphi \cdot \cos\delta + \sin\varphi \cdot \sin\delta) \quad \textbf{(4-9)}$$

where:

- φ is the local Latitude.

$$\text{Azimuth: } a_s = \begin{cases} 180^o - \arccos\frac{\sin\gamma_s \cdot \sin\varphi - \sin\delta}{\cos\gamma_s \cdot \cos\varphi} & \text{for LAT} \leq 12{:}00\text{h} \\ 180^o + \arccos\frac{\sin\gamma_s \cdot \sin\varphi - \sin\delta}{\cos\gamma_s \cdot \cos\varphi} & \text{for LAT} > 12{:}00\text{h} \end{cases} \quad \textbf{(4-10)}$$

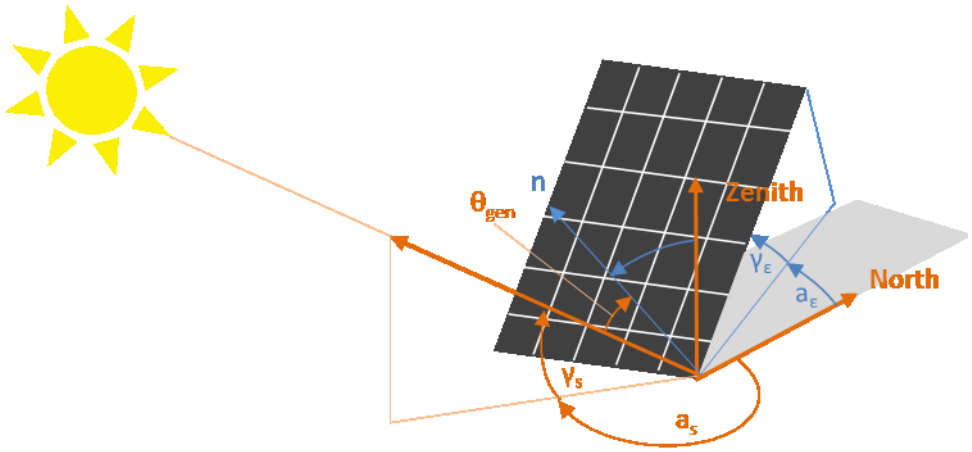

Figure 4-2: Solar incidence angle on a PV panel

Given the sun altitude and azimuth the diffuse and the direct components of the global radiation on a horizontal surface are calculated based on the model developed from Reindl et al. [115-116]. The decomposition of the global radiation is essential for the further calculations of the diffuse and direct parts of the radiation reaching the inclined panel. The clearness index k_T (ratio of hourly global horizontal to hourly extraterrestrial radiation) [115] and the solar zenith angle γ_s are the variables which determine the diffuse fraction of the global solar irradiation.

According to that:

$$k_T = \frac{E_{Global,hor}}{E_o \cdot \sin\gamma_s} \quad \textbf{(4-11)}$$

where:

- E_o is the extraterrestrial irradiance (solar constant) equal to 1360.8 W/m^2

$$E_{Diffuse,hor} = \begin{cases} E_{Global,hor} \cdot (1.020 - 0.254 \cdot k_T + 0.0123 \cdot \sin\gamma_s), & \text{for } k_T \leq 0.3 \\ E_{Global,hor} \cdot (1.400 - 1.749 \cdot k_T + 0.177 \cdot \sin\gamma_s), & \text{for } 0.3 < k_T < 0.78 \\ E_{Global,hor} \cdot (0.486 \cdot k_T - 0.182 \cdot \sin\gamma_s), & \text{for } k_T \geq 0.78 \end{cases} \quad \textbf{(4-12)}$$

Finally the direct fraction is extracted from the deduction of the diffuse part from the global radiation on the horizontal surface and is mathematically expressed from the following equation:

$$E_{Direct,hor}=E_{Global,hor}— E_{Diffuse,hor} \quad \textbf{(4-13)}$$

4.1.1 Decomposition Models

Having already assessed the direct and diffuse components of the global irradiance on the horizontal plane, the calculation of the diffuse fraction of the irradiance on the inclined surface follows. Three different computation models are applied and their accuracy is estimated. These are namely the isotropic sky model of Liu and Jordan [117], the Klucher model [118] and the Perez et al. model [119-121], and their respective equations are given below [122]:

A. Isotropic Sky Model

$$E_{Diffuse,gen}=E_{Diffuse,hor}\cdot\frac{1}{2}\cdot(1+\cos\gamma_E) \quad \textbf{(4-14)}$$

where:

- γ_E is the slope angle of the module.

In the isotropic approach it is assumed that the radiation is always the same, regardless the sky direction, which is interpreted as the beam density is uniformly distributed [114]. This model is preferred for rough estimates or when the sky is overcast. Generally though anisotropic models are more appropriate for calculating the diffuse part of the irradiance on inclined surface since the irradiance density differs greatly according to the direction of the sky. Klucher and Perez model which are next described belong to this cluster [114].

B. Klucher Model

$$E_{Diffuse,gen}=E_{Diffuse,hor}\cdot\frac{1}{2}\cdot\left(1+\cos\gamma_E\right)\cdot\left(1+F\cdot\left(\sin\frac{\gamma_E}{2}\right)^3\right)\cdot\left(1+F\cdot(\cos\theta_{gen})^2\cdot(\cos\gamma_s)^3\right) \quad \textbf{(4-15)}$$

The factor F is given by:

$$F= 1— \left(\frac{E_{Diffuse,hor}}{E_{Global,hor}}\right)^2 \quad \textbf{(4-16)}$$

The incidence angle θ_{gen} between the sun direction and the normal vector *n* perpendicular to the tilted surface can be calculated as:

$$\theta_{gen}=\arccos(-\cos\gamma_s\cdot\sin\gamma_E\cdot\cos(a_s-a_E)+\sin\gamma_s\cdot\cos\gamma_E) \quad \textbf{(4-17)}$$

where:

- a_E is the azimuth angle of the module.

C. Perez Model

The calculation of the diffuse radiation according to Perez model is requiring more effort [123] and the steps followed are shown below. First the Air Mass index *AM*, the sky Clarity Index ε and the brightness Index Δ are calculated according to the following equations:

$$\text{Air Mass: } AM=\frac{1}{\sin\gamma_s} \quad \textbf{(4-18)}$$

$$\text{Sky Clarity Index: } \varepsilon=\frac{\frac{E_{Diffuse,hor}+E_{Direct,hor}}{E_{Diffuse,hor}}\cdot\sin^{-1}\gamma_s+\kappa\cdot\theta_{hor}^{\ 3}}{1+\kappa\cdot\theta_{hor}^{\ 3}} \quad \textbf{(4-19)}$$

$$\text{Brightness Index: } \Delta=AM\cdot\frac{E_{Diffuse,hor}}{E_0} \quad \textbf{(4-20)}$$

where:

- θ_{hor} is the angle of incidence of the sunlight, expressed in rad.

The Air Mass coefficient describes the path length that the light follows through the atmosphere normalized to the shortest path it could take. Sky Clarity Index is actually depicting the pollution in the air and mixes the parts of background diffuse irradiance and the circumsolar part. Variations of Δ show actually the opacity/thickness of the clouds [120, 124].

The circumsolar and *horizon brightness* coefficients F_1 and F_2 respectively can be expressed as:

$$F_1=F_{11}(\varepsilon)+F_{12}(\varepsilon)\cdot\Delta+F_{13}(\varepsilon)\cdot\theta_{hor} \quad \textbf{(4-21)}$$

$$F_2=F_{21}(\varepsilon)+F_{22}(\varepsilon)\cdot\Delta+F_{23}(\varepsilon)\cdot\theta_{hor} \quad \textbf{(4-22)}$$

where:

- $F_{11}(\varepsilon)$, $F_{12}(\varepsilon)$, $F_{13}(\varepsilon)$, $F_{21}(\varepsilon)$, $F_{22}(\varepsilon)$, $F_{23}(\varepsilon)$ are constants stemming from the Table 4-1 [114]. The Table is formed based on eight consecutive ε-classes which correspond to eight sky-clearness indices ε-ranges.

Then the diffuse fraction is calculated from the diffuse radiation on a horizintal surface and the the abovementioned parameters and variables and is mathematically given from the equation:

$$E_{Diffuse,gen}=E_{Diffuse,hor}\cdot[\frac{1}{2}\cdot(1+\cos\gamma_E)\cdot(1-F_1)+\frac{a}{b}\cdot F_1+F_2\cdot\sin\gamma_E] \quad \textbf{(4-23)}$$

where:

- $\alpha=\max(0;\cos\theta_{gen})$, $b=\max(0.087;\sin\gamma_s)$.

Table 4-1: Constants for the determination of F_1 and F_2 as a function of ε

ε-Class	1	2	3	4	5	6	7	8
ε	*1.000… 1.065*	*1.065… 1.23*	*1.230… 1.5*	*1.500… 1.95*	*1.950… 2.8*	*2.800… 4.5*	*4.500… 6.2*	*6.200… ∞*
F_{11}	-0.008	0.13	0.33	0.568	0.873	1.132	1.06	0.678
F_{12}	0.588	0.683	0.487	0.187	-0.392	-1.237	-1.6	-0.327
F_{13}	-0.062	-0.151	-0.221	-0.295	-0.362	-0.412	-0.359	-0.25
F_{21}	-0.06	-0.019	0.055	0.109	0.226	0.288	0.264	0.156
F_{22}	0.072	0.066	-0.064	-0.152	-0.462	-0.823	-1.127	-1.377
F_{23}	-0.022	-0.029	-0.026	-0.014	0.001	0.056	0.131	0.251

The direct part of the radiation in each case on the tilted panels is obtained by the equation:

$$E_{Direct,gen}=E_{Direct,hor}\cdot\frac{\cos\theta_{gen}}{\sin\gamma_s} \quad \textbf{(4-24)}$$

Model Evaluation

At the evaluation part of the three different transposition models, since measured data of diffuse irradiance on inclined surfaces are not available for the region, so as to examine the deviation between measured and calculated values, the statistical comparison has been carried out between measured output power from the photovoltaic plant mounted on the roof top of Faculty and simulated output power with input the newly computed values of global irradiance on the tilted panels.

In order to compare the different extracted outputs from the applied methods a statistical indicator, namely the Mean Bias Error (*MBE*) was applied, so as to estimate the systematic error of the models. The indicator was calculated according to the following equation:

$$MBE/A=\frac{1}{n*\overline{P}}\sum_1^n(P_{i,sim}-P_{i.meas}) \quad \textbf{(4-25)}$$

where:

- $P_{i,sim}$ is the simulated AC Output Power;
- $P_{i.meas}$ is the measured AC Output Power;
- n is the number of Data;

- $\overline{P}$ is the mean of the measured values.

The total errors calculated in a period of one year (2013) are shown in Table 4-2. Although it would expected that the model from Perez as it is computationally more demanding would produce better outputs this is not the case here. According to the presented results we notice that the minimum MBE is calculated for the Isotropic Model. It should be noted that a great percentage of the produced errors in all cases is due to the heavy winter conditions during the first months of the year 2013, when snow accumulation on the PV panels hindered the production of energy which corresponded the respective on-site available radiation.

Table 4-2: Total Error of Output Energy in 2013

Diffuse Fraction Models	**Total Measured Energy in 2013: 4,866 kWh**	
	Calculated Energy	***%MBE/A***
Perez Model	5,288 kWh	8.2%
Isotropic Model	5,211 kWh	7.1%
Klucher Model	5,415 kWh	11.6%

As Klucher has self-concluded, Liu's and Jordan's model (isotropic) yields better results under overcast conditions. Taking into account the fact that the climate in the area of Wolfenbüttel is characterized as temperate, but major rainfalls during the year represent also a high level of cloudy hours/days [123] it is expected that the isotropic model fits better the real data.

4.2 Lead Acid Battery Model

As it is in Section 2 explained the Lineal Modell is to be adopted for simulating the behavior of the on-site installed lead acid battery system. The conceived Simulink model is based on the battery model developed from Brendel et al. [125] and was further enhanced and parametrized in the framework of the Bachelor thesis of Kügler [58]. It is composed from single components which are based on the circuit diagrams presented in Chapter 2 (Figure 2-10) and are in detail explained in the following paragraphs [58].

The flow chart diagram which depicts the calculation steps in the frame of the simulation is depicted in Figure 4-3:

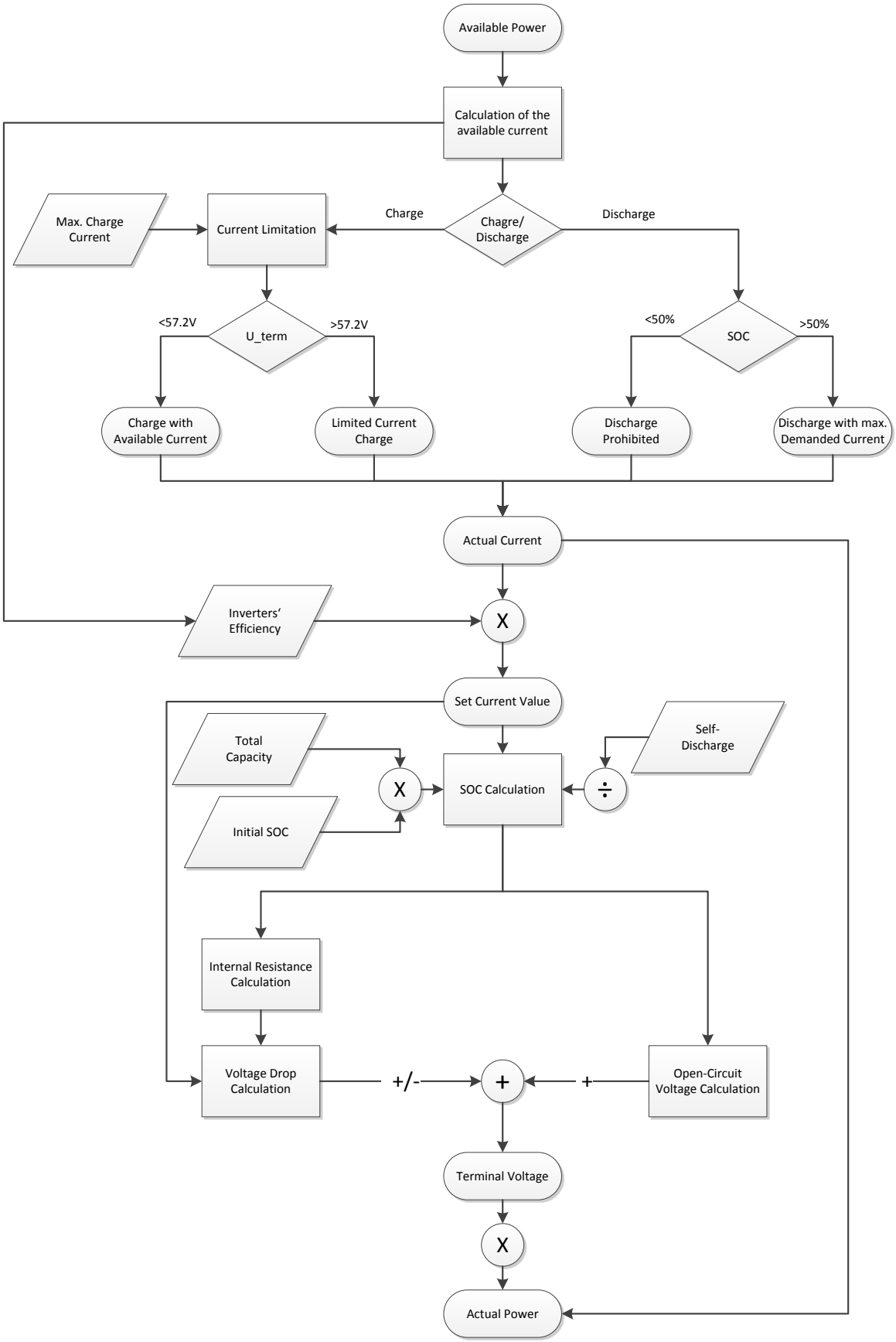

Figure 4-3: Flow Chart Diagram of the Lead Acid Battery Model

The behavior of a real battery can be divided into a static and a dynamic battery behavior. While the static battery behavior is determined by charge-dependent parameters, such as the open-circuit voltage and the resistances, the dynamic behavior depends on factors such as aging and temperature - both factors not individually observed in the model, but only generally by calculation of the overall internal resistance.

Each individual component of the simulation model, namely the open-circuit voltage and the internal resistance, are provided with charge-dependent parameters and converted as a lookup table. Alternatively, an implementation as polynomial regression is also possible in a Matlab function. Though in this case the regression of the measured values would lead to misleading results since it cannot accurately represent particularly strong changes [58].

Battery control

In order to be able to fully charge the batteries during the charging process, current controllers are internally regulated by the inverters. This utility is subsequently adjusted in a Matlab function and is graphically described in Figure 2-9. In the battery control, the battery is charged with the uncontrolled current when the terminal voltage is less than 57.2V, according to test measurements. When this voltage threshold is reached, the charging current is automatically reduced until it reaches the minimum value of approximately 1.6 A (self-discharge compensation). In the Matlab function this behavior is taken into account with a selection of the maximum calculated current and the minimum set current of 1.6 A

Moreover, a discharge at a state of charge (SOC) of less than 50% [126] is not allowed in order to protect the system from unnecessarily reduction of its battery life.

Capacity & State of Charge

The battery is self-discharged due to the losses that are caused from the inverters. The actual charge current that is fed to charge the battery is thus lower due to self-discharge while the actual discharge current appears higher and the state of charge is falling faster. According to installation guidelines of the inverters the self-discharge power rate is 50W.

In order to take this phenomenon into account a $I_{eff}(t)$ is calculated at each moment according to:

$$I_{eff}(t) = I_{set}(t) - I_{self} \tag{4-26}$$

where the parameter I_{self} describes the self-discharge current and $I_{set}(t)$ is the corrected current value before the losses of the inverter are taken into account.

The calculation of the battery capacity is stemming from the integration of the actual current:

$$C(t) = \int I_{eff} dt + C_0 \quad \textbf{(4-27)}$$

The capacity C_0 describes the battery capacity at initial conditions and is calculated based on the following equation:

$$C_0 = SOC_0 \cdot C_N \quad \textbf{(4-28)}$$

where SOC_0 is the initial state of charge and C_N the nominal capacity.

Finally the state of charge at each moment is dependent on the battery capacity at time step t and the nominal one:

$$SOC(t) = \frac{C(t)}{C_N} \cdot 100\ \% \quad \textbf{(4-29)}$$

Inverter Efficiency

Another significant factor for the calculation of state of charge is the efficiency of the inverter. The efficiency grade during charge process is calculated as the fraction of the actual stored charge (Q_{ch}) to the supplied one (Q_{sup}), while during discharge the efficiency results from the ratio of the used charge (Q_{used}) to the actual charge (Q_{dis}) withdrawn from the battery and represented from the two following equations:

$$\eta_{ch} = \frac{Q_{ch}}{Q_{sup}} \approx \eta_{WR} \quad \textbf{(4-30)}$$

$$\eta_{dis} = \frac{Q_{used}}{Q_{dis}} \approx \eta_{WR} \quad \textbf{(4-31)}$$

The described losses are represented from the manufacturer diagram (Figure 4-4):

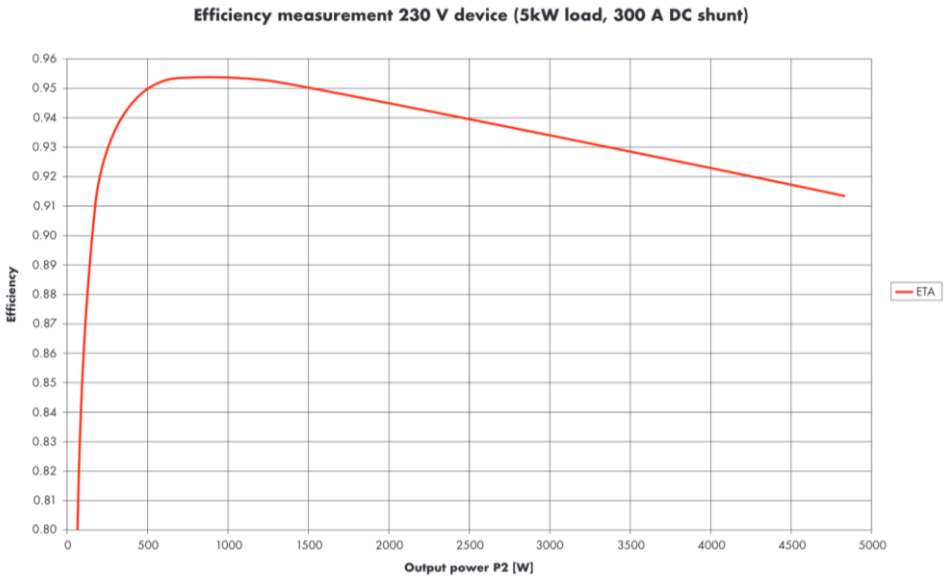

Figure 4-4: Efficiency of the Inverter Sunny Backup 5000

At these efficiencies, the set charge current (which is related to the galvanic cell) is reduced and the set discharge current is amplified as shown from the following equations:

$$I_{set,ch}(t) = I_{ch}(t) \cdot \eta_{WR}(P) \quad \textbf{(4-32)}$$

$$I_{set,dis}(t) = I_{dis}(t) \cdot \frac{1}{\eta_{WR}(P)} \quad \textbf{(4-33)}$$

Open-Circuit Voltage

When galvanic cells are connected in series, the open circuit voltage is built up in a battery block, which depends on the charging state and can be multiplied by series connected battery blocks. It characterizes a battery when no load is connected to its terminals. So as to determine it, test measurements were conducted during which the voltage was measured after a 10% drop in the state of charge of the battery during a discharge process. In Figure 4-5 the extracted results are illustrated:

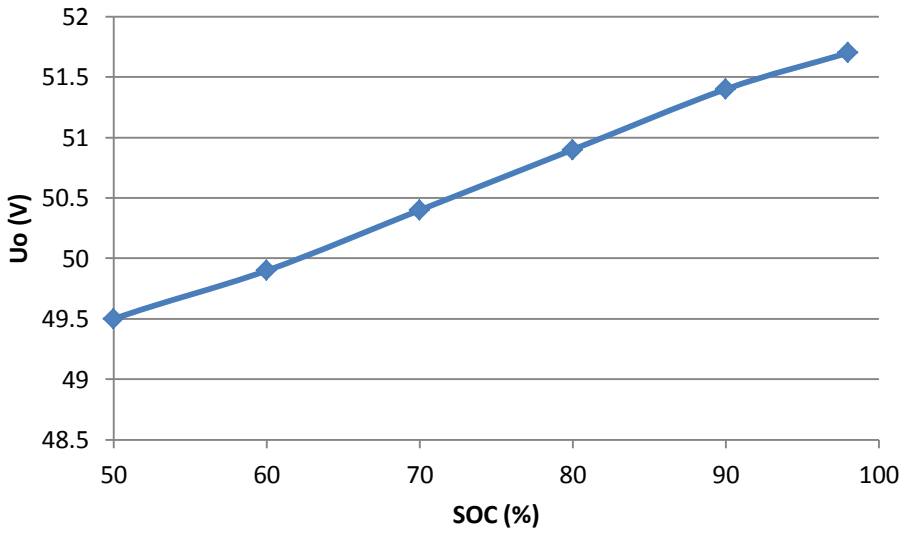

Figure 4-5: Open-Circuit Voltage as function of State of Charge

Internal Overall Resistance

The internal overall resistance was defined for two different conditions, namely during charging and discharging process. It was calculated after a series of experiments, when the battery was discharged/ charged and at different SOCs the open-circuit voltage was measured. The resulted overall resistance for the two cases is dependent on the SOC and their relation is on Figure 4-6 shown:

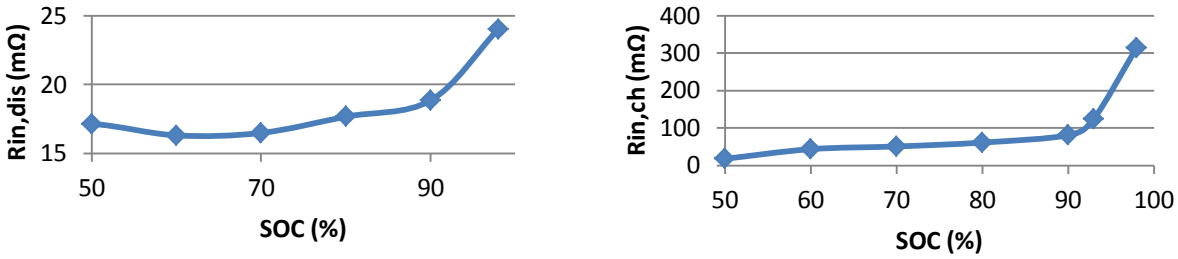

Figure 4-6: Internal Charge & Discharge Resistance as function of State of Charge

The voltage drop on the internal resistance is then calculated using the Ohm's law:

$$U_R = f(SOC, I) = R_i(SOC) \cdot I \qquad \textbf{(4-34)}$$

As already explained previously the charge process is controlled from the inverters that are connected to the battery so as to protect it. When the terminal voltage of 57.2V is reached the current is steadily decreased. So as to calculate the time constant τ of the decay function the first derivative of the current function at the point "0" and the intersection with the abscissa is searched (Figure 4-7).

$$y'(0) = g(t) \qquad g(\tau) = 0 \qquad \textbf{(4-35)}$$

In seconds it is $\tau = 2.735\ sec$.

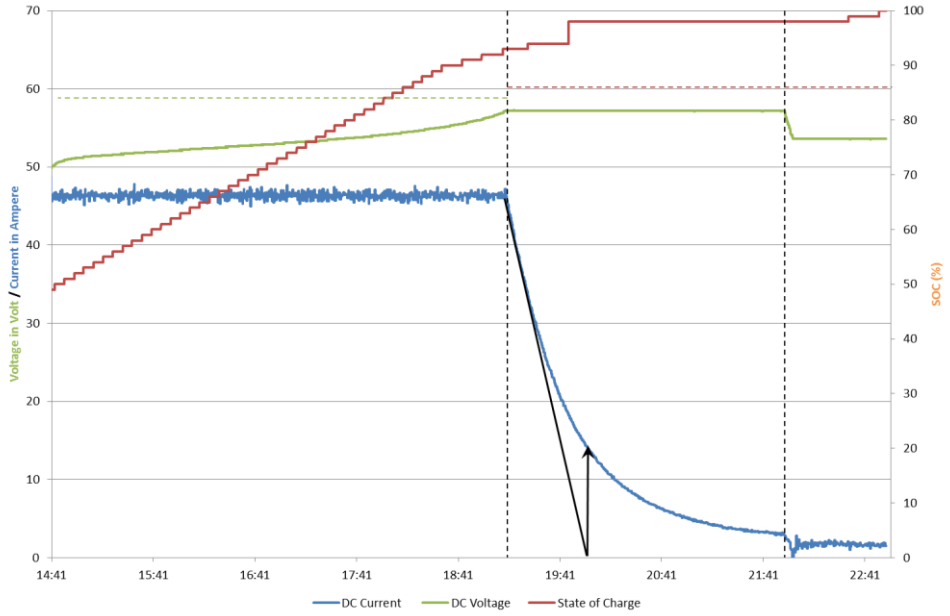

Figure 4-7: Graphical Illustration of the Voltage, Current & SOC during Charge

Terminal Voltage

Finally, the voltage that appears at the terminals of the battery is composed of the open-circuit voltage U_0 and the voltage drop on the internal resistance U_R and is calculated according to the following equation:

$$\begin{aligned} U_{term} &= U_0 + U_R \\ &= U_0 + R_{dis/ch} \cdot I \end{aligned} \quad \textbf{(4-36)}$$

It is to be noted that during charging process, the terminal voltage is higher than the open-circuit voltage, because the voltage drop across the resistors leads to a voltage increase, whereas during discharge (negative current), it is lower than the open circuit voltage. If from the abovementioned equation the U_{term} exceeds the nominal charge cut-off voltage, for simulation reasons the U_{term} is replaced with the constant value 57.2V which equals the maximal measured terminal voltage.

Model Evaluation

So as to compare the extracted simulated results with the measured ones a validation test was performed and the output SOC given a specific charge and discharge power was registered. In each case the respective MAPE was calculated and the results are presented in the following figures:

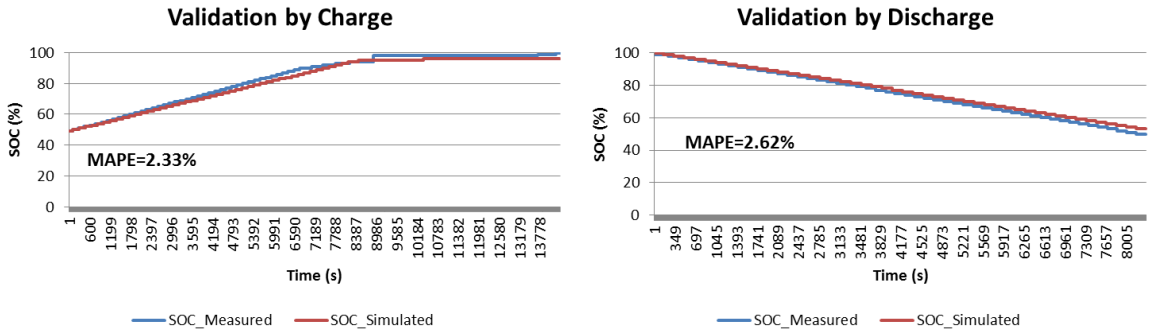

Figure 4-8: The installed PV Power plants of (a) 5.1kWp Plant with 30 modules; (b) 1.02kWp Plant with 12 modules

With a MAPE less than 3% it can be concluded that the designed model represents the real system with a satisfactory accuracy.

4.3 Vanadium Redox Flow Battery Model

As already explained in Chapter 2 the selected model is based on the doctor thesis of Baumann [18] and has been validated with real data stemming from the on-site vanadium redox flow battery. The respective electrical model is composed of resistances which represent the power losses and a voltage source and current sink to describe the open-circuit voltage and the power demand of the auxiliary parts respectively.

Voltage Equilibrium

The voltage equilibrium of one cell U_{eq} is calculated according to Nernst equation and is dependent on the $U_{OCV,SOC=50\%}$, which is the measured open circuit voltage at $SOC|_{50\%}$, R which is the ideal gas constant (8.314 J/molK), T which is the electrolyte temperature (K), n which represents the number of electrons transferred and F which is the Faraday constant (96,485 As/mol) [18, 127]:

$$U_{eq} = U_{OCV,SOC=50\%} + \frac{R \cdot T}{n \cdot F} * ln\left(\frac{SOC^2}{(1-SOC)^2}\right) \quad \textbf{(4-37)}$$

Due to slight deviations that occurred between measured and simulated data of the open circuit voltage, the equation was readapted and a correction factor had been added in order to overcome this divergence:

$$U_{eq} = U_{OCV,SOC=50\%} + \frac{R \cdot T}{n \cdot F} \cdot ln\left(\frac{SOC^2}{(1-SOC)^2}\right) + \underbrace{(C_1 \cdot SOC + C_2)}_{correction\ term} \quad \textbf{(4-38)}$$

The newly introduced parameters C_1 and C_2 of the correction term are estimated after a series of experiments and measurements, and the defined values are C_1= 0.0818 V/% and C_2= -0.04 V.

Since the abovementioned system is composed of 36 cells the respective voltage on stack is then subsequently calculated from the following equation:

$$U_{stack} = n_{cells} \cdot U_{eq} \quad \textbf{(4-39)}$$

Internal Resistance

So as to calculate the internal power losses an analogous resistance R_{eq} which represents mathematically the voltage drop was defined. This was computed independently for charge and discharge.

$$R_{eq,charge/discharge} = \left|\frac{U_{battery} - U_{stack}}{I_{stack}}\right| \quad \textbf{(4-40)}$$

where $U_{battery}$ is the output voltage.

Avoiding the creation of a Look-up table and extrapolating the values or using constant values as the majority of the existing studies proposes, the respective resistances were calculated based on the following two equations:

Charge: $$R_{eq,charge} = A_1 \cdot I_{stack} + A_2 \cdot I_{stack}^2 + B_1 \cdot \left(\frac{SOC}{100\%}\right)^2 + B_2 \cdot \left(\frac{SOC}{100\%}\right) + C \quad \textbf{(4-41)}$$

Discharge: $$R_{eq,discharge} = D_1 \cdot I_{stack} + D_2 \cdot I_{stack}^2 + E_1 \cdot \left(\frac{SOC}{100\%}\right)^2 + E_2 \cdot \left(\frac{SOC}{100\%}\right) + F \quad \textbf{(4-42)}$$

It is obvious that their values are functions of the SOC and the stack current. The coefficients of the variables occur after applying the curve fitting function of the Matlab software using as input data measured value sets. Their experimentally defined values are shown in Table 4-3:

Table 4-3: Calculated coefficients for R_{eq} [18]

Charge	A_1	A_2	B_1	B_2	C
	$1.85 \cdot 10^{-4}$ Ω/A	$9.36 \cdot 10^{-7}$ Ω/A^2	0.0414 Ω	-0.0361 Ω	0.0562 Ω
Discharge	D_1	D_2	E_1	E_2	F
	$-4.097 \cdot 10^{-4}$ Ω/A	$1.16 \cdot 10^{-6}$ Ω/A^2	0.0592 Ω	-0.0723 Ω	0.0913 Ω

Shunt Resistance

A similar approach has been adopted for the estimation of the shunt resistance R_{sh}. In particular this resistance represents the coulombic losses and is a function of stack current as shown from the following equation:

$$R_{sh} = R_{s,1} * |I_{stack}|^{R_{s,2}} \quad \textbf{(4-43)}$$

The extracted values from the curve fitting are thus $R_{s,1}$=311.5 Ω/A and $R_{s,2}$=-0.753.

After the calculation of the shunt losses, which are modelled as a resistor in parallel with the controlled voltage source, the effective stack current $I_{stack,eff}$ can be simply calculated by applying Kirchhoffs' 1st Law:

$$I_{stack,eff} = I_{stack} + I_{sh} \quad \textbf{(4-44)}$$

where I_{sh} is the shunt current and can be calculated by:

$$R_{sh} = \frac{U_{stack}}{I_{sh}} \quad \textbf{(4-45)}$$

State of Charge

The SOC of the system is continuously predicted based on the open circuit voltage of a single reference cell. It is mathematically extracted from its value on time step $t-1$ and the difference occurred in the next time step t and is expressed as a fraction of the stored energy to the maximum energy capacity of the battery:

$$SOC_{t=n} = SOC_{t=n-1} + \Delta SOC = SOC_{t=n-1} + \int_{t=n-1}^{n} \frac{n_{cells} \cdot U_{eq} \cdot I_{stack,eff}}{E_{capacity}} dt \qquad \textbf{(4-46)}$$

At this point it should be noted that between the calculation from the controller of the SOC and the mixing of the electrolyte in the tanks a time delay is noticed which is approximately six minutes according to measurements and is in the model integrated through the abovementioned equation.

Approximation of power consumption of the auxiliary devices

The last step to be taken into account for modelling the vanadium redox flow battery is the estimation of the power needed to supply the BOP system which actually supplies the actuators, the pumps and the sensors with the required energy.

Due to the fact that the electrolyte pumps are consuming a substantial amount of power but no hydraulic model has been developed or integrated to the current model because a more electrical approach was chosen, the power demand was defined based on the different states of charge and the respective stack current. In each case and after a series of experiments a power demand estimation was defined as shown in Table 4-4:

Table 4-4: Estimated Power Consumption of the Auxiliary Systems [18]

I_{stack}	$SOC < 36\%$	$36\% < SOC \leq 66.2\%$	$SOC > 66.2\%$
$0 > I_{stack} > -50A$	500 W		
$I_{stack} \leq -50A$	520 W		
$0 < I_{stack} \leq 35A$	225 W	177 W	228 W
$35A < I_{stack} \leq 80A$	360 W	260 W	365 W
$I_{stack} > 80A$	508 W	365 W	518 W

Finally the output system power is given from the following equation:

$$P_{system} = P_{stack} - P_{aux} \qquad \textbf{(4-47)}$$

Model Evaluation

All these individual modelling parts were integrated into one single model in Matlab/ Simulink environment and finally a validation test was conducted to prove the accordance of the simulated with the measured data during charge and discharge process. With a MAPE of 0.5% it can be concluded that the simulated model represents sufficiently the

performance and behavior of the real system, succeeding a high accuracy as it is shown in Figure 4-9:

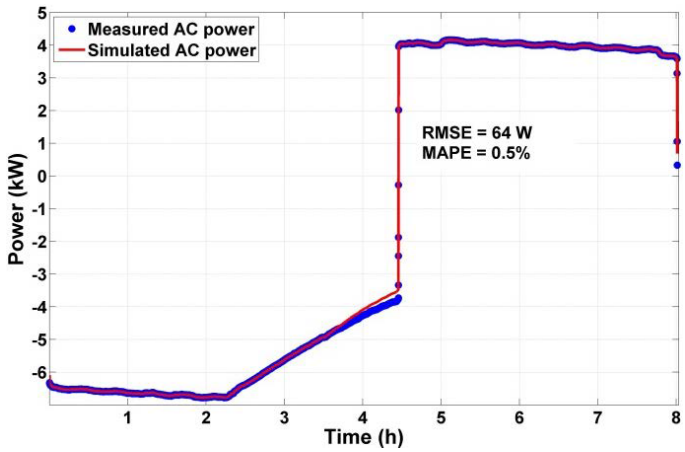

Figure 4-9: Validation Test Results [18]

4.4 Residential Load Demand Model

In the next section the calculated house load demand of a one-family house is presented. The selected technique to model the load demand of such a dwelling is justified in Section 2 and the arguments which advocate to this direction are already previously reported.

So as to determine the reference domestic electric load profiles of a single-family house the following parameters were taken into account according to the guideline VDI 4655 [81]:

- Climate Zone of the Site of the Building;
- Number of occupants;
- Type of the Day (Workday, Sunday);
- Typical-day category (Cloudy or Fine Day);
- Type of Season (Transition/ Summer/ Winter).

The house is assumed to be located North-West German Lowlands, a region which is characterized from changeable overcast weather and the defined number of occupants is four. Moreover, in order to define the type of day category the cloud amount had to be considered; if the one-day average cloud amount is less than 5/8 the day is fine, otherwise the day is characterized as cloudy. The type of the season was also dependent on the mean temperature of the day. When the mean temperature ranged between 5 °C and 15 °C the day was described as transition day, for temperatures over 15 °C it was characterized as summer day and for temperatures below 5 °C as winter day.

Based on the predefined parameters electric load profiles are generated and presented in Table 4-5. This matrix depicts ten day categories, for which a different reference domestic electric load profile was computed and attributed. The reference load profiles are calculated on a one minute time frame. A graphical representation of a typical reference load profile for

a summer workday (SWX) is shown in Figure 4-10. Power peaks in the morning, and earlier and later in the afternoon depict the activity trace in summer during a working day for a family with four members.

Table 4-5: Typical-day categories

	Fine (H)	Cloudy (B)	Fine (H)	Cloudy (B)
Transition (T)	TWH	TWB	TSH	TSB
Summer (S)	SWX		SSX	
Winter (W)	WWH	WWB	WSH	WSB

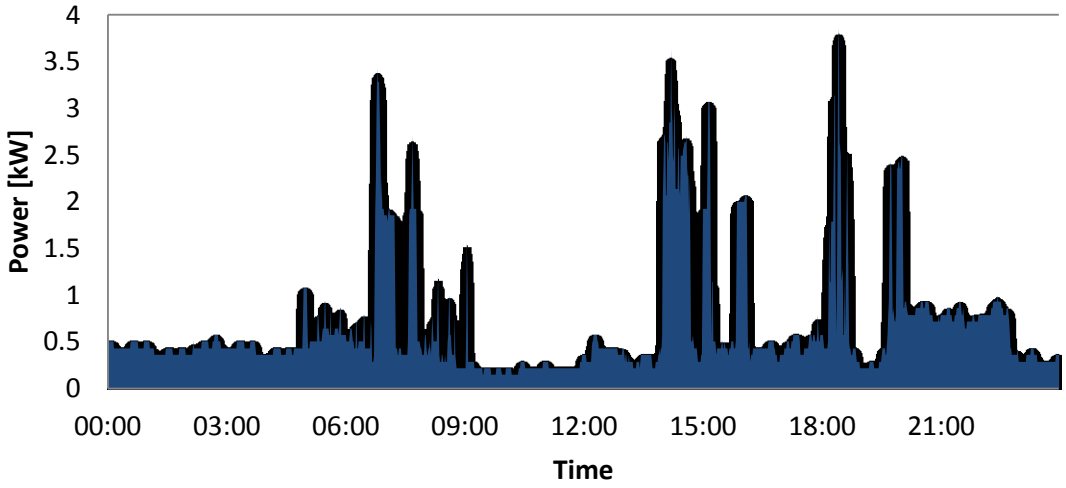

Figure 4-10: Typical Reference Load Profile for a Summer Workday (SWX)

Given the mean daily temperature, which is registered from the on-site weather station and the cloud amount data obtained from the German Meteorological Service (Deutscher Wetterdienst - DWD), the respective reference domestic electric load profile for each day in 2013 has been selected and the yearly house load demand of a single family house with 4 occupants in North-West Germany for the whole year 2013 was calculated in Matlab.

4.5 Electric-Vehicle Load Demand Model

After presenting the domestic load calculation the load demand of an E-Vehicle which always charges at home is given. Concluding to a more static charging model for the E-vehicle for reasons which are explained in Chapter 2, the mean daily trip-distance in Germany was required. According to the VDE Studie Elektrofahrzeuge [93] the mean daily vehicle distance travelled in Germany for a passenger car is approximately 60km. After performing a real driving combined cycle of 60km [128] with the fully charged Peugeot iOn, the E-vehicle was recharged at the charging station of the Faculty and the whole charging process was registered with the Power Quality Analyser PQ-Box 100 until the SOC of the 14.4kWh Lithium iOn battery was again 100%. This charging process is depicted in Figure 4-11:

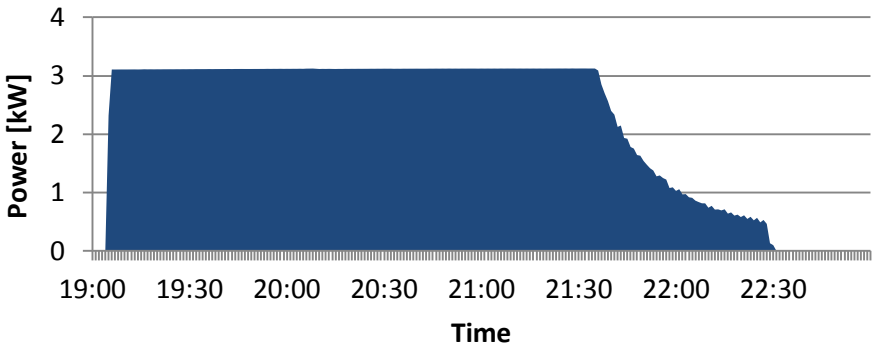

Figure 4-11: Electric Load Demand of the 14.4 kWh Lithium iOn Battery of the Peugeot iOn after a Real Driving Combined Cycle of 60km

This charging imprint is utilized as the prerequisite load demand of the E-Vehicle of the family for each day.

Generation of the Overall Load Profile for 2013

Subsequently, the cumulative house load per day amplified with the charging process of the 14.4kWh Lithium iOn battery from a Peugeot iOn was compiled assuming that the charging process each day begins at 19:00 every day. An indicative example of the overall daily load demand for a Summer Workday is described with the following diagram (Figure 4-12):

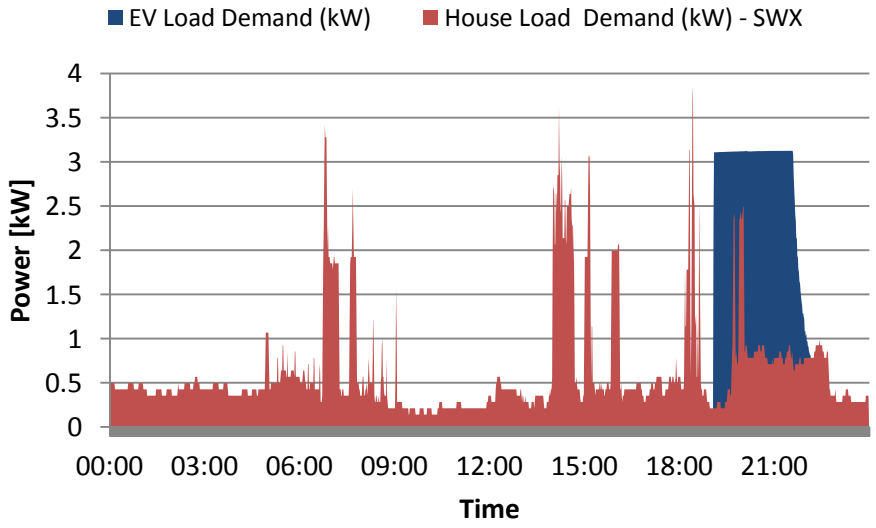

Figure 4-12: Cumulative Daily Load for a Summer Workday (SWX)

Finally the yearly house load demand was extracted and an overall load demand for 2013 was generated based on the above calculated data.

4.6 Grid Model

After covering the individual models that represent an existing physical key element of the conceptualized system in the previous sections, another block is introduced so as to depict the occurred power exchange between the building and the grid. In particular, an additional block is added to the system representation in Matlab/ Simulink which encapsulates and extracts the $P_{grid}(t)$. This variable is calculated after the energy management system (which will be presented in detail in Section 5) allocates the arisen power difference (i.e. the instantaneous local load demand deduced from the respective energy produced from the PV panels at the same time logging) to the available storage systems. Then another power balance computation is executed, estimating the residual power that is missing (in case the local demand is not yet fully covered) or is redundant and must be fed to the public grid and is described mathematically from the following equations:

$$P_{grid}(t) = P_{diff}(t) - P_{battery}(t) \quad \textbf{(4-48)}$$

$$P_{grid}(t) = \begin{cases} P_{grid_{draw}}(t), if P_{grid}(t) > 0 \\ P_{grid_{feed}}(t), if\ P_{grid}(t) < 0 \end{cases} \quad \textbf{(4-49)}$$

Finally, it should be noted that the charging of the batteries from the public grid is prohibited in this configuration in order to minimize the system losses.

5 Energy Management System

After describing the overall context which forms the simulation and test environment in the previous section, it is considered logical consequence to proceed to the reporting of the designed and developed system management which is actually based on the Markov Decision Process (MDP) and under which a delegated agent is assigned to apply the two storage systems in a rational sequence based on the input parameters and the boundary conditions which are framed from the examined HESS. In the next paragraphs a comprehensive introduction in MDP will be presented and the applied techniques are to be thoroughly explained.

5.1 Introduction to Markov Decision Process

A Markov Decision Process is a widely applied technique from the reinforcement learning field and is commonly used to solve problems with stochastic dynamics. It is actually configuring the mathematical framework of modeling a problem which demands a decision making at regular time intervals.

A MDP is formulated from:

- a set of discrete time epochs $T = \{1, \dots, N\}$;
- a set of States $S = \{s_1, \dots, s_n\}$;
- a set of Actions, $A = \{a_1, \dots, a_m\}$;
- a matrix of assigned Rewards R: $S \times A$ for taking action a in state s;
- a Transition Model $P: S \times S \times A \to [0,1]$, which specifies the probability of transitioning from state i to state j on taking action a.

In particular, an agent, which is actually the decision maker, considering the current state s and the available actions that can be taken makes a decision so as the process to move to state s', while a reward $r(s, a)$ is assigned for this choice. The executed action is not completely randomly selected, but based on the transition probabilities $p(s'|s, a)$ which are predefined. The upper target is to define a policy (based on decision rules) according to which the utility (or value) function is maximized. Decisions are made also on finite time steps (decision epochs). A graphical illustration of the previously mentioned procedure is depicted in Figure 5-1.

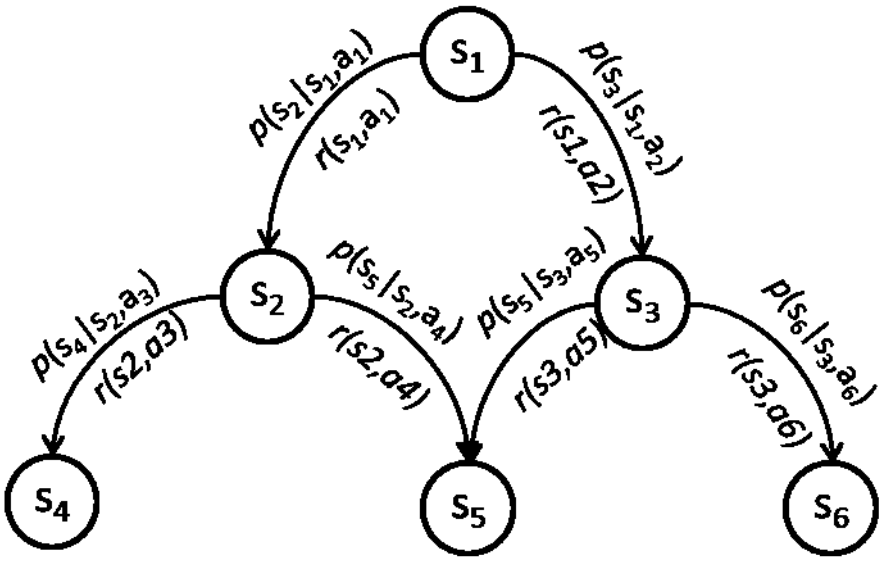

Figure 5-1: A graphical illustration of a MDP model

Therefore a selection of objects with the structure:

$$\{T, S, A_s, r\ (s, a), p\ \}$$

is formulating a Markov Decision Process.

It is should be noted that according to [129] the reward could be:

- a lump sum which is calculated prior to the next discrete time epoch;
- computed constantly during the present time epoch;
- an ambiguous value which occurs from the system state in the next time epoch;
- a blend of the abovementioned cases.

When referring to the type of decision rules that shall be applied different clusters are identified. We classify the existing decision rules as Markovian or history dependent if the decision made depends on the previous states only through the current state and or if it is linked to the history through the whole sequence of applied actions and states respectively. Moreover the differentiation between randomized and deterministic emerges from the grade of certainty that characterizes the chosen action.

In a finite horizon problem the Utility function for discounted Markov Decision Problems is defined as follows:

$$U(s_0, \dots.) = R(s_0) + R(s_1) + .. + R(s_N) \quad \textbf{(5-1)}$$

In the above function the result may be arbitrarily large and the amount of time epochs must be known in advance. On the other hand, in an infinite horizon problem the Utility function for discounted Markov Decision Problems is defined as follows:

$$U(s_0, \dots.) = R(s_0) + \gamma R(s_1) + .. + \gamma^N R(s_N) + .. \quad \textbf{(5-2)}$$

The parameter γ is the discount factor and conduces to the convergence of the function. If γ is close to 0 then more attention is paid on instant gratification and the faster the convergence is, otherwise (γ close to 1) future rewards are considered more important.

The agent is obliged to find an optimal policy π, which is a sequence of actions, that maximizes the abovementioned utility function which can be rewritten in a more generalized form as follows:

$$U_\pi(s) = R(s) + \gamma \sum_{s'} T(s, \pi(s), s')\, U_\pi(s') \quad \textbf{(5-3)}$$

In general, we need |S|²x|A| numbers to store all the transitions probabilities.

Markov Decision Problems with infinite horizon can be solved based on two different techniques:

- value iteration;
- policy iteration.

Value iteration is the most widely used tactic to solve indefinite horizon problems. Given the fact that all the parameters are already known the optimal policy is to be found by solving the Bellman's equation:

$$U_{\pi^*}(s) = max\left[R(s,a) + \gamma \sum_i P^a_{ss'}\, U_{\pi^*}(s')\right] \quad \textbf{(5-4)}$$

where π^* is the optimal policy for state s and U_{π^*} the value of the respective state when the policy π^* is applied.

The abovementioned equation converges and is proved to have a unique solution which is extracted after multiple iterations of the function. In this case we begin with the initialization of the value function so as to have a comparison metric for computing the convergence.

When policy iteration is chosen the agent makes a decision by starting with an arbitrary policy π_0 and proceeds with the estimation of the utility function. If the convergence between two consecutive policies is satisfactory then the iteration stops. Otherwise another policy is selected and the process is repeated. The evaluation criterion remains the maximization of the following component of the utility function and so is the policy in the next time step selected. Target is to create a sequence of decision rules and actions where the respective rewards are monotonically increasing.

$$\pi_{k+1}(s) = argmax\left(\sum_i P^a_{ss'}\, U_{\pi_k}(s')\right) \quad \textbf{(5-5)}$$

During value iteration the optimal value function is computed and then the policy is concretized. The optimal value function is attained with convergence after an iterative approximation. During policy iteration, policy is primarily defined and then the value of the function is calculated. The method is iteratively transformed till it cannot be further

improved and can be preferred since regularly an optimal policy can be extracted sooner as the difference of two successive utility function calculations gets close enough to the predefined threshold value.

5.2 Designed Markov Decision Process Controlling

As already explained in Section 3.3.4 the addressed problematic can be systematically and methodically interpreted from a MDP algorithm. Therefore, after explaining the theoretical background around the Markov Decision Process it is time to proceed to the analysis of the control concept which was developed in the frame of this thesis in order to manage the energy flow of the photovoltaic installation and intelligent allocate it to the two different storage systems.

5.2.1 Battery Efficiencies and Previous Work

It is to be noted that the instantaneous on-site house consumption (including the demand for charging the E-vehicle) is by priority served so as to avoid energy losses. The remaining (the power difference between the locally produced renewable energy and the direct consumed one from the instant loads) is actually the assigned fraction to the battery systems.

Apparently the conceptual approach should not be applicable in a case study as the one examined in this thesis. The reason would be that the one of the two applied batteries, namely the lead acid battery, has always a higher efficiency during both charging and discharging process, on same power levels. In Figure 5-2 a graphical illustration of the described event is presented. In particular, based on the created validated models a comparative simulation analysis is performed. The two systems are charged and discharged with the same power values at various power levels and the overall efficiency was in each case calculated.

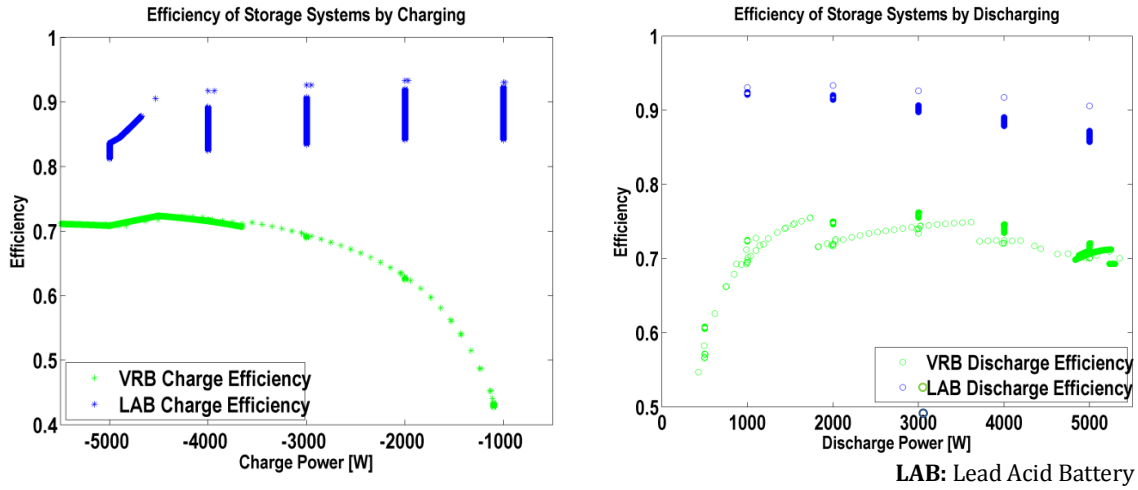

LAB: Lead Acid Battery
VRB: Vanadium Redox Flow Battery

Figure 5-2: Efficiency Grades of Storage Systems

It is obvious that at first glance there is no need for an energy management system since the vanadium redox flow battery performs always worse as the lead acid battery. Several reasons could explain this phenomenon. First, VRBs are still a commercially immature technology, meaning that there is still a lot to be accomplished so as this battery type to reach efficiency levels of technologies which are in market for years. In addition, although it is in literature otherwise argued, the examined system (which is commercially available and not only a test unit for demos and experiments) is characterized by higher losses as theoretically claimed if all coulombic and peripheral losses are taken into account.

Nevertheless, it is identified that there are power regions where the VRB has improved performance records, favoring its function between these areas. The energy management system is therefore so designed to detect these power ranges and try to operate the VRB at an overall higher efficiency. This is succeeded through a reward/ penalty policy which is by default integrated into the MDP and was respectively adapted.

A similar approach is also adopted in the study of Qiu [17]. A thorough description of this case is presented in Section 3.3.4 though it should be stressed out here that although the examined systems appear ostensibly to have a similar structure the internal characteristics of the storage systems have in Qiu's study dictated a different handling method in designing the respective control unit. In particular, the efficiency grades of the selected storage systems in that case intersect at a power level, setting the implementation of a MDP as more trivial as in any other case. To this respect the applied method cannot be generalized in cases when the adopted systems efficiency curves do not have an intersection point, as it is in this case study. Therefore it was decided it was acute to develop a new MDP algorithm which would also incorporate more system configurations.

5.2.2 Markov Process of the Examined System

The designed discrete MDP includes the definition of the various states, actions, rewards and transition probabilities and are in detail analyzed in the following section. A design approach with a continuous state MDP is not attempted in the frame of this thesis since according to literature continuous MDP problems are mainly solved through discretization of the states, leading thus to an exponential increase of the number of states [130]. In addition, as it subsequently described the state space is already sufficiently fragmented representing a considerable amount of states.

It should be also stated that target of this study is not to recognize the optimal storage capacities' combination that can be coupled with the given size of the PV installation and the type of domestic load demand, which is extracted as it is described in Sections 4.4 and 4.5, rather it was attempted to identify a method that can optimally allocate/ serve the available power excess or occurring power demand in an experimental space with predefined storage types and sizes, which though remain in a scale that matches the needs of a dwelling with such a load time series and an on-site PV power generation, in order to succeed grid stability.

States' Definition

The decision of the states' choice is key constituent for the overall process and before proceeding to its definition it is considered wise to assess what a meaningful state space stands for. The determination of the variables that should be integrated in the state matrix must be carefully selected so as to attribute the model needs and the environment characteristics to the control management unit, without exaggerating in the contained information and by keeping the content fully observable. The energy management unit should allocate the arising power difference after consideration of the SOC of the respective storage system. The physical characteristics of the batteries, such as the internal resistances or the maximum current are not considered here, since they are in modelling part integrated. On the other hand, the capacity of the systems, which is obliquely related to the SOC, as well as the value of the arising power difference are affecting the design part. In the examined case the selected states were defined from the state of charge of the two storage systems and the power difference which constitutes the demand or the surplus of energy which arises after subtracting the instant power demand from the on-site renewable energy generation.

It should be noted that the applied technique as concept is identical during charge and discharge phases and differentiates only numerically by the different efficiencies of the storage systems which are given as input to the MDP algorithm.

In particular, the range of the arising power difference was divided in six discrete intervals from $[0 \dots 6kW]$ (the occurring P_{diff} was extended in this range; in any other case the limits can be accordingly scaled). The designed algorithm observes the sign of the parameter (negative P_{diff} corresponds to power excess and positive value to power deficit) and applies respectively the matching method. The SOC ranges were respectively defined by creating SOC level partitions, one for each system. The lead acid battery, whose minimal SOC is limited to 50% of the installed capacity, has a SOC range from $[0 \dots 10]$ in the designed MDP, and the SOC of the vanadium redox flow battery is described from a range of states in the scale from $[0 \dots 20]$. These SOC ranges were selected based on the capacities of the storage systems. In particular, the useable SOC range of the VRB (33% till 74%) corresponds to a stored energy of almost 20 kWh, while the lead acid battery, with an exploitable SOC above 50% for safety reasons is with only 10 kWh full. The numerical interpretation of these discretized states is experimentally investigated and a trial-and-error process advocated for the empirical distributions:

$$SOC_{LAB} = \{[0\ 0.5)\ ,\quad [0.5\ 0.545), [0.545\ 0.59) \cdots [0.905\ 1]\ \} \tag{5-6}$$

$$SOC_{VRFB} = \{[0\ 0.33)\ ,\quad [0.33\ 0.3505) \cdots [0.699\ 0.7195\ ), [0.7195\ 0.74]\ \} \tag{5-7}$$

$$P_{diff}\ (W) = \{[0\ 1000)\ , [1000\ 2000) \cdots [4000\ 5000), [5000\ 6000]\ \} \tag{5-8}$$

So each defined state is represented in the model as follows:

$$S_{n_{i,j,k}} = \left\{SOC_{LAB_i}, SOC_{VRFB_j}, P_{diff_k}\right\}, i = 1 \cdots 11, j = 1 \cdots 21, k = 1 \cdots 6, n = 1 \cdots N, \quad N = i \cdot j \cdot k \tag{5-9}$$

Actions' Definition

After specifying the selected states and composing the state space the actions that can be taken are defined. These are namely the command to charge/discharge the lead acid battery system (A_{LAB}) or the vanadium redox flow battery (A_{VFRB}) or to perform no action (A_{none}). At this point it should be stressed out that for each time interval only one battery may operate and the occurred power difference is not divided in arbitrary or analogous to the each system characteristics partitions. The actions' set A contains the three distinct actions :

$$A = \{A_{LAB}, A_{VFRB}, A_{none}\} \tag{5-10}$$

Rewards' Definition

The instant reward is respectively formulated based on the efficiency of the two storage systems at each charge/ discharge level. This was calculated by estimating the instant power losses according to the efficiency grade that each system is attributed with at the respective power level (see Figure 5-2). In addition reward takes into account special cases like avoiding charging a fully charged battery and preventing charging none of the batteries when both batteries are not fully charged.

In general, except for the special cases mentioned above, the instant reward R is defined as follows:

$$R = -|P_{loss}| \tag{5-11}$$

Since the charge power states P_{diff} include a range of values and due to the non-linearity of the efficiency curves, due to the fact that the efficiency is dependent not only to the power value but also to the current SOC as illustrated in Figure 5-2, we have to assume that for each P_{diff_k}, the batteries have a constant Eff_{LAB_k} and Eff_{VFRB_k} correspondingly. This assumption applies only for the calculation of the rewards and not when modeling the battery performance later. By definition the useable amount of power is the product of the power difference to the respective facility efficiency ($P_{useable} = Eff * P_{diff}$). So the losses which are in the designed algorithm the opposite of the reward function, occur from the complement of the useable power (P_{loss}= $(1 - Eff) * P_{diff}$). The reward is calculated as following:

$$R(s,a)|_{s\in S, a\epsilon A} = \begin{cases} (Eff_{LAB_k} - 1)\cdot P_{diff_k} : \quad a = A_{LAB} \\ (Eff_{VFRB_k} - 1)\cdot P_{diff_k} :, a = A_{VFRB} \\ -c_1 : a = A_{none}, SOC_{LAB_i|i\neq 11}, SOC_{VFRB_j|j\neq 21} \\ 0 : a = A_{none}, SOC_{LAB_i|i=11}, SOC_{VFRB_j|j=21} \\ -c_1 : a = A_{LAB}, SOC_{LAB_i|i=11} \\ -c_1 : a = A_{VFRB}, SOC_{VFRB_j|j=21} \end{cases} \quad \textbf{(5-12)}$$

In cases when the system decides to take no action, the reward is either an arbitrary large negative reward " $-c_1$" (lowest than any other assignable reward) if both batteries are not fully charged (line 3 in Equation (5-12)) or 0 (the highest assigned reward) if both batteries are full (line 4 in Equation (5-12)). In cases that the action tries to charge an already fully charged battery (lines 5 and 6 in Equation (5-12)), the same large negative value is assigned in order to prevent such actions being preferred.

Transition Probabilities' Definition

The last step is to calculate the state transition probabilities. As it is in the MDP theory stated, the new state which is reached after taking an action depends only on the previous state and the decided action and it is not affected from the previously states [129]. This involves calculating for a given charge power P_{diff_t} and battery SOC at time step t the transition probability $P^a_{s,s'}$, when performing action a:

$$P^a_{s,s'} = P(s_{t+1} = s' | s_t = s, a = a_t) \quad \textbf{(5-13)}$$

In the continuous time space, when the battery has X^{wh}_t Wh stored, after applying a constant P_{diff} for a given time duration, the energy stored $X^{wh}_{t'}$ in Wh at time $t' = t + dt$ will be :

$$X^{wh}_{t'} = X^{wh}_t + P_{diff} \cdot \text{Eff} \cdot dt, \quad \textbf{(5-14)}$$

and by setting $dt = 1h$ and $E_{charge/discharge} = P_{diff} \cdot \text{Eff}$

$$X^{wh}_{t'} = X^{wh}_t + E_{charge/discharge} \quad \textbf{(5-15)}$$

Taking as example the lead acid battery and assuming that the battery state is SOC_{LAB_i} at time t, this means that the actual stored energy $X^{wh}_{LAB\_t}$ is in the range $[a_i\ b_i)$. When considering the $X^{wh}_{LAB\_t}$ as a uniformly distributed random variable across the boundaries $a_i\ b_i$ with probability density function (PDF) $f_S(s)$, and considering also that the E_{charge_t} is also uniformly distributed random variable in the range$[a_k\ b_k)$ with PDF $f_P(p)$, then the $X^{wh}_{LAB\_t}$, is the convolution of the two distributions [131].

$$f_{S'}(s') = \int_{-\infty}^{+\infty} f_S(s)\, f_P(s' - s) ds \quad \textbf{(5-16)}$$

Now the state transition probabilities can be calculated for each battery (given the state of the non-charging battery remains the same).

$$P\left(SOC_{LAB}^{t+1} = SOC_{LAB_{i'}} | SOC_{LAB}^{t} = SOC_{LAB_i}, a = A_{LAB}\right) = \int_{a_{i'}}^{b_{i'}} f_{s'}(s') \cdot ds' \quad \textbf{(5-17)}$$

where $a_{i'}$ and $b_{i'}$ result from the synthesis of the limits of the $f_S(s)$ and $f_P(p)$.

We can use the following illustration, which is a custom environment instance (Figure 5-3) to visualize the probability calculation. Let's assume that at time t the $SOC_{LAB}^{t} = SOC_{LAB_4}$ ($X_{LAB\_t}^{wh} = X_{LAB\_4}^{wh}$) and that $P_{diff^t} = P_{diff_2}$ ($P_{charge_t} = P_{charge_2}$).This means that the energy stored in the LAB battery is between 6350W and 6800W and the energy provided to the battery is between 1 kW and 2 kW. According to the efficiency diagram of the lead acid battery, we can assume that the efficiency with this energy supply is 0.9, so that means that 900 Wh to 1800Wh can be stored in the battery in one hour.

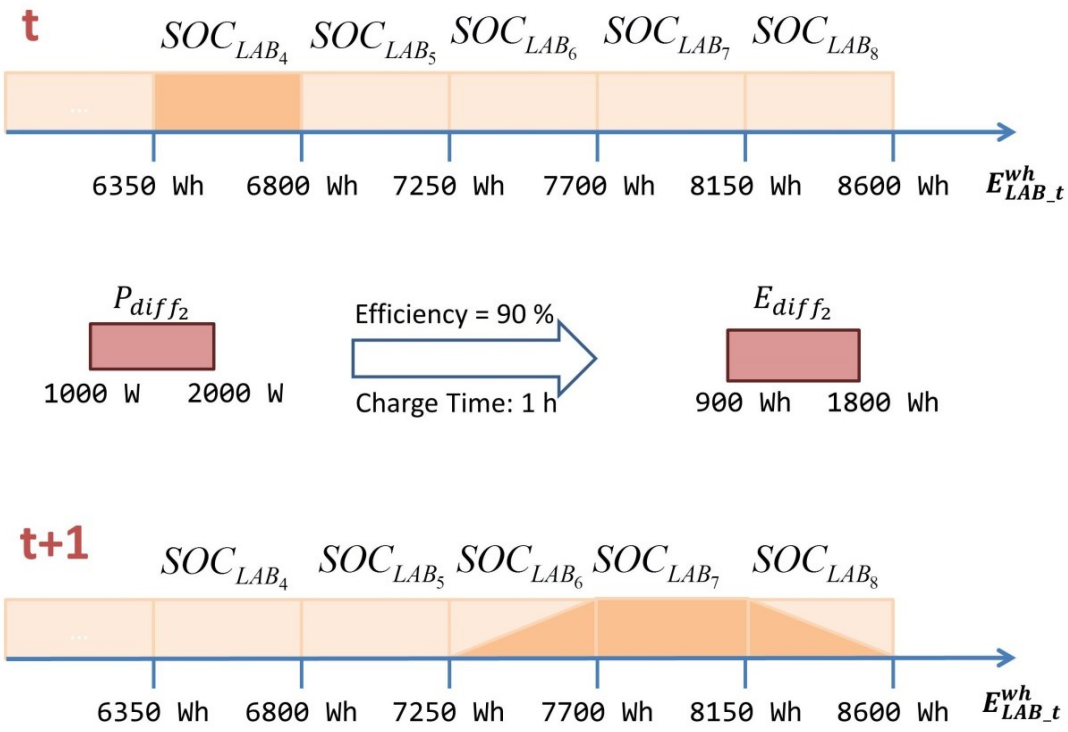

Figure 5-3: Graphical Illustration of the SOC_{LAB}^{t} transition

In the above figure it can be seen that the state transition probability is the integral of the trapezoid part that coincides with the state. I order to calculate for each single state the transition probability the following ritual is applied:

In particular, P_{charge_2} is a continuous uniformly distributed random variable in [900, 1800] or P_{charge_2}~U(900,1800) and is defined as follows:

$$E_{charge_2} = \begin{cases} c\,, 900 \leq p \leq 1800 \\ 0, elsewere \end{cases} \quad \textbf{(5-18)}$$

Due to the fact that the probability density function is always a positive number and the total area under the graph of the respective illustrated function should be 1 the normalizing constant c is given as follows:

$$P\left(-\infty < E_{charge_2} < +\infty\right) = 1 \Rightarrow \int_{-\infty}^{+\infty} E_{charge_2}(p)\, dp = 1 \Rightarrow$$
$$\int_{-\infty}^{900} E_{charge_2}(p)\, dp + \int_{900}^{1800} E_{charge_2}(p) dp + \int_{1800}^{+\infty} E_{charge_2}(p) dp = 1 \Rightarrow \quad \textbf{(5-19)}$$
$$\int_{900}^{1800} E_{charge_2}(p) dp = 1 \Rightarrow c = \frac{1}{1800-900} \Rightarrow c = \frac{1}{900}$$

Similarly is also estimated the normalizing constant d for the SOC_{LAB_4} state and its uniformly random function $X_{LAB\_4}^{wh}$ ($X_{LAB\_4}^{wh} \sim U(6350,6800)$) which is defined accordingly:

$$X_{LAB\_4}^{wh} = \begin{cases} d\,, 6350 \le s \le 6800 \\ 0, elsewere \end{cases} \quad \textbf{(5-20)}$$

Respectively, the constant d is given from the following equations:

$$P\left(-\infty < X_{LAB\_4}^{wh} < +\infty\right) = 1 \Rightarrow \int_{-\infty}^{+\infty} X_{LAB\_4}^{wh}(s)\, ds = 1 \Rightarrow$$
$$\int_{-\infty}^{6350} X_{LAB\_4}^{wh}(s)\, ds + \int_{6350}^{6800} X_{LAB\_4}^{wh}(s) ds + \int_{6800}^{+\infty} X_{LAB\_4}^{wh}(s) ds = 1 \Rightarrow \quad \textbf{(5-21)}$$
$$\int_{6350}^{6800} X_{LAB\_4}^{wh}(s) ds = 1 \Rightarrow d = \frac{1}{6800-6350} \Rightarrow d = \frac{1}{450}$$

The sum of the two distributions is extracted from the Equation (5-17). Thus if $S' = X_{LAB\_4}^{wh} + E_{charge_2}$ defined in [7250, 8600], then:

$$f_{S'}(s') = \int_{-\infty}^{+\infty} X_{LAB\_4}^{wh}(s) \cdot E_{charge_2}(s'-s) ds = \int_{-\infty}^{+\infty} \frac{1}{450} \cdot E_{charge_2}(s'-s) ds \quad \textbf{(5-22)}$$

The following cases are identified:

If $s' \le 7250$, then $f_{S'}(s') = 0$.

If $7250 \le s' \le 7700$, then $6350 \le s$ & $s' - s \ge 900 \Rightarrow s' - 900 \ge s$. Thus:

$$f_{S'}(s') = \int_{6350}^{s'-900} \frac{1}{450} \cdot \frac{1}{900} ds = \frac{1}{450} \cdot \frac{1}{900} \cdot (s' - 7250) \quad \textbf{(5-23)}$$

If $7700 \le s' \le 8150$, then $900 \le p \le 1800 \Rightarrow 6350 \le s \le 6800$. Thus:

$$f_{S'}(s') = \int_{6350}^{6800} \frac{1}{450} \cdot \frac{1}{900} ds = \frac{1}{450} \cdot \frac{1}{900} \cdot 450 = \frac{1}{900} \quad \textbf{(5-24)}$$

If $8150 \le s' \le 8600$, then $6800 \ge s$ & $s' - s \le 1800 \Rightarrow s' - 1800 \le s$ Thus:

$$f_{S'}(s') = \int_{s'-1800}^{6800} \frac{1}{450} \cdot \frac{1}{900} ds = \frac{1}{450} \cdot \frac{1}{900} \cdot (8600 - s') \quad \textbf{(5-25)}$$

If $8600 \leq s'$, then $f_{S'}(s') = 0$.

Finally, the probability of transition to the new states is the integral of each part of the newly created piecewise function $f_{S'}(s')$ in each respective state space. So:

$$P\left(SOC_{LAB}^{t+1} = SOC_{LAB_6} | SOC_{LAB}^{t} = SOC_{LAB_4}, a = A_{LAB}\right) = \int_{7250}^{7700} f_{s'}(s') \cdot ds' = \int_{7250}^{7700} \frac{1}{450} \cdot \frac{1}{900} \cdot (s' - 7250)\, ds' = 0.25 \quad \textbf{(5-26)}$$

$$P\left(SOC_{LAB}^{t+1} = SOC_{LAB_7} | SOC_{LAB}^{t} = SOC_{LAB_4}, a = A_{LAB}\right) = \int_{7700}^{8150} f_{s'}(s') \cdot ds' = \int_{7700}^{8150} \frac{1}{900} ds' = 0.5 \quad \textbf{(5-27)}$$

$$P\left(SOC_{LAB}^{t+1} = SOC_{LAB_8} | SOC_{LAB}^{t} = SOC_{LAB_4}, a = A_{LAB}\right) = \int_{8150}^{8600} f_{s'}(s') \cdot ds' = \int_{8150}^{8600} \frac{1}{450} \cdot \frac{1}{900} \cdot (8600 - s')\, ds' = 0.25 \quad \textbf{(5-28)}$$

This procedure is repeated for every possible SOC of each battery and every possible provided or requested power difference and in such a way the transition probability matrix is created and filled with the respectively calculated values. The extracted matrix $NxNx3$ combined with the reward vector are the inputs to the Markov model and the optimal policy is concretized and entered into the Simulink model.

It should be noted that if $A = \{A_{none}\}$ then the $f_{S'}(s') = 0$. Moreover, if the resulting SOC is beyond the defined ones (the battery cannot accept more energy to be stored), then the again $f_{S'}(s')$ is equal to 0 in that case. In addition an analogous procedure is applied for the discharge modus. In this case though the trapezoid part has a reverse moving (the stored energy in the battery is reduced).

Finally, the Utility function integrates the discount factor γ which is assigned with the value 0.99 for the described method and set to 0.001 if the naive approach is applied.

5.2.3 Implementation

As a basis for the implementation the MDP toolbox [132] was used. MDP toolbox contains functions related to the resolution of discrete-time Markov Decision Processes and are

implemented in different programming environments. In this work the Matlab implementation was used.

In Figure 5-4 the implementation architecture is visualized. Following the logical flow presented in 5.2.2, in the first step the states and actions are defined. Each state is represented as a three element vector as described in Equation (5-9):

$$S(n_{i,j,k}) = [i\ j\ k], n = 1 \dots N \tag{5-29}$$

Then by taking in to account the battery efficiencies and Equation (5-17) the state transition probabilities are calculated as a three dimensional matrix with size $NxNx3$. Each element describes the transition probability between two states with a given action:

$$P\_Prob_{(l,m,u)} = P(S_l^{t+1} | S_m^t, a = A_u)|_{A_u \in A, S_l^t S_m^t \in S} \tag{5-30}$$

The last programming step involves the calculation of the rewards, which are also described in a matrix with size $Nx3$ and calculated according to Equation (5-12). The reward of an action $a = A_u$ at state S_n^t is $R(n,u)$. The matrixes P_Prob and $R(n,u)$ are then given as input to the MDP Toolbox which performs the Markov optimization process. The result is a vector with N elements containing the optimal policy for each state. This vector is then used by the Simulink model in the simulation environment. The policy iteration is the applied method for the resolution of discounted MDP.

In the Simulink model the arising power difference between the load demand and the PV generation is assigned to the respective P_{diff^t} and the same is repeated for each state of charge of the two batteries (SOC_{LAB}^t, SOC_{VRB}^t). The sign of the occurred P_{diff^t} activates the correct algorithm ("-" stands for excess of energy, thus "Charge modus", and "+" stands for demand, thus "Discharge modus" should be triggered). According to these three elements the optimal action is chosen based on the predefined optimal MDP policy and the corresponding control command is passed on to the chosen battery.

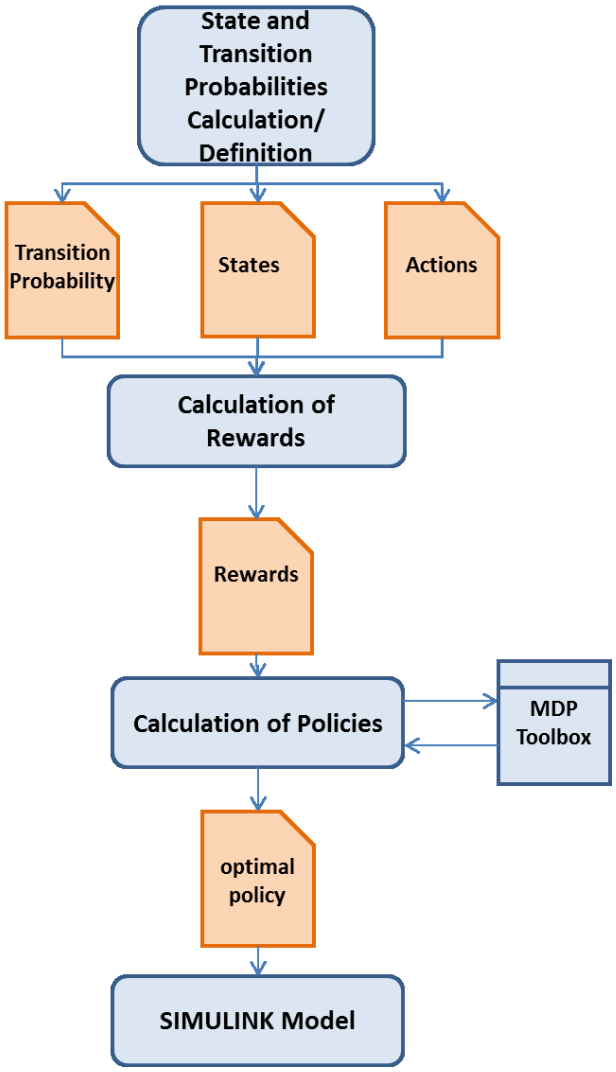

Figure 5-4: Implementation Architecture

In addition it should be stressed out that the search for the optimal policy is developed not only for charging the storage systems but also for discharging them. In this case the same approach is adopted and the main body of the designed algorithm remains unchanged. What differentiates charge and discharge state are the battery efficiencies, which during the two processes vary given the same SOC and power (Figure 5-2).

Schematically the designed strategy can be illustrated as a switch (Figure 5-5). The MDP is making the decision which facility is going to serve in each case the respective load demand or power excess among the three available choices (operation of the lead acid battery, operation of the vanadium redox flow battery, electrical grid). The occurring P_{diff} is then attributed to the chosen system and the process is repeated for the next time period.

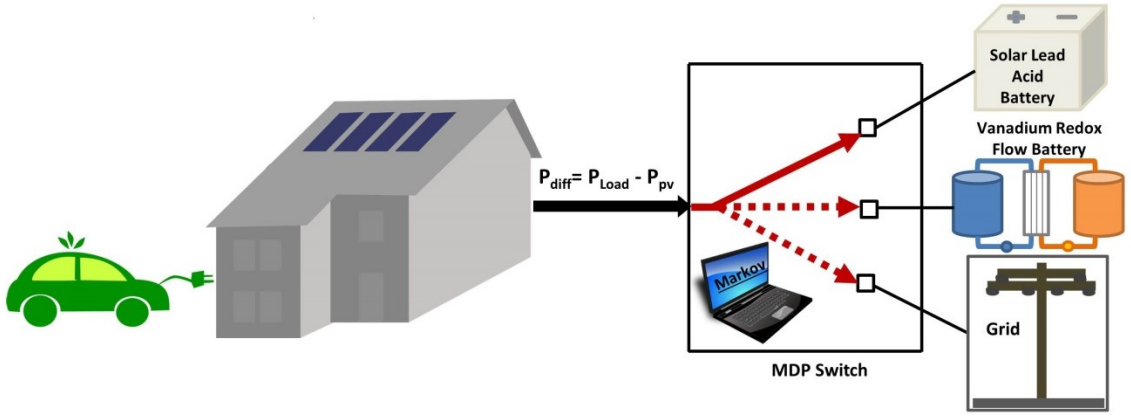

Figure 5-5: Schematic Illustration of the Applied Strategy

5.3 Naive Approach-Benchmark Method

A benchmark method (or naive approach) is needed to estimate the robustness of the applied algorithm. This is traditionally defined in every newly developed method so as to assess how efficient the new technique is performing. The conceptualized approach is implemented through a naive policy which is based on the fact that the efficiency grade of the lead acid battery system is always higher than the one of the vanadium redox flow battery, no matter which power fraction is drawn from or fed in the storage systems and regardless of the state of charge of the operating system. Therefore the control management was designed in this case by giving always higher priority to the storage system with the higher efficiency, if the boundary conditions allow it. That means the benchmark scenario is designed based on the "apparent" optimal energy allocation, which would be the prioritization of the lead acid battery if an excess or a deficit of energy occurs and the extracted results are stemming from this naive policy.

So as to implement that, instead of designing a different algorithm from scratch, it was decided to set the discount factor of the already designed MDP close to zero, thus the applied algorithm was paying attention on the instant gratification which in this case was always higher for the lead acid battery system. The same energy management architecture was therefore retained and only the tuning of a parameter could differentiate the two examined energy allocation approaches. In particular, the regarding equation (which is already presented in Section 5.1):

$$U_{\pi^*}(s) = max\left[R(s,a) + \gamma \sum_i P_{ss'}^a U_{\pi^*}(s')\right] \quad \textbf{(5-31)}$$

is attributing the optimal policy by minimizing the second term of the sum in brackets since:

$$\gamma \to 0. \quad \textbf{(5-32)}$$

It is the instant reward $R(s,a)$, given from Equation (5-12), which is actually always higher for the lead acid battery as shown in Figure 5-2, that determines the actions to be taken and subsequently the overall policy pattern.

Then the two applied approaches have been compared on the basis of the evaluation criteria presented in Section 3.3.5, namely the supply cover factor, which describes the proportion of the self-energy consumption and the grid interaction index, which describes the fluctuations of the energy which is fed to or drawn from the grid and the superiority of the designed technique was reviewed.

5.4 Overall Model - Interactions of the Models

After finalizing the implementation of designing the algorithm for the optimal energy conversion the complete Simulink model is formed (Figure 5–6) and the only design step missing is the sketching of the interactions among the different blocks. As it can be ascertained from the illustrated layout of the overall system the on-site power generation from the photovoltaic installation is primarily calculated based on the temperature and radiation data stemming from the weather databank. In parallel the "actual" load demand which ensues from the house load demand of an one-family house, calculated as described in Section 4.4 and from the load demand for charging the electric vehicle, computed as explained in Section 4.5, is drawn. The instant values of the previously referred parameters are consecutively fed in the energy management block.

The instantaneous local load demand is covered by priority directly from the energy produced from the PV panels, thus minimizing the amount of energy exchanged with the grid and lowering the power losses due to energy conversion reasons. These correlations are described with the following equations:

$$P_{diff}(t) = P_{load}(t) - P_{pv}(t) \tag{5-33}$$

$$P_{diff}(t) = \begin{cases} P_{battery_{discharge}}(t), if\ P_{diff}(t) > 0W \\ P_{battery_{charge}}(t), \quad if\ P_{diff}(t) < 0W \end{cases} \tag{5-34}$$

The resulting power difference after extracting the direct load demand from the on-site renewable energy production is then the fundamental parameter along with the SOC of the two storage systems which determine the optimal charge/ discharge policy for the operation of the batteries. Moreover, it is always preferred to completely charge/ discharge the storage systems before "commanding" the grid to serve the occurring P_{diff} .

Finally, the energy management system assigns the signal with the arisen power difference to the available storage systems and after letting the models process the given input the real stored or extracted power is directed to the grid block, where the final power balance computation is executed.

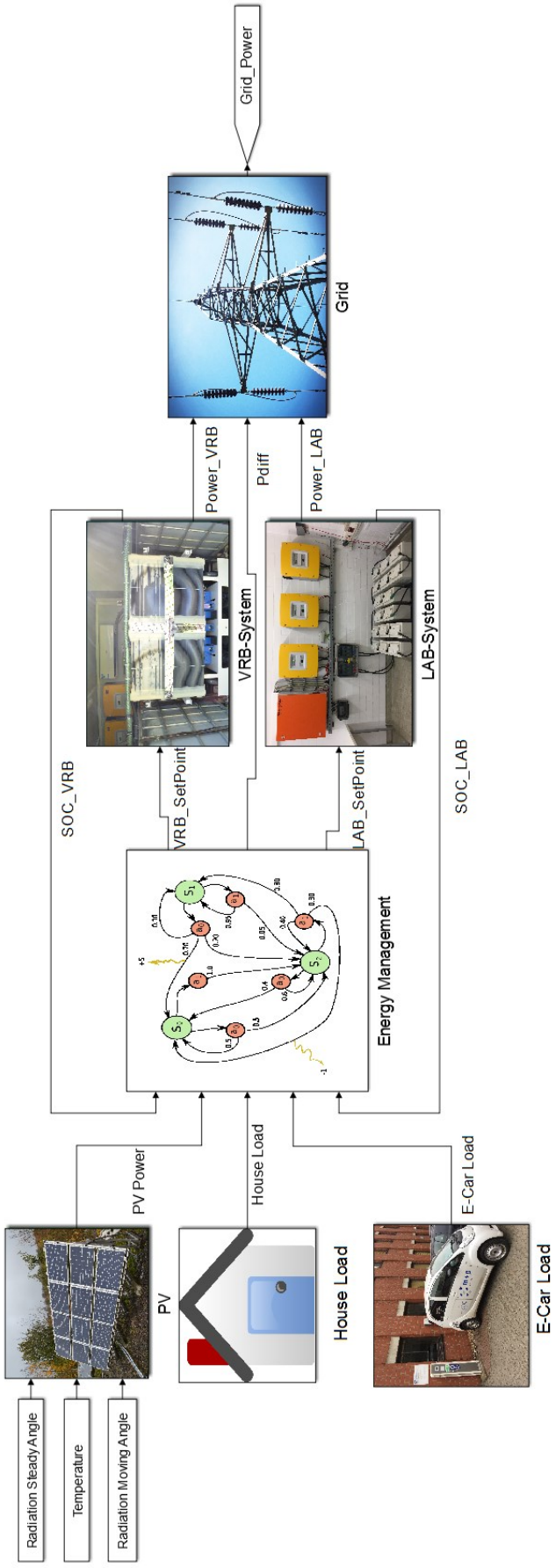

Figure 5–6: Simulink Model Layout [133-135]

6 Simulation Results & Discussion

In the previous section a thorough description of the applied technique is provided accompanied from the theoretical background around the Markov theory and Markov Decision Processes. A benchmark method was also defined which was extracted from the physical characteristics of the storage systems and which meant to be used as an estimation criterion. The analysis of the developed algorithm was sketched out based on the fundamentals of the MDP and in detail presented. In this section the outputs from the two applied methods are reported through graphical and tabular data and a comparative report is provided.

6.1 Simulation Results with one Storage System

The idea is to present results and outputs from one year simulation. The incremental step of one hour which was adopted matches the hourly decision making which is extracted from the methodology presented in the previous section. Since the available data availability comes with an at least minute time-scale, it was decided to calculate the mean average value per hour for each input parameter and consequently feed it to overall system which will simulate the output performance of the observed installation.

Due to the fact that the on-site produced PV energy was limited during the overcast months of the year it was further investigated a time span with high on-site energy generation, so as to inquire whether a different system dynamic could influence the results substantially. This time period was defined between the dates of the 3rd June 2013 till 11th June 2013, when the global radiation received from the PV panels was reaching peak values. In Figure 6-1 and Figure 6-2 it is depicted the annual PV production as well as the domestic load demand for the one-family house, accumulated with the power demand of charging an E-Vehicle at home. Moreover in Figure 6-3 the respective data are illustrated for the selected characteristic sunny period, which are indicatively chosen to examine batteries' behavior when there is a great surplus of on-site energy generation.

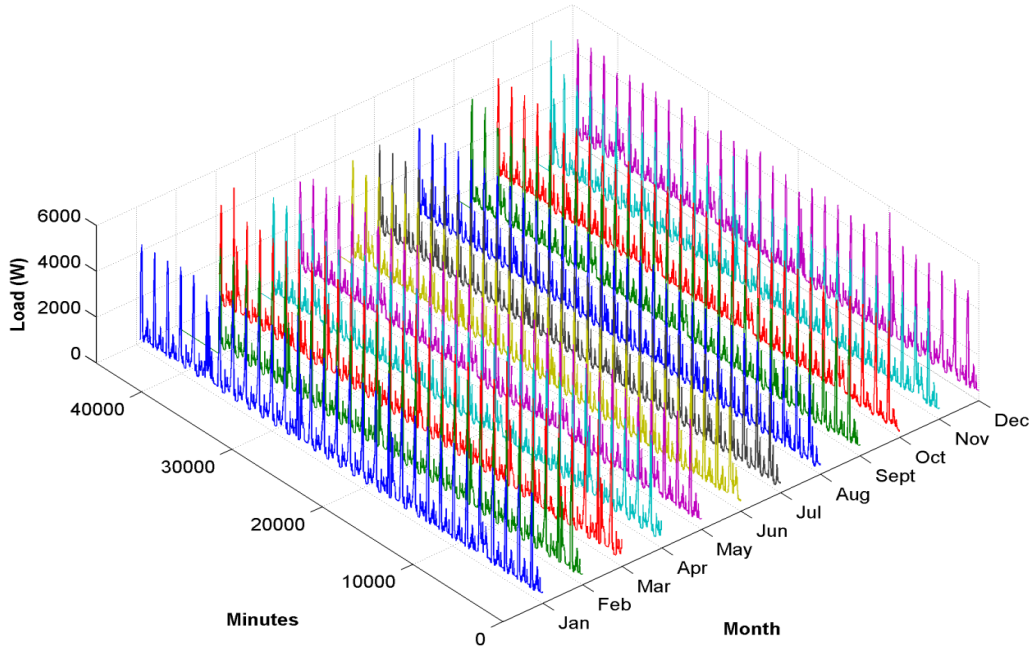

Figure 6-1: A graphical illustration of the Annual Load Profile

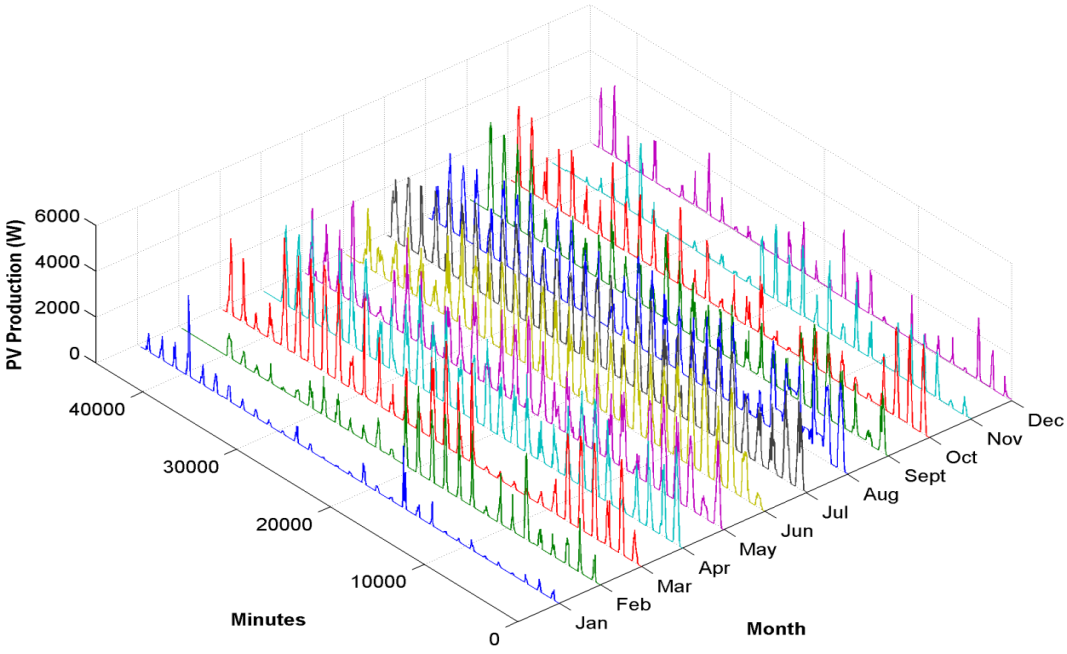

Figure 6-2: A graphical illustration of the annual PV production

From Figure 6-1 and Figure 6-2 it can be recognized that although the chronological trend of the load demand is almost the same among the days, months and seasons, it is not the same case for the PV time series. In a north-central German city the radiation fluctuations correspond to a great diversity in the output power of a PV installation creating a rather

random profile of the $P_{diff}(t) = P_{load}(t) - P_{pv}(t)$, as stated in Equation (5-33). Although during the colder months a generally low irradiation succeeds to cover just a really small amount of the on-site load demand, in the sunnier months the percentage of load coverage may reach 100% with the given sizing and dimensioning of the installed facilities. This can be identified for instance in June 2013 when for nine consecutive days there was a total energy demand which is below the PV generation as it is stated in Table 6-1.

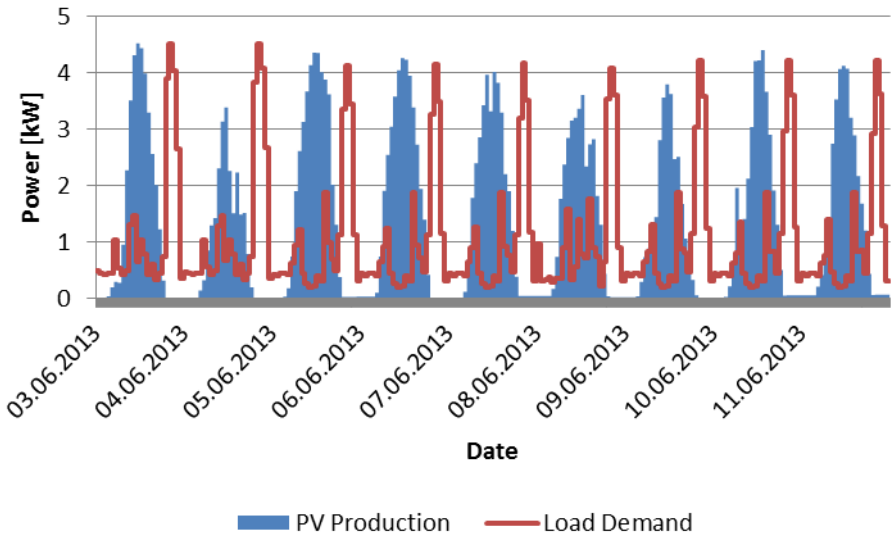

Figure 6-3: A graphical illustration of load demand and the PV production from 3rd till 11th of June 2013

Moreover, it is obvious from Figure 6-3 that the peak of load demand is not synchronized with the peak of PV generation although the peak values are of the same power level and are only shifted in the day. It is noticed that load demand peaks are registered during evening hours when the occupants are usually at home, while the peak PV production is dependent on the global radiation which escalates during noon. It is thus proved to be substantial the role of battery systems for the optimal energy allocation.

In the next Section the results referring to the system with one storage device are thoroughly presented and extensively explained.

A. Outcomes with Lead Acid Battery

After running the simulation for the installation including only the LAB as the one and only storage device of the system the following numerical outputs are extracted and shown in Table 6-1:

Table 6-1: Simulation Energy Results (with LAB)

Energy Metrics	2013	03.06.2013-11.06.2013
Total Energy Demand (House and Electric Vehicle Load)	10.17MWh	227kWh
PV generation	5.21MWh	299kWh
PV energy instantaneously consumed from loads	2.20MWh	86kWh
Battery energy charge	2.30MWh	115kWh
Battery energy discharge	1.80MWh	89kWh
Grid Feed	0.70MWh	96kWh
Grid Draw	6.16MWh	52kWh
Efficiency $\eta_{energy,AC}$	78.26%	77.39%

With a total annual PV generation of 5.21MWh and a yearly load demand of 10.17MWh (almost the double amount) it is considered wise to try and consume the majority of the locally produced energy instead of feeding it to the grid, by taking advantage of the integrated storage devices. Since in this case only one storage system supports the energy apportionment, it was possible to consume 2.20MWh (42%) of the overall renewable energy to cover the instantaneous load demand and 2.30MWh (44%) was fed to the LAB, so as to be used later, when the domestic demand rises. Finally only 0.7MWh (14% of the locally produced energy) is fed to the grid.

However, when the analysis focuses on the period between the 3rd and the 11th of June, the system analytics differentiate substantially. In particular, the PV generation exceeds the respective local demand in the overall examined time period while the instantaneous local demand is directly consuming only the 29% of the locally produced energy. The battery is charged with the 39% of the on-site energy production, and the rest of it (32%) is fed to the grid.

It is thus ascertained that with this dimensioning of systems and such a locally load demand a LAB is proved to be insufficient for exploiting the majority of the PV energy, if the target is to minimize the interaction with the grid when the global radiation favors the peak production. Yet it is not such a great misuse when a greater time frame is observed.

B. Outcomes with Vanadium Redox Flow Battery

The same procedure as abovementioned has been repeated; however in this case study the single storage device was the VRB. Table 6-2 presents the annual results as well as the results for the selected representative sunny period:

Table 6-2: Simulation Energy Results (with VRB)

Energy Metrics	2013	03.06.2013-11.06.2013
Total Energy Demand (House and Electric Vehicle Load)	10.17MWh	227kWh
PV generation	5.21MWh	299kWh
PV energy instantaneously consumed from loads	2.20MWh	86kWh
Battery energy charge	2.43MWh	183kWh
Battery energy discharge	0.92MWh	82kWh
Grid Feed	0.58MWh	29kWh
Grid Draw	7.05MWh	59kWh
Efficiency $\eta_{energy,AC}$	37.86%	44.81%

In this case in a time period of one year the percentage of the direct energy consumption remains as previously unchanged (42%) while the amount of the renewable energy directed to the VRB is equal to the 2.43MWh (47% of the locally produced PV energy). The grid feeding rises to 11%.

When the results of the sunny period are examined, it is noticed again that 86kWh (29%) is fed to the instant load demand and 183kWh (61% of the PV energy) is stored in the VRB. Finally the energy exported to the grid is no more than 10%.

Evaluating the extracted numbers, it can be concluded that the behavior of the VRB is significantly improved when the available power is kept in higher ranges (see Figure 5-2), as it noticed from the 3rd till the 11th of June. This can be inferred also by observing the efficiency values in both cases. An increase of 18% to the efficiency grade is considered the key explanation to the appropriateness of such a system when the domestic renewable sources produce a considerable amount of energy.

Results Evaluation

It is noticed that the efficiency of the LAB is slightly reduced when the battery is storing the excess of energy during the sunny days of the year. This is due to the fact that the efficiency of the battery is curved downwards when the power levels which are fed to the system are

high (see Figure 5-2). Since in the sunny period the produced energy is significantly higher than in the overcast days, it is realistic that the efficiency ratio drops.

On the contrary the exactly opposite performance is remarked by the VRB. In particular, the efficiency during higher power rates is elevated and thus the respective losses are minimized. It is consequently anticipated that the calculated efficiency of the system rises during sunny days (as it is the selected time frame).

When the grid interaction comes under consideration it is detected that when the LAB is the only storage device of the examined system then in both case studies the grid export is higher than that which is attributed to the system with the VRB and the grid import is lower. This is explained from the efficiency of the storage systems. Although the VRB was capable of accepting a higher amount of energy in order to reassign it to the loads when needed, its extended internal power losses are prohibiting the complete reallocation of the stored energy.

Finally, after a quick glance at the charge and discharge values it is found out that although the VRB can receive a higher amount of energy than the LAB, due to its narrow efficiency rate only a smaller percentage of it in comparison to the one delivered from the LAB is reassigned to the domestic loads. On the other hand the LAB is capable of a higher allocation rate and in absolute numbers of a higher discharge amount, since the internal losses are not lavishing the stored energy.

6.2 Simulation Results with Two Storage Systems

After studying the advantages and deficits of the individual battery systems when they operate as unique storage devices in an one family house, it is time to proceed to the examination of the combination of storage equipment, in order to create a hybrid system where the batteries are operating in turn supporting thus the enhancement of the on-site consumption of the locally produced renewable energy. In the next sections the results for year simulations as well as for the representative selected sunny period are presented for the applied control methods, namely the Naive and the Markov based, which are in detail explained in Section 5.

A. Outcomes from Naive Approach

After combining the two storage systems, simulations for one year and for a sunny period of nine days are performed while the chosen control algorithm is based on the naive approach that represents that the optimized outputs will be extracted when the battery system, namely the LAB, is prioritized against the VRB, which is in any case inferior to the first one.

Table 6-3: Annual Simulation Energy Results (Naive Policy)

2013 (Naive Policy)	Vanadium Redox Flow Battery (MWh)	Lead Acid Battery (MWh)
Total Energy Demand (House and Electric Vehicle Load)	10.17	
PV generation	5.21	
PV energy instantaneously consumed from loads	2.20	
Battery energy charge	0.46	2.21
Battery energy discharge	0.17	1.74
Grid Feed	0.33	
Grid Draw	6.06	
Efficiency $\eta_{energy,AC}$ (%)	36.95	78.73

Table 6-4: Simulation Energy Results for Sunny Period (Naive Policy)

03.06.2013-11.06.2013 (Naive Policy)	Vanadium Redox Flow Battery	Lead Acid Battery
Total Energy Demand (House and Electric Vehicle Load)	227 kWh	
PV generation	299 kWh	
PV energy instantaneously consumed from loads	86 kWh	
Battery energy charge	75 kWh	104 kWh
Battery energy discharge	32 kWh	82 kWh
Grid Feed	33 kWh	
Grid Draw	27 kWh	
Efficiency $\eta_{energy,AC}$ (%)	42.66	78.85

If the abovementioned results are interpreted in percentage values, it is recognized that when two storage systems as those integrated into the conceived scenario are combined

under the Naive Policy the annual consumed PV energy amounts to 94% of the locally produced energy and only 6% is fed to the grid based on the annual simulation results for the year 2013 (Figure 6-4). The efficiency of the batteries is slightly improved in comparison to their stand-alone operation as described in the previous sections, verifying the axiom that the combination of two different storage devices is generally offering an overall ascent to the current status of the system.

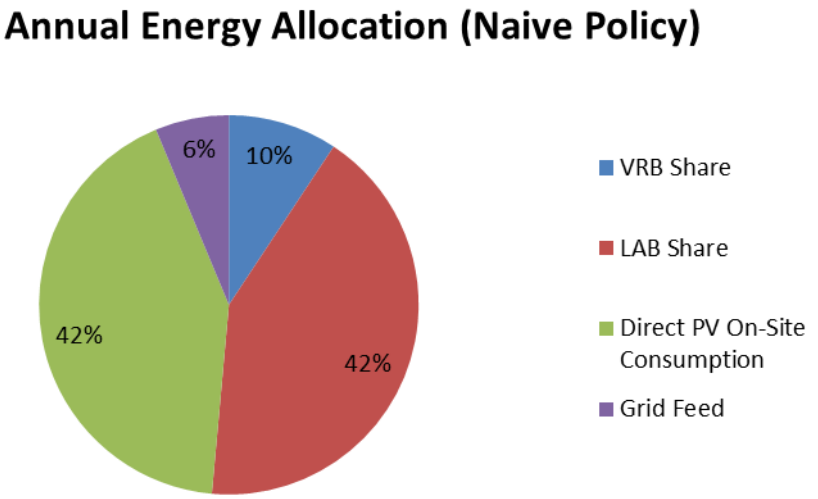

Figure 6-4: Annual Percentage Breakdown of the On-Site Power Generation (Naive Policy)

In the sunny period case the 89% of the on-site PV production was able to be locally exploited and the remaining 11% should be offered to the grid. It is thus detected that the percentage distribution is minor reduced when the PV proportion increases. The efficiency of the two storage systems is analogous to the one observed previously, when the described system is composed only from one battery. In particular, the efficiency grade of the VRB increases and the respective one of the LAB decreases as we switch from annual to sunny period data. The key reason for this lies behind the described efficiency behavior as illustrated in Figure 5-2, where the LAB presents a deterioration of its efficiency at higher power levels while the VRB shows a complete reverse performance.

B. Outcomes from Markov Decision Process Controlling

In this section the same procedure as previously is repeated but the energy management is undertaken by the designed Markov Decision Process, which examines the optimal operation fields of the selected battery systems, i.e. according to power levels demanded/ fed to them, their SOC and their efficiency and consequently the optimal policy is selected.

Table 6-5: Annual Simulation Energy Results (Markov Policy)

2013 (Markov Policy)	Vanadium Redox Flow Battery (MWh)	Lead Acid Battery (MWh)
Total Energy Demand (House and Electric Vehicle Load)	10.17	
PV generation	5.21	
PV energy instantaneously consumed from loads	2.20	
Battery energy charge	1.83	1.10
Battery energy discharge	0.78	0.96
Grid Feed	0.10	
Grid Draw	6.23	
Efficiency $\eta_{energy,AC}$ (%)	42.62	87.27

Table 6-6: Simulation Energy Results for Sunny Period (Markov Policy)

03.06.2013-11.06.2013 (Markov Policy)	Vanadium Redox Flow Battery	Lead Acid Battery
Total Energy Demand (House and Electric Vehicle Load)	228 kWh	
PV generation	299 kWh	
PV energy instantaneously consumed from loads	86 kWh	
Battery energy charge	125 kWh	79 kWh
Battery energy discharge	59 kWh	57 kWh
Grid Feed	9 kWh	
Grid Draw	25 kWh	
Efficiency $\eta_{energy,AC}$ (%)	47.2 (36.74% SOC)	72.15 (84.68% SOC)

If the Markov Policy is applied to HESS then the following findings are noticed: Annually the 98% of the on-site PV generation is locally exploited and only 2% is fed to the grid.

Moreover during a sunny time period the respective proportional shares are almost identical with minor deviations. This conclusion proves that with the Markov Policy it is irrelevant whether or not the PV generation reaches nominal peak values, since the algorithm allocates wisely the arising energy amount, thus ideally serving the designed purpose. As regards the efficiency reliable conclusions cannot be drawn since at the end of the sunny period none of the batteries has the same SOC as it had when we started examining the system behavior. However, at a quick glance it is again confirmed that the higher the power rates, the lower the LAB energy efficiency and the higher for the VRB.

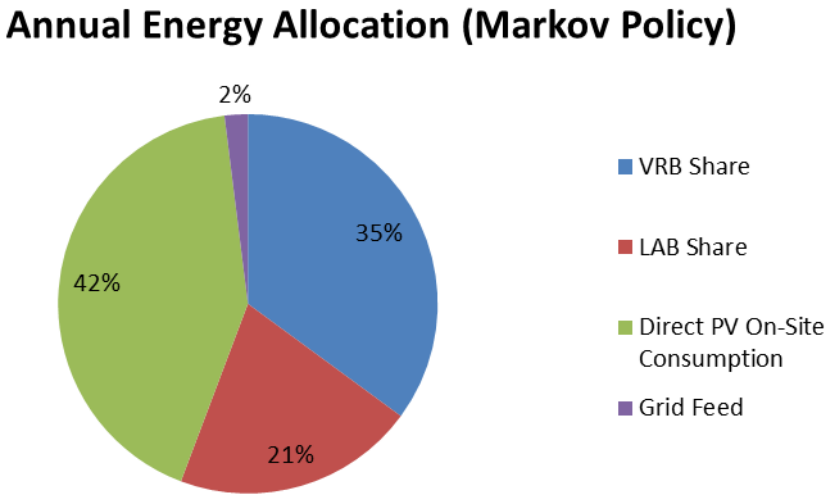

Figure 6-5: Annual Percentage Breakdown of the On-Site Power Generation (Markov Policy)

Results Evaluation

When we cross-examine the arising annual results from the two applied techniques it is reconfirmed the so far adopted argue that an optimal design of a control algorithm contributes to a wiser energy allocation in a HESS. In particular, none of the battery systems is functioning poorly or underperforms, exploiting at its maximum the strengths of its battery. Although at a quick glance it was considered dummy to intervene in the way the storage facilities are being charged or discharged since the LAB is by far the most effective, it was ascertained that this scenario would not lead to an optimal energy allocation. Great deviations are not clearly observable, due to the overall poor efficiency grade of the VRB when low power ranges ought to be served. Grid draw values affirm the poor behavior of such a peculiar storage facility, since the Markov Policy does not guarantee the overall lower losses. Nevertheless the grid export, which is lower when Markov Policy is applied, still offers a better energy balance to the poor reaction of the VRB.

If we concentrate on the representative sunny period time the arising energy flow confirms the initial statement of this dissertation, namely a well-designed energy management algorithm provides the optimal solution for the energy assignment in a dwelling with an E-Vehicle, a PV installation and a combination of two storage devices. The efficiency

enhancement of the VRB, which occurs due to the fact that larger energy quantities ought to be managed, leads to a grid interaction reduction and to a higher self-energy consumption.

6.3 Evaluation & Discussion of Results

As explained and in detail presented in Section 3.3.5 the evaluation criteria for the applied method are two indexes which describe the grid exchange and the consumption grade of the on-site PV energy. These are the grid interaction index and the supply cover factor and their role is to confirm or reject the claim that the Markov Policy outperforms the Naive. In Table 6-7 and Table 6-8 the annual outputs as well as the results from the selected sunny period are presented. It is identified that while annually the grid interaction index does not substantially differentiate between the two methods, the supply cover factor is 5% higher when the Markov Policy is applied.

Table 6-7: Evaluation Criteria (2013)

2013	Naive Policy	Markov Policy
Supply Cover Factor	92.80%	97.46%
Annual grid interaction index	20.99%	20.78%

If we focus though on the sunny period time then the differences escalate and it becomes more obvious why there is a need for a control algorithm when a hybrid system operates. A 10% higher supply factor and a 5% lower grid interaction index confirm the hypothesis, that a wisely designed energy management system may enhance the performance of a HESS which is composed from a renewable energy source, domestic loads and two different storage facilities.

Table 6-8: Evaluation Criteria (Sunny Period)

03.06.2013-11.06.2013	Naive Policy	Markov Policy
Supply Cover Factor	85.77%	95.77%
Annual grid interaction index	17.77%	12.46%

Trying to better assess the adequateness of the designed technique the results for the two evaluation criteria are examined per month and graphically illustrated in Figure 6-6 and Figure 6-7. In this spectrum it becomes clearer that the developed methodology delivers better outputs and this is more obvious during sunnier months of the year when the PV generation does not show great fluctuations. In particular, the supply cover factor is almost identical for the cold months (November, December, January) while for the rest of the months lower or greater differentiations are more than evident. It is thus observed that the higher the on-site power production, the greater the rate of the consumed amount from the local loads when Markov policy is applied. This conclusion is theoretically grounded, since the VRB is operating more efficient, being able to receive greater proportions of renewable energy, and supporting the LAB in terms of replenishing its inadequateness in capacity. Furthermore, the grid interaction index is respectively reduced in sunnier months and when

higher levels of solar radiation reach the PV panels if the Markov policy is adopted, thus succeeding a limited random exchange with the public grid, while avoiding to stress it.

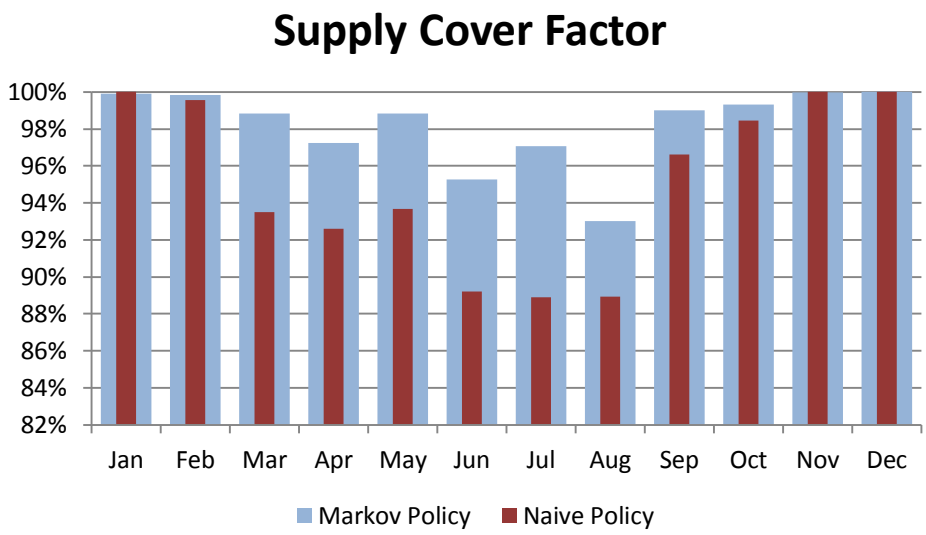

Figure 6-6: Monthly Illustration of Calculated Supply Cover Factor

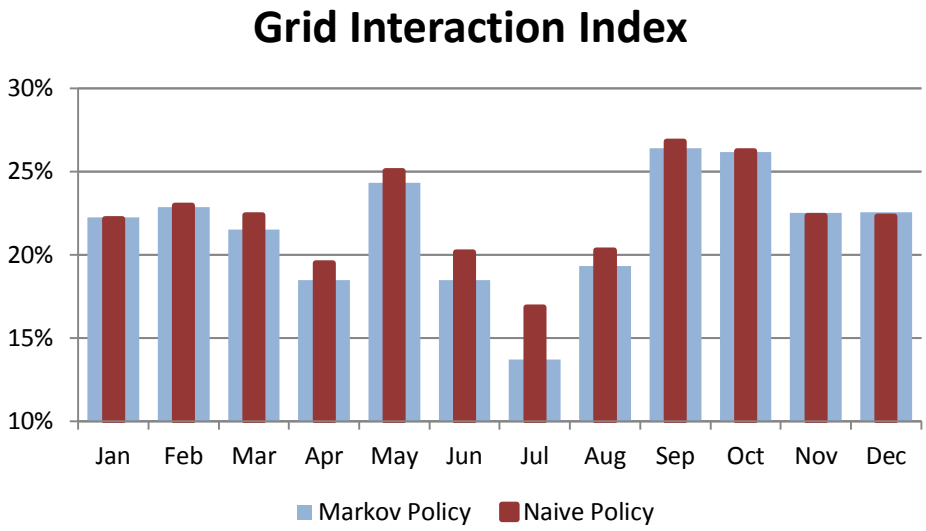

Figure 6-7: Monthly Illustration of Calculated Grid Interaction Index

When the overall system energy efficiency ratio (EER) is considered the results attest to the efficiency rates depicted in Figure 5-2. In order to estimate this, the consumed energy over the period of one year, which corresponds to the energy of the domestic load demand, is compared to the energy fed to the loads, either from the grid or from the PV installation, as shown from Equation (6-1):

$$EER = \frac{E_{House} + E_{Car}}{E_{PV} + E_{Grid_{Draw}}} \cdot 100\% \quad \textbf{(6-1)}$$

The respective ratios for the two examines cases, namely the Markov and the Naive approach, for the year 2013 are then subsequently presented in Table 6-9:

Table 6-9: Overall System Energy Efficiency Ratio

2013	**Naive Approach**	**Markov Policy**
Overall System Energy Efficiency Ratio	90.23%	88.90%

It can be noticed that the EER of the system is slightly worse when the Markov policy is applied to allocate the available excess of the locally produced energy or to serve the on-site load demand. However, this conclusion should not be false interpreted, questioning the optimality of the designed algorithm. The result is fully explained from the curves presented in Figure 5-2. In particular, after applying the Markov policy the system optimally allocates the respective power so as to take advantage of both storage systems, while its logic is not based on the minimization of the losses but on the maximization of the consumption of the on-site produced energy which subsequently leads to the reduction of the fluctuations that occur when the grid is commanded to be the exclusive electricity player. Thus, although the Markov policy delivers a higher self-consumption rate, the VRB is in this case more often in operation and subsequently the overall losses are increased since this battery has a substantially lower efficiency grade than the LAB.

As for the self-energy consumption, by examining the four individual cases that are previously described, namely the system composed only from one battery, either the LAB or the VRB, and the HESS composed of two batteries and operated by two different management policies, the Naive and the Markov, it is concluded that the higher rate is accomplished when two battery systems are in operation according to the Markov Policy. In particular, when the annual energy balance is considered and estimated, which is composed of the share of the direct on-site energy generation from the instant loads, and the share allocated to the battery systems, it is verified that the HESS with Markov policy succeeds a 98% rate of self-energy consumption. The same system, controlled over the Naive policy reaches 94% of self-energy consumption and when the examined concept with only one storage installation is considered rates of 91% and 87% are respectively achieved for the LAB and VRB configuration.

If the respective proportion is calculated for the sunny period which is indicatively selected it is noticed the system configuration with only the LAB for storage purpose is considered almost insufficient with the current dimensioning, since only a 67% of the locally produced energy can be directly consumed from the on-site demand. Though, when the battery is replaced from a VRB then the respective rate rises to 90%, showing the appropriateness of such a storage system when the renewable production is maintained at high levels. If two storage systems are combined, an 8% raise in self-energy consumption is recorded confirming and validating the original assertion that an employment of a suitably designed storage control policy improves substantially the efficiency of the complete system.

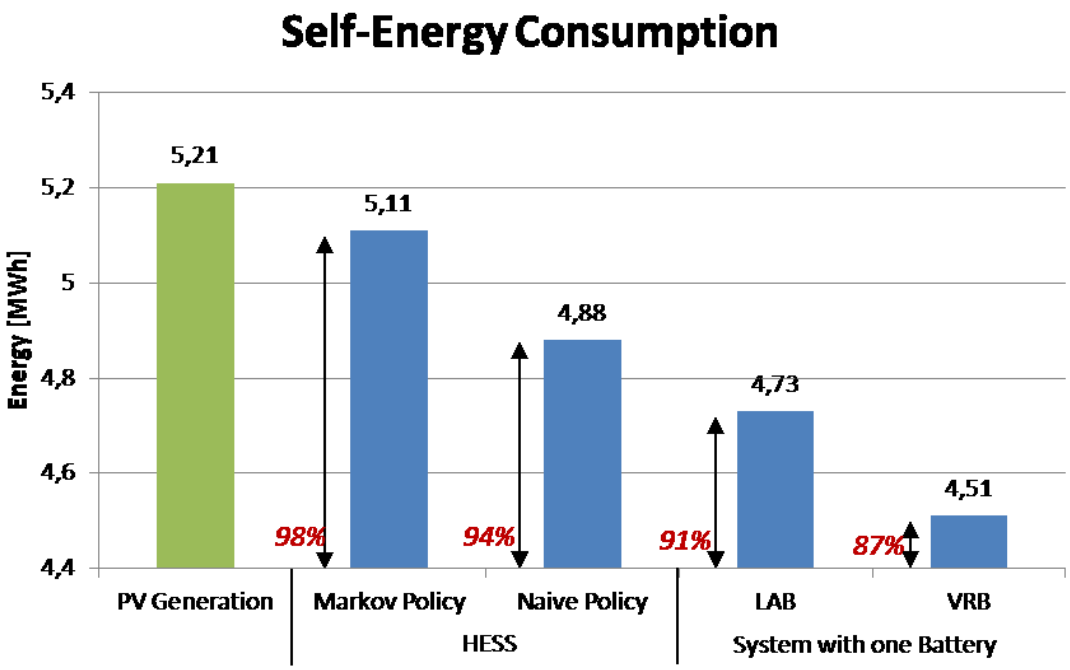

Figure 6-8: Annual Rate of Self-Energy Consumption for 4 Case Studies

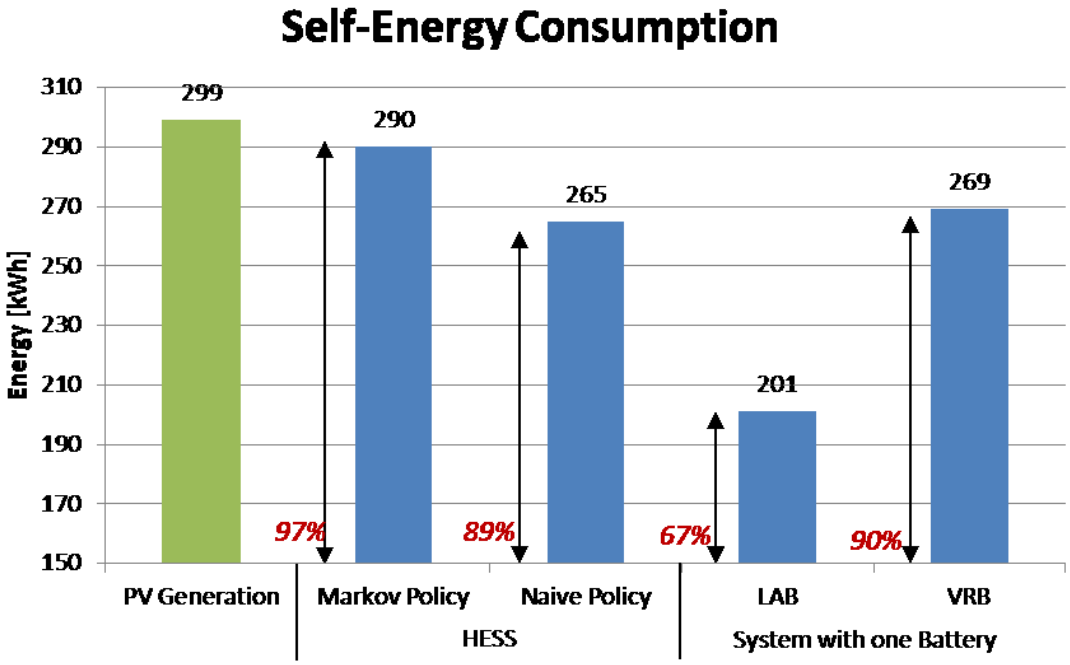

Figure 6-9: Rate of Self-Energy Consumption for 4 Case Studies during a Sunny Period

Finally, the energy allocation per month is distributed in the following two diagrams, showing the effectiveness of the applied Markov policy in optimal exploitation of the available facilities. It is therefore identified that the greater amount of energy has been assigned to the VRB (illustrated with the purple color bar) when the Markov Policy is deployed, leading to a more thoughtful operation of the LAB and thus minimizing its operating cycles and increasing the battery life. In parallel it is detected that during a really overcast month, as January is, an installation with two storage systems is not contributing

substantially to the rate of the self-energy consumption as only a really narrow proportion of energy (17%) can be further allocated to the storage systems in both cases. In July however 66% of the on-site PV generation is assigned to the storage systems if Markov Policy is applied and 59% if the Naive Policy is used. Moreover, as regards the frequency that an order is given by the energy management unit for taking an action, the LAB system is mandated 26% of the overall given orders to operate (charge or discharge), the VRB 48%, and 26% of the ordered actions are assigned to the grid if the Markov Policy is applied, while the rates for Naive Policy are 39%, 36% and 25% respectively. It is obvious that the LAB is commanded more often when Naive policy is applied as expected since priority is given to the battery with the overall higher efficiency grade. On the other hand, the VRB system is favored to operate more frequently when the Markov policy is chosen. The grid is in both cases almost equally in frequency strained.

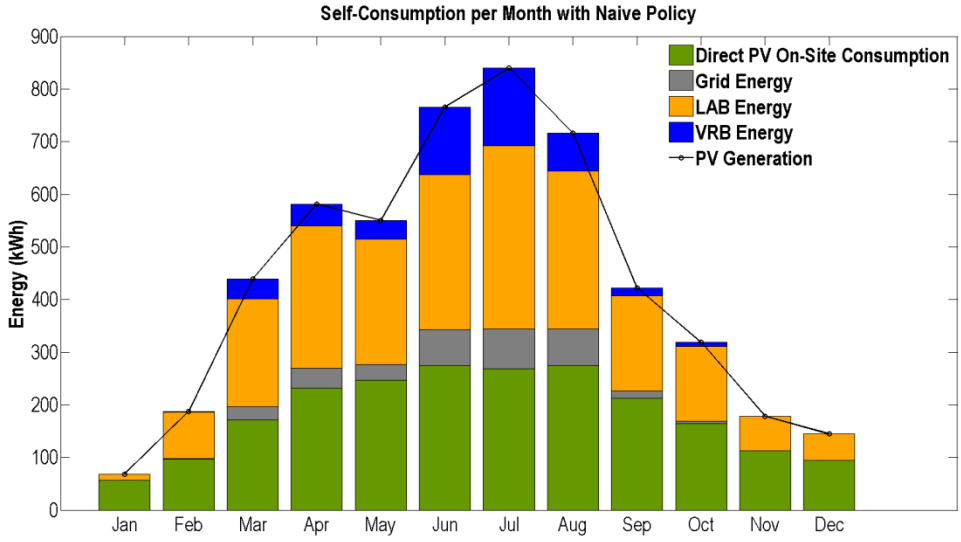

Figure 6-10: Monthly Energy Allocation of the On-Site Generation (Naive Policy)

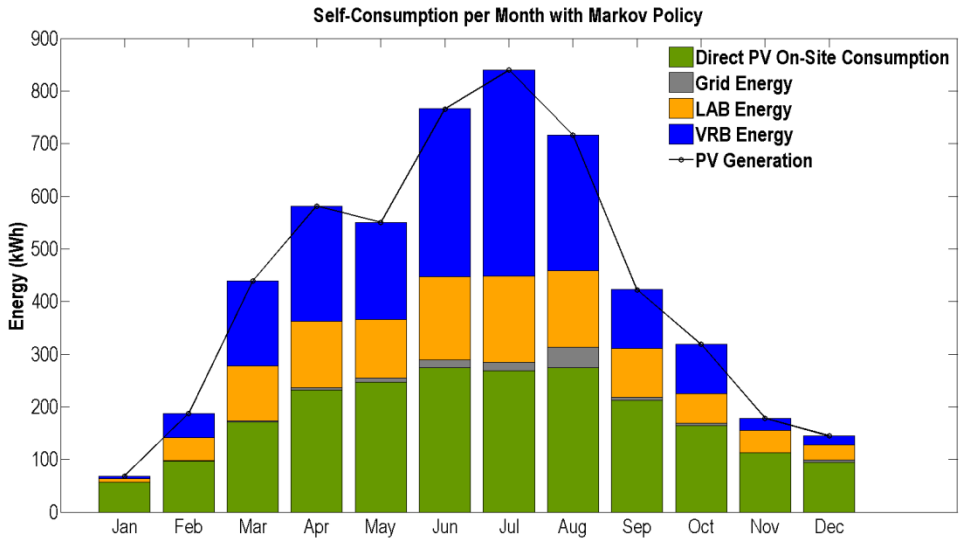

Figure 6-11: Monthly Energy Allocation of the On-Site Generation (Markov Policy)

7 Conclusions & Perspective

The evolution of the building sector in the context of the energy market renovation after the fierce introduction of the renewable energy sources as small scale installations have set as critical and urgent the reformation of the existent energy allocation. The repeatedly grid feed of energy from smaller domestic renewable systems has strained its stability while the radically reduced feed-in-tariffs offer no more incentive in selling the locally produced energy to the grid operators. The potential in self-energy consumption when storage facilities are missing from a household installation is particularly low, due to the fact that the peak of load demand is not timed to coincide with the peak of PV generation although the occurring peak power values range among the same power levels and are only shifted in the day. This fact sets the implementation of a battery connected facility as essential if target is to minimize the randomness in the energy exchange between the grid and the building. Furthermore, the establishment of the electromobility as the next step in the transfer sector has differentiated lately the load profiles of households. The combination of the abovementioned components would be an ideal application to explore optimally the on-site power generation and would offer an improvement in the decentralization of the power sector.

The integration of one battery system in a household is already a common tactic nowadays and is considered an extensively explored field in the literature. The coupling though of two different types of storage systems is not thoroughly investigated and is intrinsically interesting to be examined. Such a pairing of battery systems is mentioned in the nomenclature as a hybrid energy storage system (HESS) since two different types of storage devices are combined to operate in turn. It is explicitly of greater interest how an HESS reacts when the two chosen storage systems operate alternately and not in parallel and simultaneously as it is until now preferred and registered in the literature.

In the frame of this thesis it was attempted to investigate the performance of an HESS which is integrated in a one-family house which is located in a central north region of Germany. The HESS is composed of a renewable energy source that partially covers the local energy demand which occurs from the daily load needs of a four people household and an E-Vehicle that is used for commuting reasons of the family and always charges at home and of two storage devices that are operated in order to increase the self-energy consumption rate and reduce the grid interaction. In particular, the previously referred systems are two PV plants of 5.1kWp and 1.02kWp power, a lead acid battery (LAB) system of 22 kWh capacity, a vanadium redox flow battery (VRB) of approximately 20 kWh capacity and the synthesis of the domestic load demand aggregated by the load demand of charging the EV. All of this facilities exist at the premises of the Ostfalia University of Applied Science in Wolfenbüttel and are a smaller configuration of a more complex installation.

Such a topology was until now not fully reported or deeply examined in the existing literature although similar attempts have already been described, but in these cases one of the main storage facilities which was preferred to be integrated in the HESS was a supercapacitor. The main part of this thesis is the design of a control algorithm which decides and commands the storage systems when to operate, namely when to charge or discharge. Such a management framework for controlling the storage systems was till now

trivially explored while the various techniques that were applied were not appropriate for a solution approach for the designed case study. In this thesis, the advantages of a combined VRB/LAB storage facility in the domestic field were detailed reported and the performance of such an HESS was also juxtaposed to simpler syntheses, where only one storage device was each time available.

Consecutively, the main research question which was addressed has been formulated as follows:

- *"How can the energy flow in a single-family house be managed efficiently, so as to maximize the self-consumption of the produced renewable energy and minimize the grid interaction by controlling two different stationary storage systems?"*

So as to handle and in detail examine the primary research problematic three further subquestions had to be tackled and analysed. These referred to the identification of the appropriate models to represent precisely the existing facilities, the detection of the optimal method to be applied in order to implement the selected energy management policy so as to control the charging and discharging process of two stationary storage systems and ultimately the evaluation of the designed technique.

In particular, these are formulated as follows:

- *"Which are the appropriate models to represent the existing facilities?"*
- *"Which method is optimal to be applied in order to implement the selected energy management policy so as to control the charging and discharging process of two stationary storage systems?"*
- *"How can the chosen technique be evaluated?"*

In the whole process great importance has been attached to the plausibility of the input and extracted data, by applying the management algorithm on a designed block of models which represents precisely the operation of the abovementioned facilities, that are physically also integrated in the Energy Park of the Ostfalia University. These models were conceived and created in the Matlab/ Simulink environment and a joint block system was generated. With models that are explicitly designed to depict the exact performance of real devices, but incorporating also the generalization factor, it was prevented to create an ideal system with null losses that most of the case studies apply in the literature. On the contrary, the system operation is fully analogous to the exact devices of the utilized test bed, which nevertheless correspond to a great variety of the existing market available and commercially mature systems.

The main research topic which was handled in the current study was the development of the energy management system which would be considered a strategic approach to charge and discharge the given battery systems in an optimal and efficient way. The choice of the appropriate management technique emerged from an extensive literature review and from the dynamic inputs that were to be integrated in its logic, according to the degree of influence they had on the extracted decision output. It has been advocated that the control policy should be based on the Markov Decision Process, a technique stemming from the reinforcement learning field which is commonly used to solve problems with stochastic dynamics. This method is also appropriate for problems which require a decision making at

regular time intervals as in the examined case study. The main integrated variables that were considered in the design process regarded the power difference between the instant on-site PV power generation and the direct load demand, the SOC of the storage devices and the efficiency of these at the respective power levels. The described method was designed in such a way that would also be applicable in any other hybrid storage system where the efficiencies of the batteries are not considered constant, though they are dependent on the SOC and the power and are in advance known, while the financial aspect was neglected.

So as to evaluate the extracted outputs a benchmark method had been applied, which is based on the performance of the two storage devices, namely their efficiency grade under various charge/discharge power levels. In addition, the comparative metrics which were computed for the designed and the benchmark method are two factors which are related to the self-energy consumption and the grid interaction, i. e. the supply cover factor and the grid interaction index.

The simulation process included the examination of two research periods. The first one is the reference year 2013 and real registered data of temperature, global radiation and cloud factor were used as input so as to acquire a plausible depiction of the conceived scenario. Due to the fact that the PV generation remains limited for an extended time span during a year in the examined region it was decided to examine system's behavior and performance for an indicative sunny period. In this framework nine consecutive sunny days (from the 3rd until the 11th of June 2013) were selected and the simulation process was repeated.

In addition the observed case studies were divided into two categories; the first referred to a system with only one storage system as backup solution and the second referred to the complete HESS as it was initially presented. Target was to compare the appropriateness of the two arrangements as well as to evaluate how far a control technique may improve the performance of an HESS.

In the one battery system topology, if the chosen battery was the LAB system 86% of the locally produced energy was consumed locally in the time frame of one year whereas when the VRB was the one only storage device of the system the overall self-energy consumption rose to 89%. The respective proportions for the sunny period were 68% and 90%. It is obvious that the LAB is sufficiently scaled for long-term use, though when the same concept would be transferred in a sunnier region this storage device would be inadequate. On the contrary the VRB operates in such a way that allows almost the equal percentage of self-energy consumption regardless of the on-site energy generation.

When the complete HESS was considered, there was an increase in these ratios since a higher capacity offered a higher flexibility to the allocation mechanism. The application of the Naive policy which is related to the benchmark method, and is extracted from the efficiency of the two storage devices, yielded a renewable energy consumption of 94%. When though the control technique designed according the Markov Decision Process theory is preferred then the respective annual ratio rose to 98%. Under high global radiation circumstances (during the selected sunny period time) the percentage dropped to 89% for the Naive policy while for the designed Markov technique remained unaffected. It is thus proved the superiority of the applied method towards a trivial approach and the necessity of

a control strategy so as to succeed a high degree of optimal use of the considered storage devices.

The juxtaposing of the two case studies (the one storage system case and the HESS) illustrated also the weakness of a stand-alone LAB to support such a synthesis of loads and decentralized production when there is increased on-site generation, while the VRB system proved to be more flexible, even in the domestic field in which is not yet extensively employed.

In addition, the calculation of the evaluation criteria which were the two factors that depicted the self-energy consumption and the grid interaction support the initial claim that two different storage devices which must operate in turn to serve the same domestic installation, should be externally controlled in order to fully utilize their attributes. For both the annual and the sunny period results it is determined that an intelligent designed algorithm offers a better exploitation of the self-produced energy, since a higher score in self-energy consumption is accomplished while the grid interaction is reduced.

Future Work

Although the complete mechanism has been tested and simulated with input data, that represent to a great extent the real demand, generation and responses of the individual components, it would be of great interest if the designed architecture could be additionally tested in the real facilities so as to further examine the plausibility of the simulated results. The integration of the examined concept and control technique in the context of a project would offer valuable information on the suitability of the designed method and would reveal perhaps unconsidered aspects.

In addition a sensitivity analysis of succeeding an ideal scaling of all the facilities analogous to the needs of the domestic load demand could be also proved significant for extracting conclusions for topologies with the same morphology but with different sizing. However in this case, a possible theoretical scaling of the integrated components of the system may involve risks and may end up to a misleading output, since it is possible that not all the considered parameters are allowed to be respectively scaled. Nevertheless, an analysis in a practical context and a juxtaposition of the outcomes would be meaningful and is open for future research.

References

1. European Commission. European Climate Change Programme, EU Action, European Commission. Link: http://ec.europa.eu/clima/policies/eccp/index_en.htm,
2. The National People's Congress of the People's Republic of China. The Renewable Energy Law of the People's Republic of China. 2009. Link: http://www.npc.gov.cn/englishnpc/Special/CombatingClimateChange/2009-08/25/content_1515301.htm
3. Bundesministerium für Wirtschaft und Energie (BMWi). Die Energie der Zukunft, Erster Fortschrittsbericht zur Energiewende, Bundesministerium für Wirtschaft und Energie (BMWi), Berlin, Germany, December 2014.
4. International Energy Agency. Transition to Sustainable Buildings Strategies and Opportunities to 2050, OECD/IEA, Paris, France, 2013.
5. D. Ürge-Vorsatz, N. Eyre, P. Graham, D. Harvey, E. Hertwich, Y. Jiang, C. Kornevall, M. Majumdar, J. E. McMahon, S. Mirasgedis, S. Murakami, A. Novikova. Energy End-Use: Building. In Global Energy Assessment - Toward a Sustainable Future, Cambridge University Press, Cambridge, UK and New York, NY, USA and the International Institute for Applied Systems Analysis, Laxenburg, Austria, pp. 649-760, 2012.
6. German Solar Industry Association (BSW-Solar). Statistische Zahlen der deutschen Solarstrombranche (Photovoltaik), German Solar Industry Association (BSW-Solar), June 2015.
7. Bundesministeriums der Justiz und für Verbraucherschutz. Gesetz für den Ausbau erneuerbarer Energien (Erneuerbare-Energien-Gesetz - EEG 2014), Bundesministeriums der Justiz und für Verbraucherschutz, Juli 2014 (BGBl. I S. 1066).
8. Degressions- und Vergütungssätze Juli bis September 2016, Bundesnetzagentur, Stand: 31.08.2016. Link: http://www.bundesnetzagentur.de/cln_1431/DE/Sachgebiete/ElektrizitaetundGas/Unternehmen_Institutionen/ErneuerbareEnergien/Photovoltaik/DatenMeldgn_EEG-VergSaetze/DatenMeldgn_EEG-VergSaetze_node.html;jsessionid=E8E8B4B4BD2F6A92322C2480D76BE3B8#doc405794bodyText4
9. C. Kost, J. N. Mayer, J. Thomsen, N. Hartmann, C. Senkpiel, S. Philipps, S. Nold, S. Lude, T. Schlegl. Stromgestehungskosten Erneuerbare Energien Studie, Fraunhofer-Institut für Solare Energiesysteme ISE, Freiburg, Germany, November 2013.
10. J. Weniger, T. Tjaden, V. Quaschning. Solare Unabhängigkeitserklärung, Photovoltaik, Oktober 2012
11. H. Wirth. Recent Facts about Photovoltaics in Germany, Fraunhofer ISE, Freiburg, Germany, 2016.
12. Bundesverband Solarwirtschaft. Infos zur neuen förderung von Solarstrom – Speichern, Informationspapier des BSW-Solar, Bundesverband Solarwirtschaft. Stand: 29.2.2016.
13. Bundesministerium für Umwelt, Naturschutz, Bau und Reaktorsicherheit – BMUB. Kurzinfo Elektromobilität, BMUB, Stand: 28.09.2016. Link: www.bmub.bund.de/P706/

14. K.-P. Kairies, D. Haberschusz, J. v. O., J. Strebel, O. Wessels, D. Magnor, J. Badeda, D. U. Sauer. Jahresbericht zum Speichermonitoring entstand im Rahmen des Forschungsvorhabens Wissenschaftliches Mess¬ und Evaluierungsprogramm Solarstromspeicher (WMEP PV¬Speicher), Institut für Stromrichtertechnik und Elektrische Antriebe der RWTH, Aachen, 2016.
15. C. Daniel, J. O. Besenhard. Handbook of Battery Materials, 2. ed. Wiley-VCH Verlag GmbH & Co. KGaA., Weinheim, Germany, 2011.
16. E. Jimenez. Resource Allocation And Load-Shedding Policies Based On Markov Decision Processes For Renewable Energy Generation And Storage, Master Thesis, University of Central Florida, Orlando, Florida, USA, 2015.
17. X. Qiu. Modeling and optimization of energy storage system for microgrid, PhD Thesis, Missouri University of Science and Technology, Missouri, USA, 2014.
18. L. Baumann. Improved System Models for Building-Integrated Hybrid Renewable Energy Systems with Advanced Storage: A Combined Experimental and Simulation Approach, PhD Thesis, De Montfort University, Leicester, UK, 2015.
19. P. Stenzel, J. Linssen, J. Fleer. Impact of Different Load Profiles on Cost Optimal System Designs for Battery Supported PV Systems, presented in the 7th International Conference on Applied Energy – ICAE2015, Energy Procedia 75, 1862 – 1868, 2015.
20. J. Dickert, T. Heß, P. Schegner, C. Felsmann. Electrical Design of an Efficiency House Plus, presented in the 3rd IEEE PES Innovative Smart Grid Technologies Europe (ISGT Europe), Berlin, Germany, 2012.
21. R. Bellman. A Markovian decision process, Journal of Mathematical Mechanics, 6 (5), pp. 679–684, 1957.
22. C. Guan, Y. Wang, X. Lin, S. Nazarian, M. Pedram. Reinforcement Learning-Based Control of Residential Energy Storage Systems for Electric Bill Minimization, Consumer Communications and Networking Conference (CCNC), 12th Annual IEEE, Date of Conference: 9-12 Jan. 2015, IEEE, 2015.
23. E. Boggasch, M. Heiser, R.D. Patzelt. Busgestütztes Energiemanagement eines Verbundes regenerativer Energieanlagen am Institut für Verbrennungstechnik und Prozessautomation an der Fachhochschule Braunschweig/Wolfenbüttel, AGIP-Forschungsvorhaben F.A.-Nr. 2003.525 Report, Wolfenbüttel, Germany, 2006.
24. Strom-Report. Photovoltaik in Deutschland, Link: www.Strom-Report.de.
25. Bundesministerium für Wirtschaft und Energie (BMWi). Zeitreihen zur Entwicklung der erneuerbaren Energien in Deutschland unter Verwendung von Daten der Arbeitsgruppe Erneuerbare Energien-Statistik (AGEE-Stat) (Stand: August 2016), BMWi, Berlin, Germany.
26. K. Schneider. Low-cost wafers for solar cells, Research News / 1.10.2015, Fraunhofer Institute for Solar Energy Systems ISE, Freiburg, Germany, 2015.
27. Photon International. Entwicklung der mittleren Wirkungsgrade von PV-Module auf Basis von mono- und multikristallinen Zellen nach dem Jahr der Markteinführung, Daten aus Photon International 2014-02.
28. Kelly Pickerel. What are the different types of solar modules?, Solar Power World, July 2015, Link: https://www.solarpowerworldonline.com/2015/07/what-are-the-different-types-of-solar-modules/

29. Energie-Experten. Wirkungsgrad von Solarmodulen im Vergleich, Link: http://www.energie-experten.org/erneuerbare-energien/photovoltaik/solarmodule/wirkungsgrad.html
30. C. F. Gay, J.H. Wilson, J.W. Yerkes. Performance advantages of two-axis tracking for large flat-plate photovoltaic energy systems, in: Photovoltaic Specialists Conference, 16th, San Diego, CA, USA, September 27-30, 1982, New York, Institute of Electrical and Electronics Engineers, pp. 1368-1371, 1982
31. D.L. King, W.E. Boyson, J.A. Kratochvil. Analysis of factors influencing the annual energy production of photovoltaic systems, Photovoltaic Specialists Conference, 2002, Conference Record of the Twenty-Ninth IEEE: pp. 1356–1361, 2002.
32. SMA Regelsysteme GmbH. Sunny Boy 2000, Technische Beschreibung, SMA Regelsysteme GmbH, 2000.
33. SMA Solar Technology AG. Sunny Boy 1200, Installationsanleitung, SMA Solar Technology AG, 2000.
34. X. H. Nguyen, M. P. Nguyen. Mathematical modeling of photovoltaic cell/module/arrays with tags in Matlab/Simulink, Environmental Systems Research 4:24, 2015.
35. T. Glotzbach. Ein Beitrag zur mathematischen Charakterisierung von Photovoltaik-Dünnschichttechnologien auf Basis realer I/U-Kennlinien, Ph.D Thesis, Kassel University Press, Kassel, Germany, December 2010.
36. D. Rekioua, E. Matagne. Modeling of Solar Irradiance and Cells, Optimization of Photovoltaic Power Systems, Chapter 2 of Green Energy and Technology, Springer-Verlag, London, UK, 2012.
37. K. Nishioka, N. Sakitani, Y. Uraoka, T. Fuyuki. Analysis of multicrystalline silicon solar cells by modified 3-diode equivalent circuit model taking leakage current through periphery into consideration, Solar Energy Materials and Solar Cells, 91, pp. 1222–1227, 2007.
38. J. A. Gow, C. D. Manning. Development of a photovoltaic array model for use in power-lectronics simulation studies, in: IEE Proceedings - Electric Power Applications, 146, pp. 193–200, 1999.
39. N. Pongratananukul, T. Kasparis. Tool for automated simulation of solar arrays using general-purpose simulators, in: Proceedings 2004 IEEE Workshop on Computers in Power Electronics, Urbana, IL, USA, pp. 10–14, 2004.
40. H. Tian, F. Mancilla-David, K. Ellis, P. Jenkins, E. Muljadi. A Detailed Performance Model for Photovoltaic Systems, National Renewable Energy Laboratory, to be published in the Solar Energy Journal, Journal Article, NREL/JA-5500-54601, July 2012.
41. O. Perpiñan, E. Lorenzo, M. A. Castro. On the calculation of energy produced by a PV grid-connected system, Progress in Photovoltaics: Research and Applications, 15, pp. 265–274, May 2007.
42. B. Borowy, Z. Salameh. Methodology for the optimally sizing the combination of a battery bank and PV array in a wind/PV hybrid system, IEEE Transactions on Energy Conversion, 11, 1996.
43. A. D. Jones, C. P. Underwood. A modeling method for building-integrated PV systems, 23, Building Services Engineering Research and Technology, 70, pp. 167-177, 2002.

44. M.R. Patel. Wind and solar power systems, CRC Press LLC, Boca Raton, Chapter 9: Photovoltaic Power Systems, 1999.
45. X. Luo, J. Wang, M. Dooner, J. Clarke. Overview of current development in electrical energy storage technologies and the application potential in power system operation, Applied Energy, 137, pp. 511–536, 2015.
46. IEC. Electrical Energy Storage, White Paper, International Electrotechnical Commission, Switzerland, 2011.
47. M. J. Baumann. A Constructive Technology Assessment of Stationary Energy Storage Systems: prospective Life Cycle orientated Analysis, IET Working Papers Series, No. WPS01/2013, IET/CESNOVA, Portugal, 2013.
48. REA-Renewable Energy Association. Energy Storage in the UK, An Overview, REA Renewable Energy Association, London, UK, Winter 2015/16.
49. A.Z. Weber, M.M. Mench, J.P. Meyers, P.N. Ross, J.T. Gostick, Q. Liu. Redox flow batteries: a review. Journal of Applied Electrochemistry, 41, pp. 1137–64, 2011.
50. H. Chen, T. N. Cong, W. Yang, C. Tan, Y. Li, Y. Ding. Progress in electrical energy storage system: A critical review, Progress in Natural Science, 19, pp. 291 – 312, 2009.
51. F.A. Farret, M.G. Simões. Integration of alternative sources of energy. John Wiley & Sons Inc., pp. 262–300, 2006.
52. R. Carnegie, D. Gotham, D. Nderitu, P. V. Preckel. Utility Scale Energy Storage Systems: Benefits, Applications, and Technologies, State Utility Forecasting Group, June 2013.
53. Bechtel National Inc. Handbook for Battery Energy Storage in Photovoltaic Power Systems – Final Report, Sandia Laboratories, CA, USA, 1980.
54. M. Baumann, B. Zimmermann, H. Dura, B. Simon, M. Weil. A comparative probabilistic economic analysis of selected stationary battery systems for grid applications, International Conference on Clean Electrical Power Renewable Energy Resources Impact, Alghero, Sardinia – Italy, 2013.
55. M. Beaudin, H. Zareipour, A. Schellenberglabe, W. Rosehart. Energy storage for mitigating the variability of renewable electricity sources: An updated review, Energy for Sustainable Development,14, pp. 302 –314, 2010.
56. P. Radcliffe, J. S. Wallace, L. H. Shu. Stationary Applications of Energy Storage Technologies for Transit Systems, 2010 IEEE Electrical Power & Energy Conference, 25-27 Aug. 2010, Halifax, NS, Canada.
57. HyperPhysics. Lead-Acid Battery, The chemistry of the production of a voltage by a lead-acid battery, HyperPhysics, Link: http://hyperphysics.phy-astr.gsu.edu/hbase/electric/leadacid.html#c2
58. P. Kügler. Aufbau eines Modells zur Abbildung des geprüften Batteriesystems der Fach-hochschule Ostfalia Wolfenbüttel in MATLAB/Simulink, Bachelor Thesis, Ostfalia Hochschule für angewandte Wissenschaften, Wolfenbüttel, Germany, 2014.
59. G. Albright, J. Edie, S. Al-Hallaj. A Comparison of Lead Acid to Lithium -ion in Stationary Storage Applications, AllCell Technologies LLC, March 2012.
60. EDC (solar-wind.co.uk). Deep-Cycle Batteries for Off-Grid & Remote Power Systems, Energy Development Co-operative Limited, Oulton Broad, Lowestoft, Link: http://www.solar-wind.co.uk/deep-cycle-dryfit-batteries-battery-uk.html
61. SMA, Sunny Backup 5000, Installations- und Bedienungsanleitung (Version 2), SMA.

62. M. Glavin. Optimisation of a Hybrid Energy Storage System for Autonomous Photovoltaic Applications, PhD Thesis, National University of Ireland, Galway, 2012.
63. P. Keil, A. Jossen. Aufbau und Parametrierung von Batteriemodellen, Technische Universität München, München, 2012.
64. F. M. González-Longatt. Circuit Based Battery Models: A Review, 2DO Congreso Iberoamericano de Estudiantes de Ingeniería Eléctrica (II CIBELEC 2006), 2006.
65. S. Pang, J. Farrell, J. Du, M. Barth. Battery state-of-charge estimation, in: Proceedings of the American Control Conference, 2, pp. 1644.1649, June 2001.
66. C. M. Shepherd. Design of Primary and Secondary Cells, Journal of The Electrochemical Society, 112, pp. 657- 664, 1965.
67. D. Sutanto., H.L. Chang. A New Battery Model for use with Battery Energy Storage Systems and Electric Vehicles Power Systems, IEEE Transactions on Energy Conversion, 4, 2, 1995.
68. J. Appelbaum, R. Weiss. An Electrical Model of the Lead- Acid Battery, IEEE International Telecommunications Energy Conference, 1982. INTELEC 1982, Washington, DC, USA, USA, pp. 304-307, 1982.
69. L. Balza, C. Gischler, N. Janson, S. Miller, G. Servetti. Potential for Energy Storage in Combination with Renewable Energy in Latin America and the Caribbean, Technical Note No. IDB-TN-626, Inter-American Development Bank Infrastructure and Environment Department Energy Division, February 2014.
70. M. L. Perry, A. Z. Weber. Advanced Redox-Flow Batteries: A Perspective, Journal of The Electrochemical Society, 163, pp. A5064-A5067, 2016.
71. C. Blanc, A. Rufer. Understanding the Vanadium Redox Flow Batteries. Paths to Sustainable Energy, Dr Artie Ng (Ed.). InTech. Link: http://www.intechopen.com/books/paths-to-sustainable-energy/understanding-the-vanadium-redox-flow-batteries, 2010.
72. M. Schreiber. Lifetime of Vanadium Redox Flow Battery, The Electrical Energy Storage Applications and Technologies (EESAT) Conference 2011, Oct. 16-19, San Diego, USA, 2011.
73. A. A. Shah, M. J. Watt-Smith, F. C. Walsh. A dynamic performance model for redox-flow batteries involving soluble species, Electrochimica Acta, 53, pp. 8087–8100, 2008.
74. J. R. Clausen, V. E. Brunini, H. K. Moffat, M. J. Martinez. Numerical Modeling of an All Vanadium Redox Flow Battery, Sandia Report, SAND2014-0190, CA, USA, 2014.
75. X. Ma, H. Zhang, F. Xing. A three-dimensional model for negative half cell of the vanadium redox flow battery, Electrochimica Acta, 58, pp. 238–246, 2011.
76. M. Li, T. Hikihara. A coupled dynamical model of redox flow battery based on chemical reaction, fluid flow, and electrical circuit, IEICE Transactions on Fundamentals of Electronics, Communications and Computer Sciences, E91-A(7), pp. 1741–1747, 2008.
77. BDEW Bundesverband der Energie- und Wasserwirtschaft e.V. Stromverbrauch im Haushalt, BDEW Bundesverband der Energie- und Wasserwirtschaft e.V., Berlin, Germany, 2016.
78. BDEW Bundesverband der Energie- und Wasserwirtschaft e.V. Durchschnittlicher Haushaltsstromverbrauch, BDEW Bundesverband der Energie- und Wasserwirtschaft e.V., Berlin, Germany.

79. H. Meier, C. Fünfgeld, T. Adam, B. Schieferdecker. Repräsentative VDEW-Lastprofile, Brandenburgische Technische Universität Cottbus, VDEW, Frankfurt (Main), Germany, 1999.
80. I. Richardson, M. Thomson, D. Infield, C. Clifford. Domestic electricity use: A high-resolution energy demand model, Energy and Buildings, 42, pp. 1878–1887, 2010.
81. Verein Deutscher Ingenieure, VDI 4655: Reference load profiles of single-family and multi-family houses for the use of CHP systems, Düsseldorf, Germany, 2008.
82. BMUB, Bundes-Ministerium für Umwelt, Natur-Schutz, Bau und Reaktor-Sicherheit. Kurzinfo Elektromobilität, 2016, BMUB, Bundes-Ministerium für Umwelt, Natur-Schutz, Bau und Reaktor-Sicherheit, 2016.
83. T. Pregger, D. L. de Tena, M. O'Sullivan, N. Roloff, S. Schmid, B. Propfe, D. Hülsebusch, B. Wille-Haussmann, S. Schwunk, C. Wittwer, T. Pollok, S. Krahl, A. Moormann. Perspektiven von Elektro-/Hybridfahrzeugen in einem Versorgungssystem mit hohem Anteil dezentraler und erneuerbarer Energiequellen, Schlussbericht, BMWi – FKZ 0328005 A-C, 2012.
84. Z. McDonald. A Simple Guide to DC Fast Charging, EV Charging, 2016.
85. P. Grahn. Electric Vehicle Charging Modeling, Ph.D. Thesis, Royal Institute of Technology, Stockholm, Sweden, October 2014.
86. Z. Darabi, F. Mehdi. Aggregated impact of plug-in hybrid electric vehicles on electricity demand profile, IEEE Transactions on Sustainable Energy, 2, pp. 501–508, 2011.
87. L. P. Fernández, T. G. San Román, R. Cossent, C. M. Domingo, P. Frías. Assessment of the impact of plug-in electric vehicles on distribution networks, IEEE Transactions on Power Systems, 26, pp. 206–213, 2011.
88. T.-K. Lee, B. Adornato, Z. S. Filipe. Synthesis of real-world driving cycles and their use for estimating PHEV energy consumption and charging opportunities: Case study for Midwest/U.S., IEEE Transactions on Vehicular Technology, 60, pp. 4153–4163, 2011.
89. D. Westermann, M. Agsten, S. Schlegel. Empirical BEV model for power flow analysis and demand side management purposes, in: Proceedings of the International Symposium Modern Electric Power Systems (MEPS), Wroclaw, Poland, 2010.
90. K. Clement-Nyns, E. Haesen, J. Driesen. Stochastic analysis of the impact of plug-in hybrid electric vehicles on the distribution grid, in: The 20th International Conference and Exhibition on Electricity Distribution - Part 2, 2009. CIRED 2009, Prague, Czech Republic, Jun. 8–11, 2009.
91. K. Clement-Nyns, E. Haesen, J. Driesen. The impact of charging plug-in hybrid electric vehicles on a residential distribution grid, IEEE Transactions on Power Systems, 25, pp. 371–380, 2010.
92. J. A. Pecas Lopes ; F. J. Soares ; P. M. Rocha Almeida. Identifying management procedures to deal with connection of Electric Vehicles in the grid, 2009 IEEE Bucharest PowerTech, Bucharest, Romania, 2009.
93. Verband der Elektrotechnik Elektronik und Informationstechnik (VDE)| Energietechnische Gesellschaft (ETG). VDE Studie Elektrofahrzeuge, Bedeutung, Stand der Technik, Handlungsbedarf, Gesamttext, VDE|ETG, Frankfurt am Main, Germany, 2010.

94. T. Bocklisch. Hybrid energy storage systems for renewable energy applications, Energy Procedia 73, pp. 103 – 111, 9th International Renewable Energy Storage Conference, IRES 2015, 2015.
95. O. H. Minoarivelo. Application of Markov Decision Processes to the Control of a Traffic Intersection, University of Barcelona, Spain, 2009.
96. S. Nicolai, P. Bretschneider, D. Westermann. Hierarchische Speichereinsatzoptimierung: Mit einem Realisierungsbeispiel auf der Insel Pellworm, Automatisierungstechnik, 62, pp. 364–374, Fraunhofer-Publica, 2014.
97. Y. Zhang, Z. Jiang, X. Yu. Control Strategies for Battery/Supercapacitor Hybrid Energy Storage Systems, IEEE Energy2030, Atlanta, GA USA, 2008.
98. W. Li, G. Joós. A power electronic interface for a battery supercapacitor hybrid energy storage system for wind applications, IEEE Power Electronics Specialists Conference, 15-19 June 2008, pp. 1762 – 1768, Rhodes, IEEE, 2008.
99. F. Li, K. Xie, J. Yang. Optimization and Analysis of a Hybrid Energy Storage System in a Small-Scale Standalone Microgrid for Remote Area Power Supply (RAPS), Energies, 8, pp. 4802-4826, 2015.
100. C. Abbey, K. Strunz, G. Joós. A Knowledge-Based Approach for Control of Two-Level Energy Storage for Wind Energy Systems, IEEE Transactions on Energy Conversion, 24, pp. 539-547, 2009.
101. K. Takeda, C. Takahashi, H. Arita, N. Kusumi, M. Amano, A. Emori. Design of hybrid energy storage system using dual batteries for renewable applications, 2014 IEEE PES General Meeting | Conference & Exposition, 27-31 July 2014, pp. 1 – 5, National Harbor, MD, USA, 2014.
102. T. Ise, M. Kita, A. Taguchi. A Hybrid Energy Storage with a SMES and Secondary Battery, IEEE Transactions on Applied Superconductivity, 15, pp. 1915-1918, 2005.
103. Y. Zhou, A. Scheller-Wolf, N. Secomandi, S. Smith. Managing Wind-based Electricity Generation in the Presence of Storage and Transmission Capacity, Research Showcase, Tepper School of Business, Carnegie Mellon University, Pittsburgh, USA, 2013.
104. M. A. Murtaza, M. Tahir. Optimal Data Transmission and Battery Charging Policies for Solar Powered Sensor Networks using Markov Decision Process, 2013 IEEE Wireless Communications and Networking Conference (WCNC), Shanghai, China, 2013.
105. Y. Xu, L. Tong. On the Operation and Value of Storage in Consumer Demand Response, 53rd IEEE Conference on Decision and Control (CDC) (invited paper), Los Angeles, CA, USA, December 2014.
106. S. Grillo, A. Pievatolo, E. Tironi. Optimal Storage Scheduling Using Markov Decision Processes, IEEE Transactions On Sustainable Energy, 7, pp. 755-764, 2016.
107. M. M. Hiksas, M. L. Aninditio. Redox Flow Batteries for small scale energy storage, 2016 IEEE Conference on Technologies for Sustainability (SusTech), Phoenix, AZ, USA, 2016.
108. J. Salom, A. J. Marszal, J. Candanedo, J. Widén, K. B. Lindberg, I. Sartori. IEA. Analysis of Load Match and Grid Interaction Indicators in Net Zero Energy Buildings with High Resolution Data: A report of Subtask A, IEA Task 40/Annex 52 Towards Net Zero Energy Solar Buildings, IEA, 2013.

109. K. Voss, I. Sartori, E. Musall, A. Napolitano, S. Geier, M. Hall, B. Karlsson, P. Heiselberg, J. Widen, J.A. Candanedo, P. Torcellini. Load matching and grid interaction of net zero energy buildings, in: Proceedings of EuroSun 2010, Graz, Austria, 2010.
110. S. Zhang, J. Yang, Y. Shi, X. Wu, Y. Ran. Dynamic Energy Storage Control for Reducing Electricity Cost in Data Centers, Hindawi Publishing Corporation, Mathematical Problems in Engineering, 2015.
111. Solar-Institut Juelich. CARNOT Blockset. Conventional And Renewable eNergy systems OpTimization Blockset, Solar-Institut Juelich, Juelich, Germany, 1999.
112. R. D'Agostino. The role of Vanadium Redox Flow Batteries in micro power systems for residential applications, Master Thesis, Ostfalia Hochschule für angewandte Wissenschaften, Wolfenbüttel, Germany, 2013.
113. Deutsches Institut für Normung. Norm: Daylight in interiors - Part 5: Measurement. DIN 5034-5:1993-01, Beuth Verlag, Berlin, 1985.
114. V. Quaschning. Regenerative Energiesysteme: Technologie - Berechnung – Simulation, 7th ed., Carl Hanser Verlag, Germany, 2013.
115. D.T. Reindl, W.A. Beckman, J.A. Duffie. Diffuse Fraction Correlations, in: Proceedings of ISES Solar World Conference 1989, Kobe, Japan, pp. 2082-2086, 1989.
116. D.T. Reindl, W.A. Beckman, J.A. Duffie. Evaluation of hourly tilted surface radiation models, Solar Energy, 45, pp. 9–17, 1990.
117. B.Y.H. Liu, R.C. Jordan. Daily insolation on surfaces tilted towards the equator, ASHRAE Transactions, 67, pp. 526–541, 1962.
118. T.M. Klucher. Evaluation of models to predict insolation on tilted surfaces, Solar Energy, 23, pp. 111–114, 1979.
119. R. Perez, R. Stewart, C. Arbogast, R. Seals, J. Scott, An anisotropic hourly diffuse radiation model for sloping surfaces, description, performance validation, site dependency evaluation, Solar Energy, 36, pp. 481–497, 1986.
120. R. Perez, P. Ineichen, R. Seals, J. Michalsky, R. Stewart. Modelling daylight availability and irradiance components from direct and global irradiance, Solar Energy, 44, pp. 271–289, 1990.
121. R. Perez, R. Seals, P. Ineichen, P. Stewart, D. Menicucci. A new simplified version of the Perez diffuse irradiance model for tilted surfaces, Solar Energy, 39, pp. 221–223, 1987.
122. S. Dimopoulou, E. Boggasch, A. Rausch. A Comparative Study of Diffuse Irradiance Models on Inclined Surfaces for Wolfenbuettel, Germany. Poster Session presented at: 4th Solar Integration Workshop, Berlin, Germany, 10-11 November 2014.
123. P.G. Loutzenhiser, H. Manz,C. Felsmann, P.A. Strachan, T. Frank, G.M. Maxwell. Empirical validation of models to compute solar irradiance on inclined surfaces for building energy simulation, Solar Energy, 81 pp. 254–267, 2007.
124. T. Muneer, C. Gueymard, H. Kambezidis. Solar Radiation and Daylight Models, 2nd ed., Oxford, Elsevier Butterworth-Heinemann, Amsterdam, The Netherlands, 2004.
125. C. Brendel, F. U. S. Tchikague, P. Schulz, V. Hristov. Modellbasierte MATLAB/Simulink Simulation einer Li-Ion Traktionsbatterie, Hochschule Bochum, Institut für Elektrotechnik, Bochum, Germany, 2014.
126. E. M. Krieger, J. Cannarella, C. B. Arnold. A comparison of lead-acid and lithium-based battery behavior and capacity fade in off-grid renewable charging applications, Energy, 60, pp. 492–500, 2013.

127. T. Sukkar, M. Skyllas-Kazacos. Water transfer behaviour across cation exchange membranes in the vanadium redox battery, Journal of Membrane Science, 222, pp. 235–247, 2003.
128. A. Oppermann, E. Boggasch, S. Dimopoulou, A. Rausch. Geographisch-individueller Fahrzyklus zur Ermittlung des Energiebedarfs eines eCars in einer Kleinstadt in ländlicher Umgebung, EUROSOLAR e.V., Solarzeitalter, 2015.
129. M. L. Puterman. Markov Decision Processes, Discrete Stohastic Dynamic Programming, AJohn Wiley &Sons, Inc., Publication, Hoboken, New Jersey 1994, 2005.
130. J. Marecki, Z. Topol, M. Tambe. A Fast Analytical Algorithm for MDPs with Continuous State Spaces, Computer Science Department, University of Southern California, Los Angeles, CA, USA, in: Proceedings of the Eight Workshop on Game Theoretic and Decision Theoretic Agents (GTDT) held at the Fifth International Conference on Autonomous Agents and Multi-Agent Systems (AAMAS'06), pp. 2536–2541, May 2006.
131. S. Holmes. Sums of Random Variables: Statistics 116. Stanford, USA, 1998. Link: http://statweb.stanford.edu/~susan/courses/s116/node114.html
132. I. Chadès, G. Chapron, M.-J. Cros, F. Garcia, R. Sabbadin. MDPtoolbox: a multi-platform toolbox to solve stochastic dynamic programming problems. Ecography 37:916-920, 2014.
133. Max Pixel. Power, Electricity, Line, Pylon, Sunset, Grid, Wire Photo. Link: http://maxpixel.freegreatpicture.com/Electricity-Wire-Sunset-Grid-Power-Line-Pylon-1549118
134. https://commons.wikimedia.org/wiki/File%3AMarkov_Decision_Process_example.png
135. House Clipart. Link: http://www.okclipart.com/house-clipart-png30smojlnny/

A. Appendix

In this appendix indicative graphical illustrations of the presented models in Section 4 which are designed in Matlab/ Simulink environment are exhibited with a correspondence to the physical equations that describe their operation.

A. PV Model

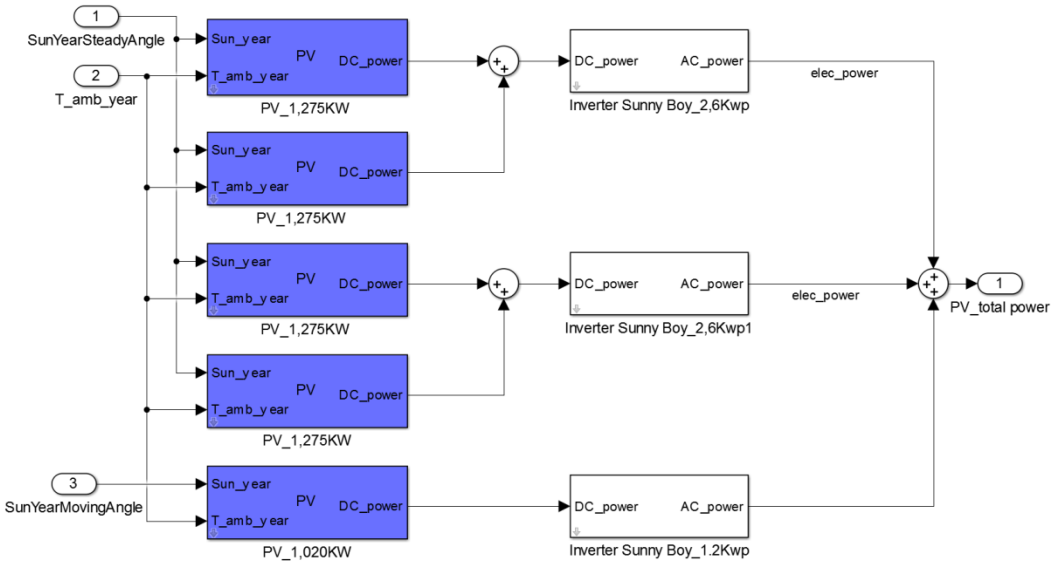

Figure A-1: A graphical illustration of the PV Model [41, 111, 112]

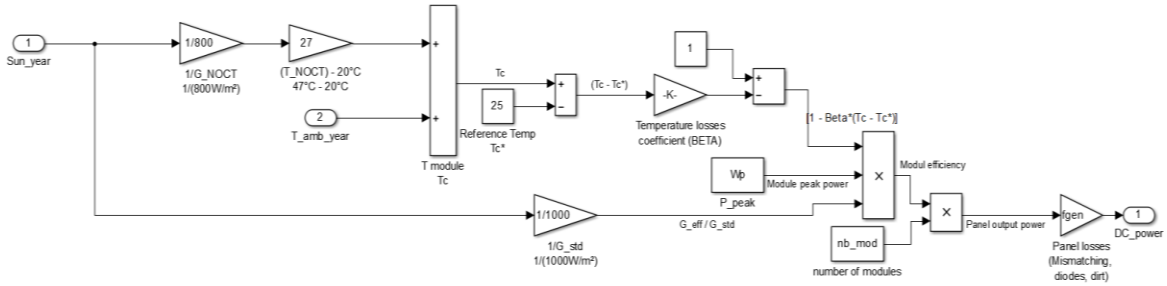

Figure A-2: DC-Power Calculation according to Perpiñan et al. [112]

B. Lead Acid Battery Model

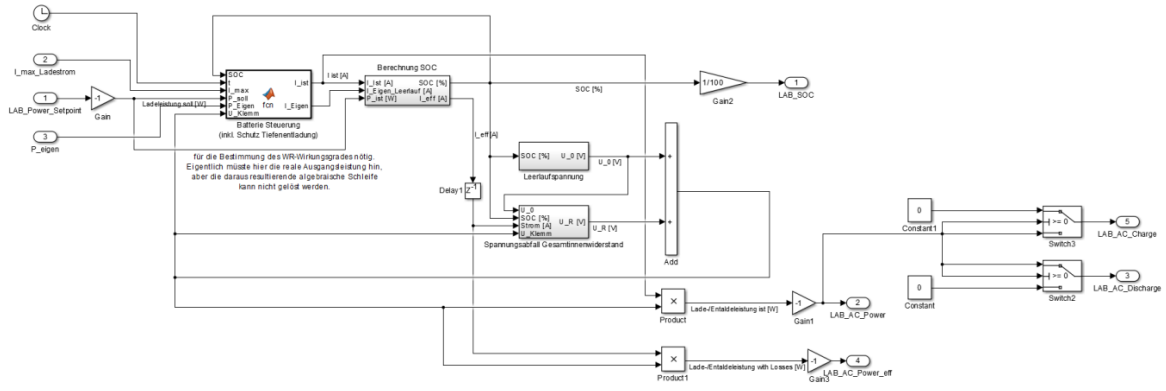

Figure B-1: A graphical illustration of the LAB Model [58, 125]

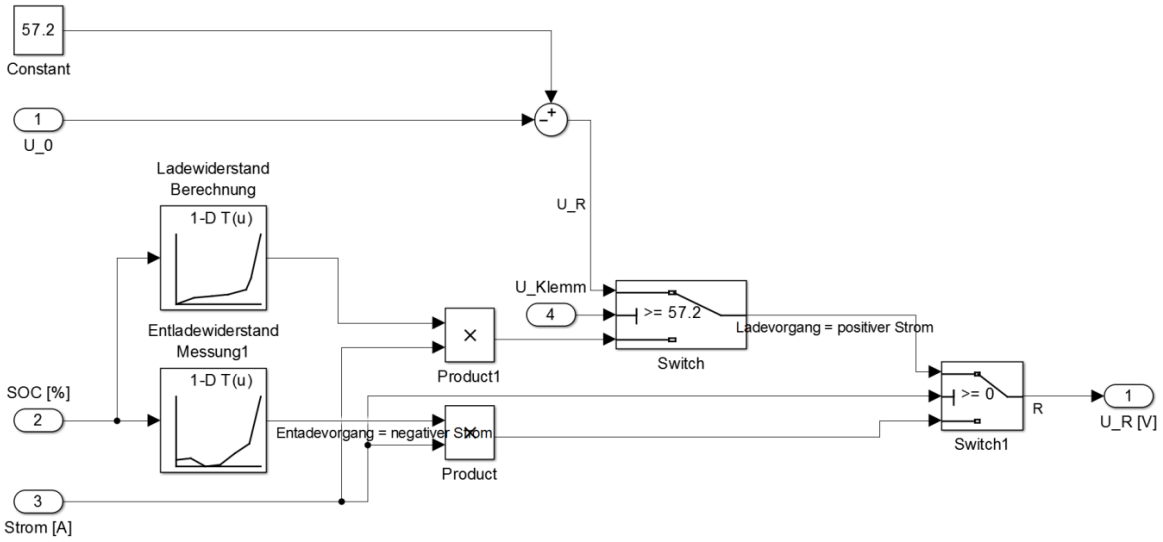

Figure B-2: A graphical illustration of the Voltage Drop on the Overall Internal Resistance [58]

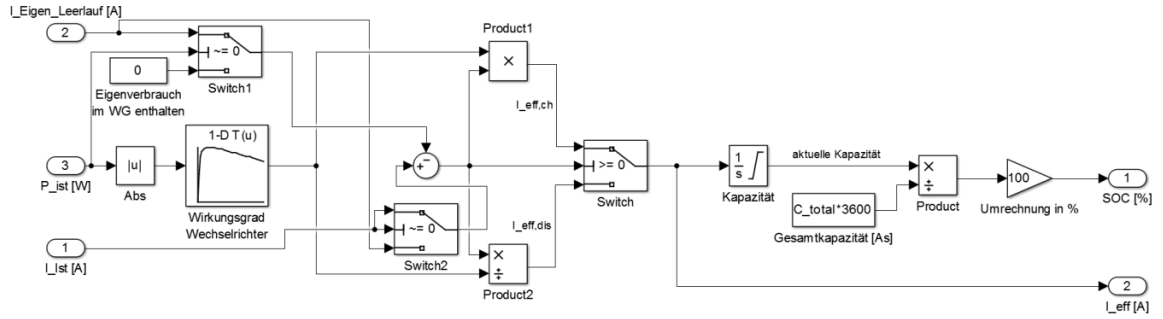

Figure B-3: SOC-Calculation for the LAB Model [58]

C. Vanadium Redox Flow Battery Model

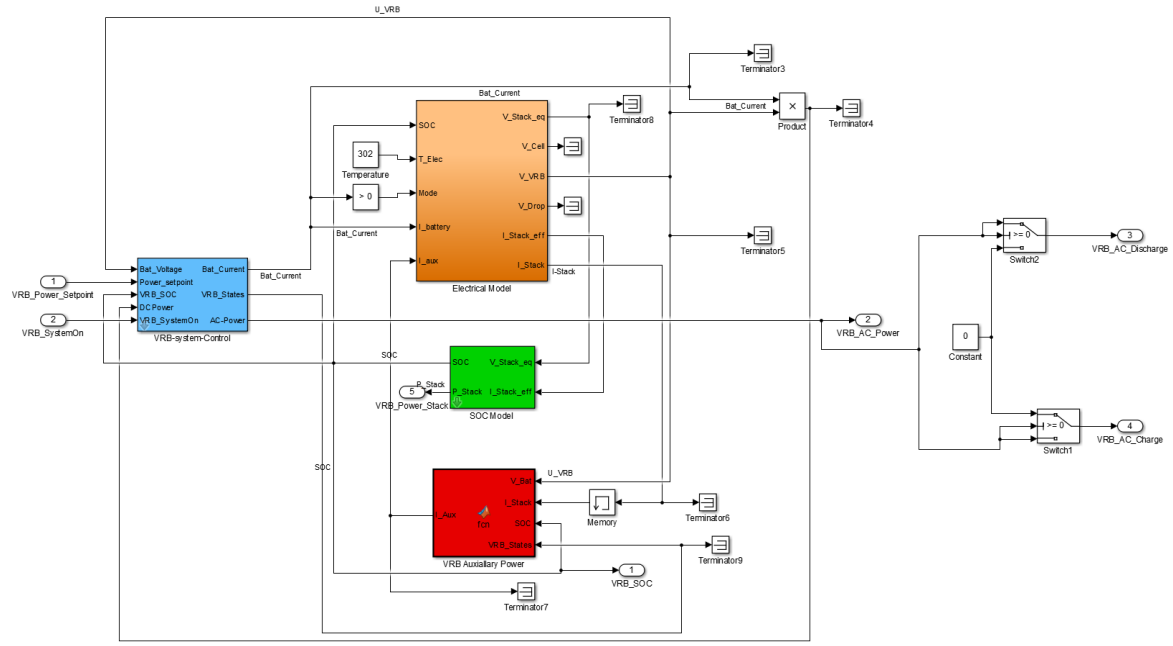

Figure C-1: A graphical illustration of the VRB Model [18]

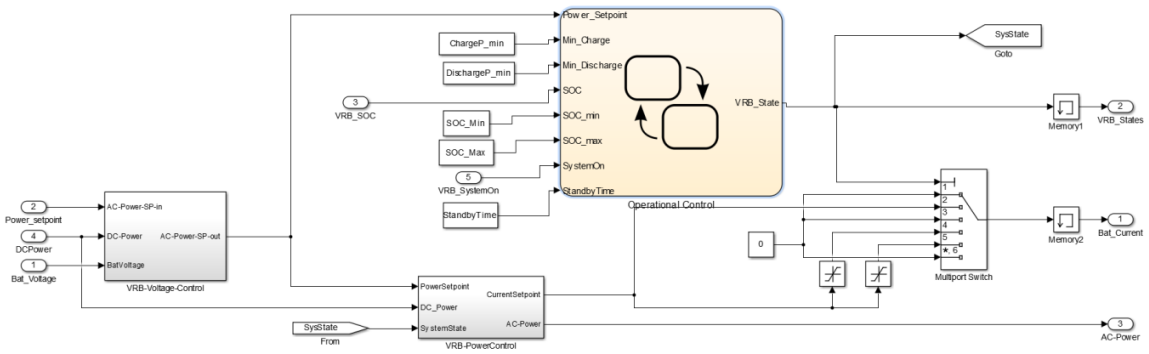

Figure C-2: A graphical illustration of the VRB System Control [18]

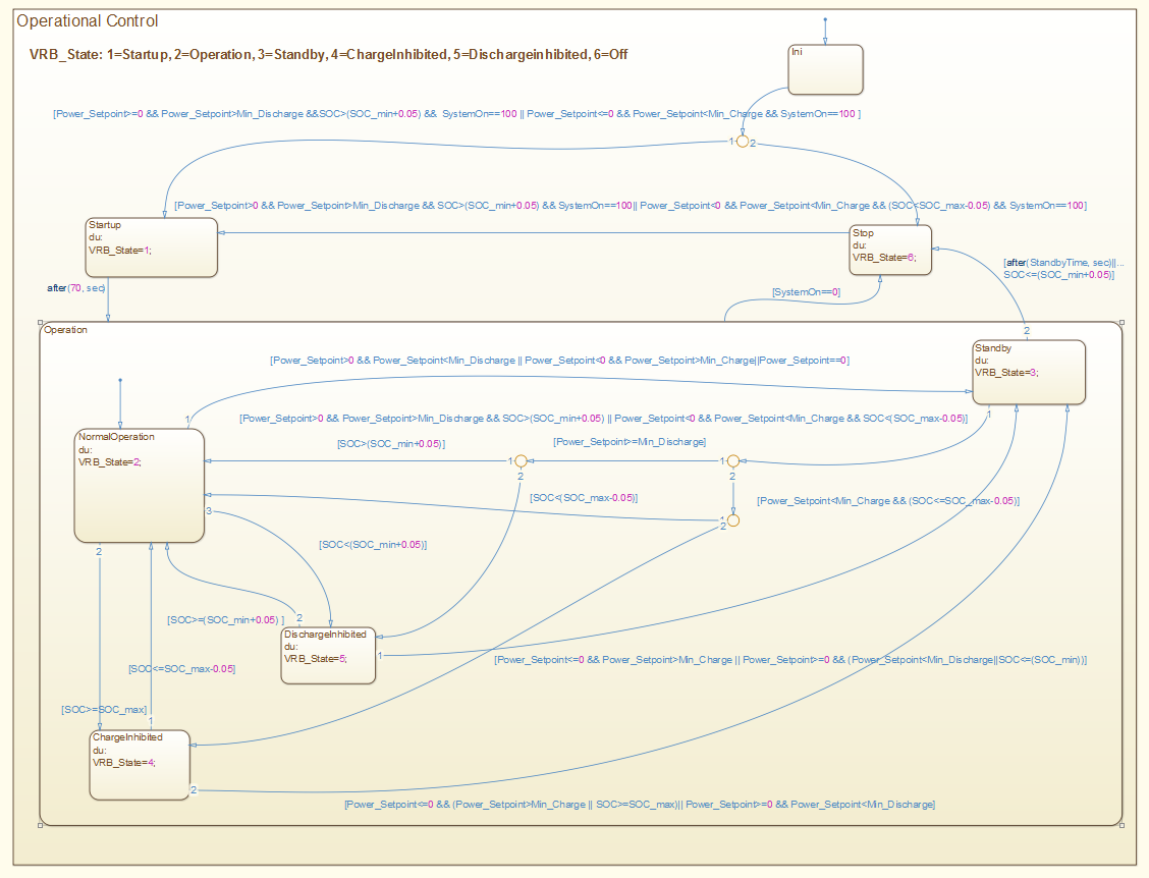

Figure C-3: A graphical illustration of the Operational Control of the VRB Model [18]

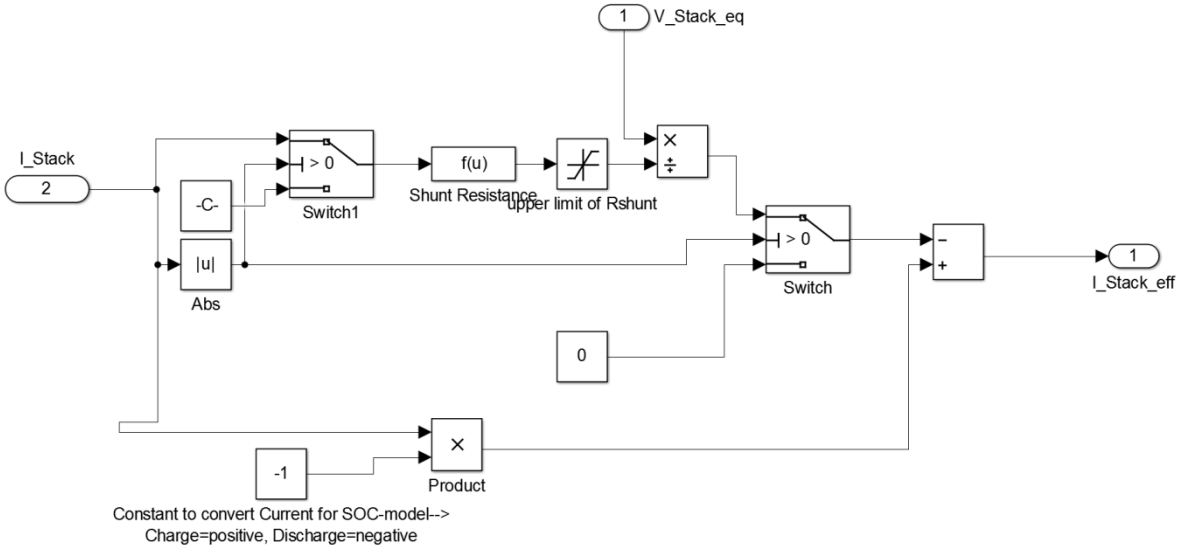

Figure C-4: Efficiency Stack Current Calculation [18]

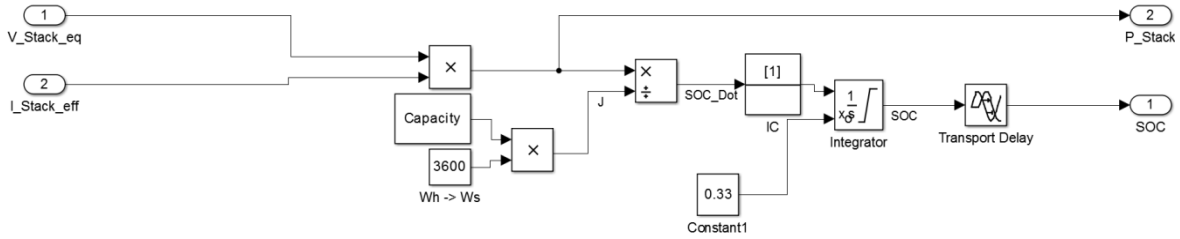

Figure C-5: SOC-Calculation for the VRB Model [18]

D. Grid Model

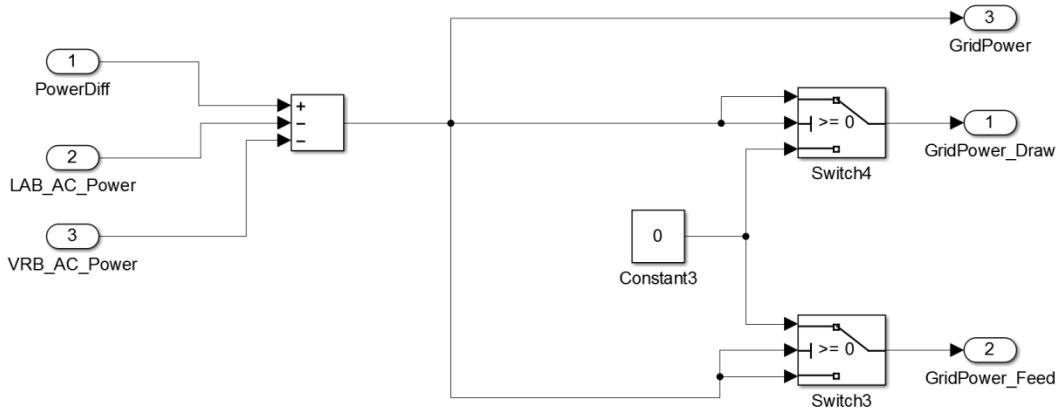

Figure D-1: A graphical illustration of the Grid Model